
Masters Theses

Student Theses and Dissertations

Fall 2016

Origin of lacustrine carbonate-dominated clinoforms in the lower-Permian Lucaogou low-order cycle, southern Bogda mountains, NW China

Yiran Lu

Follow this and additional works at: https://scholarsmine.mst.edu/masters_theses



Part of the [Geology Commons](#), and the [Geophysics and Seismology Commons](#)

Department:

Recommended Citation

Lu, Yiran, "Origin of lacustrine carbonate-dominated clinoforms in the lower-Permian Lucaogou low-order cycle, southern Bogda mountains, NW China" (2016). *Masters Theses*. 7609.

https://scholarsmine.mst.edu/masters_theses/7609

This thesis is brought to you by Scholars' Mine, a service of the Missouri S&T Library and Learning Resources. This work is protected by U. S. Copyright Law. Unauthorized use including reproduction for redistribution requires the permission of the copyright holder. For more information, please contact scholarsmine@mst.edu.

ORIGIN OF LACUSTRINE CARBONATE-DOMINATED CLINOFORMS IN THE
LOWER-PERMIAN LUCAOGOU LOW-ORDER CYCLE, SOUTHERN BOGDA
MOUNTAINS, NW CHINA

by

YIRAN LU

A THESIS

Presented to the Faculty of the Graduate School of the
MISSOURI UNIVERSITY OF SCIENCE AND TECHNOLOGY

In Partial Fulfillment of the Requirements for the Degree

MASTER OF SCIENCE IN GEOLOGY & GEOPHYSICS

2016

Approved by:

Wan Yang, Advisor
David J. Wronkiewicz
Francisca Oboh-Ikuenobe

© 2016

Yiran Lu

All Rights Reserved

ABSTRACT

Lacustrine carbonate clinoforms deposit can reflect ancient lake condition like paleoclimate and lake type. Complex lithofacies of a carbonate-dominated clinoform package in lower Permian Lucaogou low order cycle, Bogda Mountains, NW China, provide clues on clinoform-forming processes in a half-graben lake. The clinoform package is ~5.2 m thick, prograding from S to N for ~200 m with a maximum 15° dip angle, and spans ~4 km laterally. A clinoform consists of a lower siliciclastic-rich and an upper carbonate-rich beds, forming a clinoform cycle. Results of petrographic study of 30 thin sections suggest that the clinoform package is composed of mixed siliciclastic-carbonate rocks. Carbonate-rich bed is composed of diagenetically-altered lithic packstone and wackestone, and siliciclastic-rich clinoform of micritic sandstone. The foundation rock is mainly microbial boundstone, indicating a shallow littoral environment.

The carbonate-rich beds mainly consist of coarse peloids, rip-up intraclasts, aggregate grains, and volcanic lithics. The siliciclastic-rich clinoform is rich in coarse volcanic lithics. Both types of clinoforms contain abundant current laminations, indicating frequent strong current activities. The lack of evidence of unidirectional current flow suggests that the carbonate-dominated clinoform package was probably primarily formed by wave and longshore current processes. Unlike grains in wave-built terrace in the Glens Ferry Formation (Swirydczuk et al., 1979, 1980), few ooids were observed in the studied strata, which do not have local sediments as nucleus and are often broken. This indicates that the wave was not facing the lake margin directly but was more oblique to the lake margin. The carbonate-dominated clinoform package is thus interpreted as a bar or spit, controlled primarily by lake shoreline morphology and strong wave and current activities. The shift between carbonate and siliciclastic rich clinoform beds within a clinoform cycle suggests high-frequency changes in climatic conditions.

Detrital lithics were mainly derived from northern Tianshan suture zone to the south. The carbonate clasts were transported from a nearby carbonate factory at the lake margin. The Lucaogou lake was a balanced-filled lake in a semiarid, seasonal climate and had persistent longshore currents caused by strong wind and wave activities.

ACKNOWLEDGMENTS

I would like to thank my advisor, Dr. Wan Yang, for his knowledge, patience, support, and motivation both in the field and lab. This work could not be done without his help.

I also give my appreciation to my lab colleagues, Jing Duan, Jaimeson Fredricks, Xiaowei Peng, Zhixin Li, Bin Sun, Xin Zhan, and Dongyu Zheng, and also former colleagues, Dr. Abdullarh Nabhan, Qiuwan Yu, and Yizuo Shi for their ideas, help, suggestions and knowledge.

I thank my committee members, Dr. David J. Wronkiewicz and Dr. Francisca Oboh Ikuenobe for their help, support, and time.

Thank Dr. Jonathan Obrist Farner from Missouri S&T and Xin Jiao from Northwest University for their help during the microscopic petrographic study, and Dr. Mingli Wan from Nanjing Institute of Geology and Paleontology, Chinese Academy of Sciences, and Mr. Jianjun Li for their help and guidance during the summer field work.

Finally, special thanks for my parents and other family members for their support, love, and patience. I would never achieve my works without their encouragement.

TABLE OF CONTENTS

	Page
ABSTRACT.....	iii
ACKNOWLEDGMENTS	iv
LIST OF ILLUSTRATIONS.....	viii
LIST OF TABLES.....	ix
SECTION	
1. INTRODUCTION	1
1.1. GEOLOGICAL BACKGROUND	1
1.2. STRATIGRAPHY.....	2
1.3. LOWER LUCAOGOU CARBONATE-DOMINATED CLINOFORMS	3
2. METHOD AND DATA.....	7
2.1. FIELD OBSERVATIONS	7
2.2. MICROSCOPIC PETROGRAPHIC STUDY	7
3. PETROGRAPHY OF THE CLINOFORM PACKAGE	15
3.1. GRAINS	15
3.1.1. Non-Carbonate Grain (S).....	15
3.1.1.1 Monocrystalline quartz (Qm).....	15
3.1.1.2 Polycrystalline quartz (Qp)	16
3.1.1.3 Potassium feldspar (K).....	16
3.1.1.4 Plagioclase (P).....	16
3.1.1.5 Volcanic lithics (Lv).....	16
3.1.1.6 Sedimentary lithics (Ls).....	17
3.1.1.7 Accessary minerals (AM).....	17
3.1.1.8 Undifferentiated detrital grain (Lund).....	17
3.1.2. Carbonate Grain (A)	17
3.1.2.1 Intraclast (Lci)	17
3.1.2.2 Aggregate grain (Lca)	18
3.1.2.3 Ooids (Lco).....	18

3.1.2.4 Oncoid (Lcon)	19
3.1.2.5 Pisoid (Lcpi)	19
3.1.2.6 Peloid (Lcp)	20
3.1.2.7 Bioclast (Lcb)	20
3.1.3. Completely Sparry Calcite-Replaced Grains (Cr)	20
3.2. MATRIX	20
3.3. CEMENT	21
3.4. DIAGENESIS	22
3.5. PETROFACIES	24
3.5.1. Petrofacies A	26
3.5.2. Petrofacies B	26
3.5.3. Petrofacies C	26
3.6. LITHOFACIES AND THEIR DEPOSITIONAL ENVIRONMENTS	27
3.6.1. Mixed Siliciclastic-Carbonate Lithofacies	27
3.6.1.1 Diagenetic lithic packstone and wackestone subfacies	28
3.6.1.2 Micritic lithic sandstone subfacies	28
3.6.2. Microbial Carbonate Lithofacies	29
3.6.2.1 Boundstone subfacies	29
3.6.2.2 Thrombolitic microbialite subfacies	29
3.6.3. Mudrock Lithofacies	30
3.6.3.1 Interlaminated mudstone-very fine sandstone subfacies ..	30
3.6.3.2 Organic-rich mudstone subfacies	30
3.6.3.3 Calcareous shale subfacies	31
3.6.4. Highly Diagenetically-Altered Limestone Lithofacies	31
3.6.4.1 Lithic cementstone subfacies	31
3.6.4.2 Sparstone subfacies	32
3.7. LATERAL AND VERTICAL FACIES CHANGES IN CLINIFORMS	32
4. DISCUSSION AND INTERPRETATION	48
4.1. FORMATION OF CARBONATE-RICH CLINIFORMS	48
4.2. FACIES CHANGES IN CLINIFORM PACKAGE	49

4.3. PROBLEMATIC ASPECTS.....	51
4.4. LAKE CONTRACTION AND EXPANSION	52
4.5. PROVENANCE OF SILICICLASTIC SEDIMENTS.....	53
4.6. CLIMATE AND LAKE TYPE.....	54
5. CONCLUSION.....	58
APPENDICES	
A: SKETCH AND DESCRIPTIONS OF CLINIFORM PACKAGE IN DIP DIRECTION	59
B: MEASURED SECTION 2 IN STRIKE DIRECTION	64
C: MEASURED SECTION 3 IN STRIKE DIRECTION	68
D: MEASURED SECTION 4 IN STRIKE DIRECTION.....	71
E: MEASURED SECTION 5 IN STRIKE DIRECTION	75
F: MEASURED SECTION 6 IN STRIKE DIRECTION.....	79
G: MEASURED SECTION 7 IN STRIKE DIRECTION	84
H: MEASURED SECTION 1 IN STRIKE DIRECTION.....	89
BIBLIOGRAPHY.....	91
VITA	96

LIST OF ILLUSTRATIONS

Figure	Page
1.1. Location and global paleogeographic reconstruction and of the study area	4
1.2. Chrono-, litho-, and cyclostratigraphy of Permian–Triassic strata in the NE Tarloung and Taodougou sections	5
1.3. Dip section of the carbonate-dominated clinoform package	6
2.1. Geological map showing the Tarloung and Taodougou sections and locations of measured sections.....	10
2.2. A close look and sketch of the carbonate-dominated clinoform package.....	11
3.1. Photomicrographs showing various grains	42
3.2. Photomicrographs showing various grains and matrix	43
3.3. Photomicrographs showing various interesting features	44
3.4. Photomicrographs of interesting features.	45
3.5. ASMi ternary diagram showing non-microbially-induced, relatively weakly diagenetically-altered samples in clinoform package	46
3.6. Lateral change of grain size from toe to upper slope of a carbonate-rich clinoform	47
3.7. Lateral change of grain sorting from toe to upper slope of a carbonate-rich clinoform	47
4.1. Schematic diagram showing the paleogeography during the formation of the carbonate-dominated clinoform package in the study area.....	55
4.2. QpLvLs ternary diagram of detrital grains in samples	56
4.3. QmFL ternary diagram of detrital grains in samples	57

LIST OF TABLES

Table	Page
2.1. Symbols and definitions of compositional attributes documented in point counting of this study	13
2.2. Calculated derivative attributes used in statistical analysis of point-counting data ..	14
3.1. Raw point-counting data.....	34
3.2. Derivative data calculated from raw point-counting data	36
3.3. Cement spar distribution in clinoform deposits.....	38
3.4. Characteristics, interpreted depositional environments, and occurrence of lithofacies in studied samples	39

1. INTRODUCTION

Clinoforms are progradational patterns formed by deposition with sloping surfaces. Carbonate clinoforms have been studied since Bosellini (1984) in Dolomites in northern Italy, and widely investigated focusing on stacking patterns (Pomar, 1991; Jacquin et al. 1991), geometry (Mullins et al., 1983; Kenter & Campbell, 1991), and controlling factors of grain distribution (Kenter, 1990; Adams & Schlager, 2001; Quiquerez & Dromart, 2006). They are well studied in marine environments, whereas carbonate-dominated clinoforms or prograding foresets are less well known and recorded in lacustrine facies (Swirydczuk et al., 1980). Lakes are more sensitive to changes in climate than oceans; and lacustrine sediments commonly show abrupt changes of sedimentary facies in vertical sequence, reflecting variations in lake-water chemistry, physical processes, and biological activity as the result of shoreline shifting and biochemical fluctuation in lake water (Swirydczuk et al., 1980; Talbot & Allen, 1996). The origin of lacustrine carbonate is complex in comparison to shallow marine carbonate because of the strong effects from biotic factors and interference of climate, river inflow, and even lake morphology (Arp, 1995; Talbot & Allen, 1996; Gierlowski-Kordesch, 2010; Flügel, 2010). These unique aspects make occurrences of carbonate clinoforms in lacustrine facies geologically significance.

This study focuses on a carbonate-dominated clinoform package in the lower part of the Lucaogou low-order cycle (LCG LC), NW China. The lithofacies, diagenetic condition, depositional environment, forming mechanisms of the clinoforms, and type and paleoclimate of the ancient Lucaogou lake were investigated and interpreted. The interactions of coast-line morphology and climate oscillation on lacustrine carbonate deposit are explored.

1.1. GEOLOGICAL BACKGROUND

The study area covers ~4x6 km² in Tarlong-Taodonggou area and is located ~15 km north of Daheyan, Xinjiang Uygur Autonomous, NW China (Figure 1.1B, C), in the southern foothills of Bogda Mountains. The Bogda Mountains are a giant anticline and was uplifted by Early Triassic (Carroll et al., 1992; Hendrix et al., 1992; Shao et al.,

1999; Greene et al., 2005). The uppermost Carboniferous-Triassic fluvial and lacustrine deposits are exposed along the foothills (Liao et al., 1987; Cheng and Lucas, 1993; Carroll et al., 1995; Greene et al., 2005; Yang et al., 2010). The Tarlong-Taodonggou area was located in the southeastern Kazakhstan Plate, NE Pangea (Allen et al., 1995; Carroll et al., 1995; Yin et al., 1996; Scotese, 2001; Yang et al., 2010). It was located on the northwestern coast of Paleo-Tethys Sea at $\sim 30^{\circ}\text{N}$ in the arid climate zone in early Permian, at approximately 40°N in the warm temperate zone in late Permian, and moved slightly to the north into cool temperate climate zone in Early Triassic (Figure 1.1A; Scotese, 2001; Yang et al., 2010). It has a basement composed of Carboniferous volcanic arc accretionary wedge complexes formed by collision between the Junggar and Northern Tianshan plates (Allen et al., 1995; Carroll et al., 1995, Shao et al., 1999; Greene et al., 2005; Yang et al., 2010). The uppermost Carboniferous-Lower Triassic strata were interpreted to be deposited in a half graben on the basis of seismic interpretation in the nearby Turpan Basin and stratigraphic correlation by Yang et al., 2010.

The ancient Lucaogou lake in the Tarlong-Taodonggou area is interpreted as a half-graben lake, with northern Taodonggou and SW Tarlong at the ramp margin (Yang et al., 2008, 2010). It was mainly balanced-filled in a subhumid to semiarid climate condition (Yang et al., 2010). The Lucaogou LC overlies the upper Daheyan LC with a sharp erosional surface and underlies the Hongyanchi LC.

1.2. STRATIGRAPHY

The Carboniferous-Triassic chronostratigraphy in the greater Turpan-Junggar basin was poorly constrained and has been updated and improved by Yang et al., 2010 (Figure 1.2). The improvement is based on correlation of the previously-reported Permo-Triassic litho- and chronostratigraphy (Liao et al., 1987; Cheng et al., 1996; Zhou et al., 1997; Liu, 2000), zircon dating of volcanic ash layers, and calculation of average sedimentation rates.

Eight ages from five sample sites were obtained through zircon dating analyses. The average sedimentation rate is calculated by the age (301.26 Ma) of uppermost lower Daheyan, the age (281.42 Ma) at the surface ~ 38 m below the top of the Hongyanchi LC in NE Tarlong, and the thickness of the LCs in NE Tarlong section. The age of Lucaogou

LC is then calculated by the average sedimentation rate and thickness in NE Tarlong section to be between lower-middle Sakamarian and basal Artinskian (291-284 Ma).

1.3. LOWER LUCAOGOU CARBONATE-DOMINATED CLINOFORMS

Two clinoform packages in the study area occur in the lower part of Lucaogou LC. The lower clinoform package is carbonate-dominated, and the upper package deltaic. The lower clinoform package was deposited after a transgression on an alluvial-fan complex (Yang et al., 2008). The progradational platform is ~5 m thick, extending for ~200 m down dip to the north, and ~4 km laterally in an E-W strike direction. The carbonate-dominated clinoform package is composed of couplets of siliciclastic-rich and carbonate-rich clinoforms. Each couplet consists of one siliciclastic-rich clinoform and one carbonate rich clinoform, forming a clinoform high-order cycle. The couplets are 20-50 cm thick and have a maximum 15° dip angle to NE or NW (Figure 1.3). The carbonate-dominated clinoform package is sigmoidal, steepen progressively lakeward to the north. It is truncated and overlain by a 30-cm-thick sublittoral shale, upon which the upper deltaic clinoform package developed.

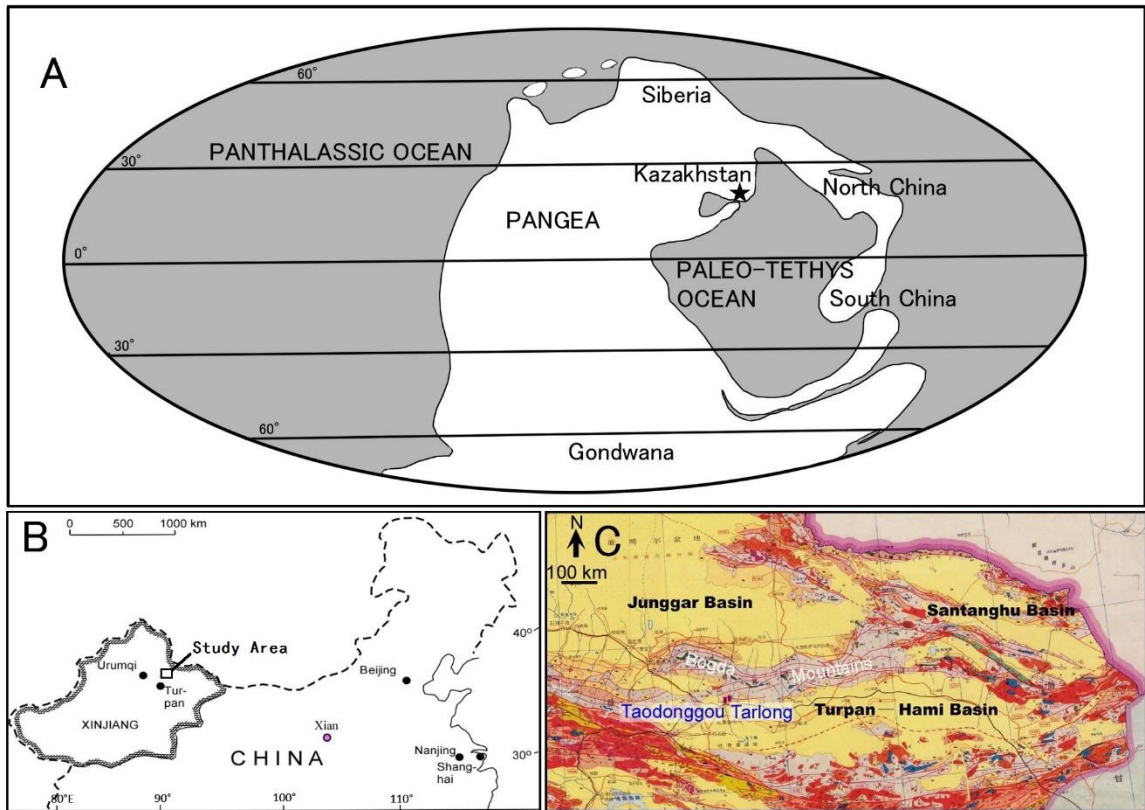


Figure 1.1. Location and global paleogeographic reconstruction and of the study area. (A) Global paleogeographic reconstruction for the early Permian. Modified from Scotese (1996). The location of the study area is marked with a star. (B) Location of the study area in Xinjiang Uygur Autonomous Region, NW China. (C) Geological map of eastern Xinjiang, showing locations of Tarlong-Taodonggou. Modified from XBGMR (1993).

System	Series	Stage	Lithostratigraphy (Formations)	Cyclostratigraphy	Improved chronostratigraphy		
				Low-Order Cycles	New dates* (from Yang et al, 2010)	Revised chronostratigraphy	
Triassic	Upper	Anisian 245.0	Karamay	Karamay		Anisian	
		Olenekian 249.7	Shaofanggou	Shaofanggou		Olenekian	
	Lower	Induan 251.0	Jiucaiyuan	Jiucaiyuan	251.0	Induan	
Permian	Upper	Lopingian	Changshingian 253.8	Guodikeng	Wutonggou	253.11 253.63	Changshingian
			Wuchiapingian 260.4	Wutonggou		254.22	Wuchiapingian
	Middle	Guadalupian	Capitanian 265.8	Quanzijie	Quanzijie		Capitanian
			Wordian 268.0	Hongyanchi	Hongyanchi	281.42	Wordian
			Roadian 270.6	Lucaogou	Lucaogou		Roadian
	Lower	Cisuralian	Kungurian	Daheyan	Upper Daheyan	295.5, 301.26	Kungurian
					Middle Daheyan		
					Lower Daheyan		
			Artinskian 284.4	Taoxigou Group		301.61, 300	Artinskian
			Sakamarian 294.6				Sakamarian
Asselian 299.0				Asselian			
Carboniferous		Gzhelian 303.9				Gzhelian	

Figure 1.2. Chrono-, litho-, and cyclostratigraphy of Permian–Triassic strata in the NE Tarlong and Taodonggou sections. Absolute ages at stage boundaries from Gradstein et al. (2004); lithostratigraphic and chronostratigraphy synthesized from Zhang (1981), Liao et al. (1987), Wartes et al. (2002), and Zhu et al. (2005). Hachured areas indicate missing strata. Wavy lines are major unconformities. Dashed lines indicate uncertain age correlations. Underlined numbers – dates from SHRIMP analysis; italic numbers – dates from $\text{Ar}^{40}/\text{Ar}^{39}$ analysis; plain numbers- dates from IDTIMS analysis. Modified from Yang et al (2010).



Figure 1.3. Dip section of the carbonate-dominated clinoform package. It shows an asymmetrical-symmetrical sigmoidal shape. The clinoforms steepen northward. Photo is tilted to make the clinoform package parallel to the horizontal. The white dashed line is the upper boundary of the clinoforms. Person is about 1.8 m tall.

2. METHOD AND DATA

Fieldwork and detailed petrographic studies were carried out to investigate the provenance and depositional mechanisms of the carbonate-dominated clinoform packages in the lower Lucaogou low-order cycle.

2.1. FIELD OBSERVATIONS

Field works was accomplished by Dr. Wan Yang and his colleagues in 2007 and 2008 (Yang et al., 2008, 2010). The author had inspected the outcrops in the summers of 2014 and 2015. Seven dip and strike stratigraphic sections were measured at a cm-dm scale in the Tarlong-Taodonggou half graben, including both of the lower carbonate-dominated and upper deltaic clinoform packages, five from NE Tarlong, one from SE Tarlong, and the other from Taodonggou, covering $\sim 4 \times 6 \text{ km}^2$ (Figure 2.1). Sections 1 to 4 in Figure 4 contain carbonate-dominated clinoform packages; and the other sections do not contain clear carbonate-dominated clinoform deposits. Lithology, sedimentary texture and structure, stratigraphic thickness, boundary relationship, and fossil content of each individual rock units were measured and described in the field. The data were used for preliminary interpretation of depositional environment, lake type, paleoclimate, tectonic setting, and stratigraphic correlation. The correlation was done by Yang et al. (2008; also see Yang et al., 2010). 80 samples were collected from the seven sections, and 38 of them were made for thin sections, including 30 for the carbonate-dominated clinoforms and 8 for the deltaic clinoforms. Detailed petrographic study was carried out using hand samples and thin sections.

2.2. MICROSCOPIC PETROGRAPHIC STUDY

Point counting method was used for a microscopic petrographic study. A two-dimensional 1 mm-spacing grid is used. Every grain, matrix, cement, or pore space, which falls at a grid point, is counted. In order to provide a sufficient accuracy of sampling, 350 points were counted for each thin section. The counted categories include grain, matrix, cement, and pore space; and for each main category, sub-categories were documented for statistics analysis of sedimentary texture. For each grain, composition,

size, shape, roundness, and contact relationship were recorded. For coated grains, such as ooid or oncoid, and aggregate grains or intraclasts with internal clasts, composition of nucleus or internal clasts was documented individually. In addition, if a grain is surrounded by a diagenetic rim, the shape of the rims was described and counted. All the information is used for further lithofacies and diagenesis studies. For matrix, its composition is recorded; and for pores space, size and pore type are recorded. Description of cement texture follows Folk's (1965) cement description principle, which includes mode, shape, crystal size, and foundation. Details of cement will be discussed in Section 3.3.

Overall thirty thin sections were observed under microscope and twenty-three of them were point counted, among which eighteen samples are from the dip section of the clinofolds that was sketched and described in detail by Dr. Wan Yang (Yang et al., 2008; Figure 2.2A, B). Other thin sections include three samples from Section 2 from strata below the foundation of carbonate-dominated clinofolds, and two from Section 3 above the carbonate clinofolds. There are 8 samples collected from one single clinofold bed. Not all the thin sections were point counted, because point counting is not effective for autochthonous organically-bounded limestones. Some siltstones and mudrocks were not counted because they are compositionally and texturally similar to other counted samples. Detailed locations of samples are shown in Appendix A, B, and C.

The point counting data were analyzed statistically to calculate the proportion of each category in the rock, and basic grain textural parameters including graphic mean size, sorting, and roundness. Size analysis was accomplished by using GRADISTAT Version 8.0, a software for grain size distribution and statistics analysis, developed by Dr. Simon. J. Blott (Blott and Pye 2001) from Kenneth Pye Associates Ltd. The software is based on formulae of Folk and Ward (1957). The graphic mean size is determined by

$$M_z = \frac{\phi_{16} + \phi_{50} + \phi_{84}}{3} \quad (2.1)$$

Where M_z is the graphic mean size of all framework grains, ϕ_{16} , ϕ_{50} and ϕ_{84} are the 16th, 50th, and 84th percentile grain size values on the cumulative curve, respectively.

Sorting is determined by the inclusive graphic standard deviation as:

$$\sigma_i = \frac{\phi_{84} - \phi_{16}}{4} + \frac{\phi_{95} - \phi_5}{6.6} \quad (2.2)$$

Where σ_i is inclusive graphic standard deviation, $\phi_5, \phi_{16}, \phi_{50}, \phi_{84}, \phi_{95}$ are the 5th, 16th, 50th, 84th, and 95th percentile values on the cumulative curve, respectively.

Most samples are mixed siliciclastic-carbonate rocks. Thus, for sandy grains in these samples, ternary diagrams from Dickinson (1985) were used for provenance interpretation. Fields in Dickinson's diagrams may not be all filled because some of component grain types are rare in mixed siliciclastic-carbonate rocks; and a small sample size would render the results unreliable. Ternary diagrams were plotted using software Triplot 4.1. Petrofacies classification follows Mount's (1985) first-order classification; and lithofacies follows Wright's (1992) revised version of Dunham's (1962) classification. For cement spars, proportions of spar size were used for diagenesis analysis, assuming the neomorphic type was aggrading, meaning that the cement spars are keeping enlarging their size during diagenesis. Detailed discussions are in Section 3. Abbreviated codes for a concise description of the counted components, are shown in Tables 2.1 and 2.2.

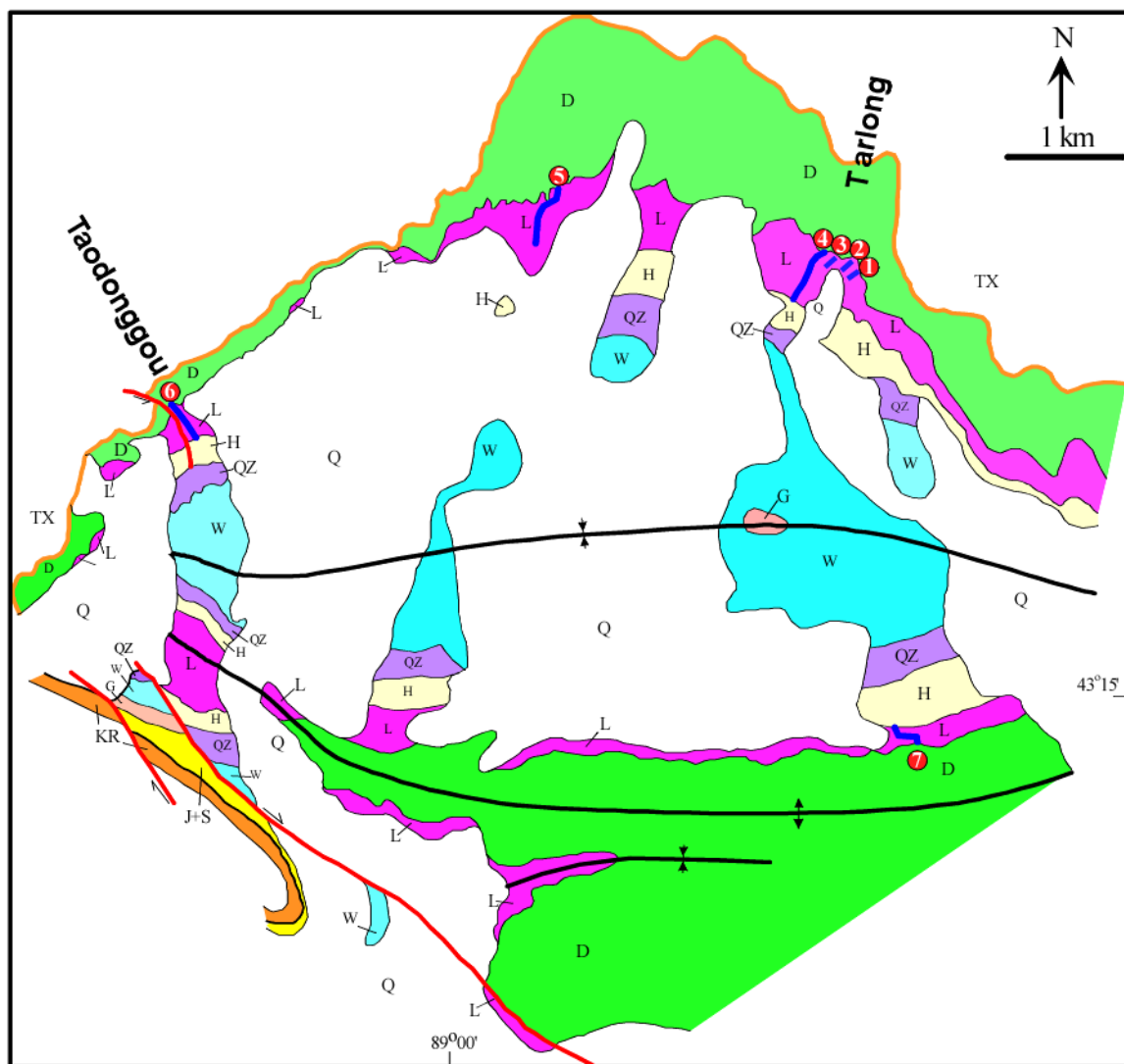


Figure 2.1. Geological map showing the Tarlong and Taodonggou sections and locations of measured sections. The Tarlong-Taodonggou area is located in a west-plunging syncline, where Permian to Lower Triassic rocks are superbly exposed. The Tarlong and Taodonggou sections were measured from 2004-2008. The measured sections are numbered as 1-7. Modified from Yang et al. (2007).



Figure 2.2. A close look and sketch of the carbonate-dominated clinoform package. (A). A close look of the carbonate-dominated clinoform package in Section 2. The package is located on a flat foundation, dipping to the northeast-northwest direction. Overall thickness is 524cm. Red hammer is 24 cm long. (B). A sketch of outcrop in (A), showing the couplet of carbonate-rich and siliciclastic-rich clinoforms. Beds with a brick pattern are the carbonate-rich clinoforms; white beds siliciclastic-rich clinoforms. Beds with circled numbers have field observations, shown in Appendix A. Photo and sketch were done by Dr. Wan Yang in 2007.

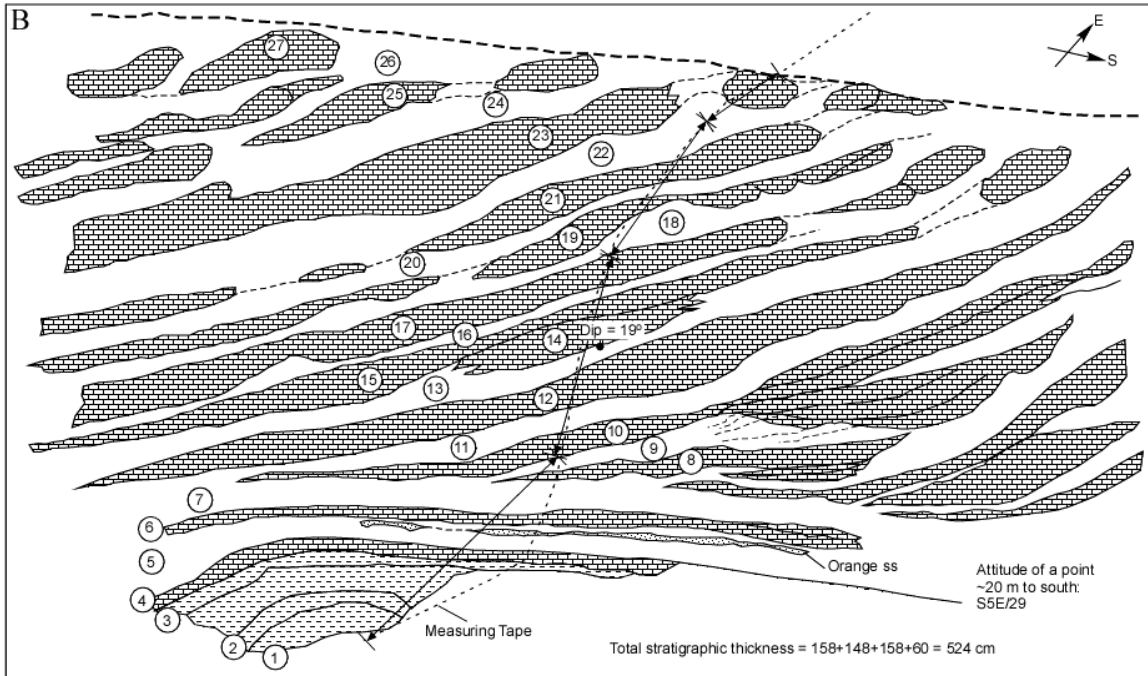


Figure 2.2. A close look and sketch of the carbonate-dominated clinofom package. (A). A close look of the carbonate-dominated clinofom package in Section 2. The package is located on a flat foundation, dipping to the northeast-northwest direction. Overall thickness is 524cm. Red hammer is 24 cm long. (B). A sketch of outcrop in (A), showing the couplet of carbonate-rich and siliciclastic-rich clinofoms. Beds with a brick pattern are the carbonate-rich clinofoms; white beds siliciclastic-rich clinofoms. Beds with circled numbers have field observations, shown in Appendix A. Photo and sketch were done by Dr. Wan Yang in 2007. (Cont.).

Table 2.1. Symbols and definitions of compositional attributes documented in point counting of this study

Symbol	Definition
G	Grain
M	Matrix
C	Cement
P	Pore-space
Qm	Monocrystalline quartz
Qp	Polycrystalline quartz
K	Potassium feldspar
P	Plagioclase feldspar
Lvt	Volcanic lithic with trachytic texture
Lvm	Volcanic lithic with microlitic texture
Lvl	Volcanic lithic with lathwork texture
Lvf	Volcanic lithic with felsitic texture
Lvv	Volcanic lithic with vitric texture
AM	Accessory minerals
Lsm	Mudrock lithic and mud clasts
Lsc	Chert
Lss	Shale and siltstone lithics
Lund	Undifferentiated detrital grain
Lci	Intraclast
Lca	Aggregate grain
Lco	Ooid
Lcon	Oncoid
Lcpi	Pisoid
Lcp	Peloid
Lcb	Bioclast
Cr	Completely replaced unknown grain
Mc	Micrite as matrix
Cc	Sparry calcite as cement

Table 2.2. Calculated derivative attributes used in statistical analysis of point-counting data

Symbol	Definition
$F=K+P$	Total feldspar grain
$L_v=L_{vt}+L_{vm}+L_{vl}+L_{vv}+L_{vf}$	Total volcanic lithic grains
$L_s=L_{sm}+L_{ss}+L_{sc}$	Total detrital sedimentary grains
$S=L_s+L_v+Q_m+Q_p+F+L_{ud}+AM$	Total siliciclastic detrital grain
$A=L_{ci}+L_{ca}+L_{co}+L_{con}+L_{cpi}+L_{cp}+L_{cb}$	Total carbonate allochems
$M_i=M_c+C_c$	Assumed total micrite

3. PETROGRAPHY OF THE CLINOFORM PACKAGE

Twenty-three samples vary in composition, texture, sedimentary structure, diagenetic products, fossil content, and stratigraphic features. They are divided into four major lithofacies and seven subfacies on the basis of characteristics above. The clinoform beds are basically composed of carbonate-dominated and sand-dominated mixed siliciclastic-carbonate lithofacies; and lateral facies change along a single clinoform bed occurs between toe to middle slope and middle to upper slope.

3.1. GRAINS

Grains in the clinoform packages can be divided into non-carbonate and carbonate grains based on their composition. Non-carbonate grains include discrete monomineralic grains of quartz, feldspar, and accessory mineral grains, lithics of a volcanic or sedimentary origin, and undifferentiated detrital grains that show some detrital characteristics but are too altered to be identified for their original composition. Carbonate grains include intraclast, aggregate grain, coated grains of ooid, oncoid, and pisoid, peloid, and bioclast. Finally, some grains are completely replaced by sparry calcite or have only minimal original features and, thus, are counted as completely replaced clasts. They are grouped into a separate grain type that is not counted as carbonate or non-carbonate grains. The detailed statistic results are shown in Tables 3.1 and 3.2

3.1.1. Non-Carbonate Grain (S). Non-carbonate grain is widespread, varies in composition, size, roundness, and sorting. They are more abundant than the carbonate grains in most lithofacies.

3.1.1.1. Monocrystalline quartz (Qm). Monocrystalline quartz is not common in the studied samples, accounting for only 0.46% in occurrence. Most Qm grains are subhedral in a crude hexagonal shape with straight edges but showing no overgrowth evidence, subrounded to angular, and poorly to non-undulatory. Generally they are medium to coarse sand-sized, but in samples S7-17 and S7-35, they are very-fine to fine sand-sized. Monocrystalline quartz grains are interpreted as derived from a volcanic origin, for their shape and undulatory type (Folk, 1980).

3.1.1.2. Polycrystalline quartz (Qp). Polycrystalline quartz grains are mostly composed of interlocking aggregate quartz crystals to form a mosaic, which have straight to slightly undulose extinction. They are rare interpreted as derived from a possible metamorphic source (Folk, 1980).

3.1.1.3. Potassium feldspar (K). Potassium feldspar grains are rare, at only 0.06%. They are subangular to angular and mostly do not have twinning. They are commonly fresh with limited alteration and some are partially replaced by calcite along the edge or internally. They are identified by typical cleavages and lower blueish grey birefringence. The K-feldspars may have been derived from either volcanic or metamorphic source rocks (Folk, 1980).

3.1.1.4. Plagioclase (P). Plagioclase grains are mostly subhedral, subangular to angular, with distinctive albite twinning (Figure 3.1A) and oscillatory or progressive zoning in some coarse grains. It is moderately common, accounting for 1.9% in total occurrence and 8% in non-carbonate grains. Plagioclase grains occur in all petrofacies, and are mostly coarse- to medium-sand-sized in the clinofom package. A few grains contain mineral inclusions. Most of the grains are somewhat altered to clay or replaced by micro- and pseudo-calcite spars. Similar to K-feldspar grains, the origin of plagioclase grains is difficult to interpret due to the limited abundance.

3.1.1.5. Volcanic lithics (Lv). Volcanic lithic is abundant in all samples, which can account for up to 40.9% in total grain content and 56% in non-carbonate content. They are mainly subangular to subrounded, fine-very fine sand to granule-fine pebble in size depending on the petrofacies, but mostly medium to coarse sand in size in the clinofom body. The absence of quartz phenocrysts indicates an andesitic or basaltic origin. The black groundmass suggests basaltic and light gray groundmass andesitic; but to differentiate the two clearly is difficult. No amphibole or pyroxene phenocrysts are observed. Lv grains are mostly altered through micritization and argillization. Hence, they are differentiated on the basis of absence of quartz and presence of phenocryst plagioclase laths. Finally, the Lv grains show a variety of microlitic, lathwork, trachytic, vitric, and felsitic texture, classified by Dickinson's principle (Dickinson, 1970) with slight modifications. Specifically, the trachytic texture (Figure 3.1B) is distinguished

from the microlitic texture because the subparallel to parallel arrangement of the phenocryst plagioclase laths in trachytic texture suggests a possible intermediate origin.

3.1.1.6. Sedimentary lithics (Ls). Non-carbonate sedimentary lithics are divided into mud clast, shale clast, and detrital chert. They account for 12.4% of all the lithics. No sandstone lithics were seen. Mudrock lithics, that is, mud and shale clasts, are the most abundant, accounting for 2.4% of the total volume. Some mudrock lithics are organic rich (Figure 3.1C), and/or have faint laminations, and are counted as shale clast. Ls grains are mostly subangular to angular, few rounded, indicating an either in-situ rip-up or extra-basinal origin. Chert grains are mainly microgranular with microcrystalline quartz crystals and, in some cases, chalcedony. Detrital chert grains are not very common. However, microcrystalline quartz may have partially altered some grains of other types. The chertified grains are differentiated from detrital chert grains. The detrital chert grains are common and vary in size and shape.

3.1.1.7. Accessory minerals (AM). Accessory mineral grains are rare, accounting for only 0.25% of the total occurrence. They include zircon, glauconite, zeolite, and some hydrothermal altered grains. Their grain size and shape vary. AM grains are mostly found in the clinofom packages or sandy part of the foundation. They are not used for provenance interpretation because of their insufficient quantity.

3.1.1.8. Undifferentiated detrital grain (Lund). Undifferentiated detrital grains account for 11.6% of total grain content. They vary in grain size and shape in different petrofacies. Most of them are highly micritized or replaced by sparry calcite, but still reserve enough original features, such as molds of phenocryst plagioclase lath and relict aphanitic or clayey patches, to be identified as detrital, . Caution was exerted to avoid overinterpretation of the original grain type of these highly altered grains.

3.1.2. Carbonate Grain (A). Carbonate grains are common in all samples. Some grain types with a microbial origin are limited to specific lithofacies. For clinofom packages, intraclast, aggregate grain, and peloid are the dominant.

3.1.2.1 Intraclast (Lci). Intraclasts are common in the body of clinofom packages, mostly subangular to angular, and medium to coarse sand-sized on average. They generally contain more organic matter and clays than the matrix, resulting in a relatively darker or browner color. In some cases, radial fibrous or bladed sparry calcite

encrusts along the grain surface to separate the intraclasts from the matrix. Many intraclasts contain one or more grains (Figure 3.1D), which can be either non-carbonate or carbonate, or the combination of both. These grains are generally fine sand-sized and commonly have a thin diagenetic calcitic rim (Figure 3.1E), oolitic coat, or microbial coat. Medium sand-sized grains are present but less abundant, and are mostly detrital clasts. For completely micritic intraclasts without internal grains, compaction-induced deformations are common. As a result, some of them show thin fractures filled by calcite spars.

3.1.2.2 Aggregate grain (Lca). Aggregate grains are mostly subrounded to subangular, with moderately lobate outlines. Some are botryoidal, with one or more thin cortices; and the others show wiggly and muddy to sparry microbial laminations or envelopes. The average size is medium to coarse sand, but varies depending on the number of bounded internal grains. The internal grains are bounded by sparry calcite cement or a combination of sparry calcite and organic-rich micrite. They have various types, such as volcanic lithics, plagioclase grains, and peloids. Volcanic lithics commonly are larger than the other types. For grains of the same type, the bounded ones in an aggregate grain tend to be smaller than the unbounded ones. This is especially true for non-carbonate grains, such as volcanic lithics and plagioclase grains. Many aggregate grains are broken, or have incomplete outlines (Figure 3.1F), suggesting “rip-up” processes that tore original bounded sediments apart. The micritic components in an aggregate grain, if present, are relatively darker than the surrounding micrite matrix, indicating that the original sediments may have been bound by microbial mats before being ripped up.

3.1.2.3 Ooids (Lco). Ooids are not abundant in the clinof orm package, relative more in the clinof orm body but less in the sandy foundation. They are rare in beds rich with microbial structures. Most ooids are radial-concentric, with or without dark organic-rich micrite laminae in cortices. Cortices are composed of needle to equant shape calcite (Figure 3.2A). Ooids cortices can be generally separated into clean type and organic rich type. Some ooids have rare or no micrite in their cortices. Those ooids are fine to coarse sand sized, commonly medium sand-sized, and contain superficial or multiple coats of two to three laminae and seldom more than four. Individual cortices have a relatively

even thickness, but differ from adjacent ones. They are mostly 5-20 μm thick, up to 30 μm and, in some extreme cases, up to 70 μm . In ooids with both sparry calcitic “clean” laminae and organic-rich “dirty” laminae in cortices, the boundary between the clean and dirty laminae are fuzzy and diffuse and, in some cases, wiggly and digitate. The clean laminae are radial or tangential, the former more common. The thickness of dirty laminae is commonly 20-50 μm and, rarely, up to 100-200 μm . In general, the light laminae have a relatively uniform thickness, whereas the micritic laminae have highly variable thickness.

The nuclei of ooids are either carbonate or non-carbonate grains, commonly volcanic lithics. Nuclei in some ooids with sparry cortices are completely replaced by sparry calcite, which may have been caused by in-situ calcitization so that only the properties of original wall structures are preserved (e.g., Richter, 1983), or dissolved to form a mold and was later filled by sparry cement. The calcitized nucleus usually keep the shape and contacting cortices better than the dissolved ones. Generally, ooids with clean cortices occur in neomorphism-rich part of the clinofom packages. In addition, very few oolitic grains are coated by non-carbonate minerals, such as possible phosphate or clay minerals. Finally, many ooids are incomplete (Figure 3.2B) with broken or partially dissolved cortices with, in some cases, only a half of the grain or a small piece of cortices preserved. This indicates that these ooids were transported away from their original depositional site and had experienced severe abrasion during transport.

3.1.2.4 Oncoid (Lcon). Oncoid grains occur only where microbial structures were well developed, such as in boundstone. Encrusting algal laminae have variable thickness and are commonly superficial. Nuclei are detrital grains which are mostly volcanic lithics, coarse to medium sand-sized, and mostly subangular to subrounded. Close to the toe of clinofoms many oncoids are highly chertified, indicating a silicification event during diagenesis.

3.1.2.5. Pisoid (Lcpi). Pisoids are only observed in the thrombotic bed directly underneath the clinofoms deposit. They are rounded to subrounded and have one or more concentric carbonate cortices. The cortices commonly are composed of finely crystalline laminae of a relatively uniform thickness. Nuclei are commonly thrombotic lumps and peloids, in some cases, detrital grains, or large pieces of aggregated algal mats.

In many cases, one pisoids contain multiple small ones, forming a compound grain. Cortices of the pisoids are smooth and complete, indicating an in-situ growing process.

3.1.2.6. Peloid (Lcp). Peloids are common in all petrofacies. They occur as grains or nuclei and are composed of micrite and micro- or cryptocrystalline carbonate sediments. Grain size is generally relatively smaller than other types of grains, especially detrital grains. Peloids have variable shapes but mostly subrounded to subangular. Fecal pellets, regarded as a special type of peloids in this study, can be identified from their small size and rod-like shape. Other non-differentiated peloids are either reworked micrite clasts, referred as mud peloid by Flügel (2010), in various shape and size, or altered grains as pelletoids of Flügel (2010), which are highly recrystallized and have diffuse outlines.

3.1.2.7. Bioclast (Lcb). Bioclasts are uncommon in thin sections but common in some outcrops. They are shell fragment, gastropods, ostracods, or calcified microbial clasts with a growth structure (Figure 3.2C). They are variously shaped and sized, depending on types of species and degree of abrasion and fragmentation.

3.1.3. Completely Sparry Calcite-Replaced Grains (Cr). Completely sparry calcite-replaced grains are present in all petrofacies, indicating severe diagenesis. They commonly have a similar size to the other grains in the same sample, and an equant shape. Some are apparently being filled by single or aggregated clean calcite spars in cavities formed by dissolution. The others were formed by sparry calcite replacing the original grain. In this case, few relict features of the original grain along the boundary (Figure 3.2D) or in the center may be preserved, but are not useful in identifying the original grain type. They are counted to reflect the grain content, but are not used for provenance interpretation and petrofacies classification.

3.2. MATRIX

Matrix grains are classified as those smaller than 0.0625 mm in siliciclastic rocks. They are classified as those between 1.25 to 2 μm by Folk (1965) and up to 4-7 μm (Folk 1962) in carbonate rocks. In the clinoforn packages, the carbonate matrix is commonly neomorphosed into micro and pseudo-spars. In this study, matrix also includes aphanocrystalline and very fine crystalline microspars that are less than 16 μm in size

(Folk, 1959) for easier point counting under a light microscope. This modification is also applied by Mount (1985) in his classification of mixed siliciclastic and carbonate sediments.

Micrite is the dominant matrix type of clinoform deposits (Figure 3.2E). It is commonly variably grey, depending on degree of recrystallization and amount of organic matter and/or clay. Micrite matrix becomes relatively darker grey in rocks close to the foundation and in the toe slope of clinoform package, probably due to increasing organic matter related to microbial activities. It is relatively lighter in middle to upper parts of the clinoform, due to the presence of abundant microspars (Figure 3.2F). The matrix content ranges from 67 to 14%, and decreases significantly in samples with a high degree of recrystallization and/or precipitation of diagenetic spars.

Other types of matrix also occur but are rare. Some matrix contain patches of microscopic rhombohedral crystals interpreted as dolomite, indicating dolomitization. Clay and organic matter is commonly mixed with micrite to form thin muddy laminae, such as thin calcareous shale partings at the toe slope. In addition, siliciclastic matrix occurs in the lowermost part of the clinoform foundation rocks as a mixture of clay mineral, micrite, calcite spars, and fine to very fine sand-sized detrital grains and form thin, interlaminated mudstone and very fine sandstone.

3.3. CEMENT

Folk (1965) summarized four basic ways in which authigenic calcite form: (a) by direct precipitation into a cavity, (b) by displacive or aggressive precipitation, (c) by neomorphism of previous calcite or aragonite, and (d) by replacement of other non- CaCO_3 minerals, and gave four codes as P, D, N, and R to reflect each mode of formation, respectively. However, due to the severe diagenesis in the samples, most of the primary depositional textures were overprinted, making it difficult to differentiate ordinary pore-filling cement (P) from the other types. As suggested, diagenetic textures must be identified beforehand to sample correctly for isotope analyses (Kelts and Talbot, 1990; Talbot and Kelts, 1990) and for interpretations of facies and their alteration through time. On the basis of lack of geochemical study, for a compromise, cement here includes all kinds of authigenic calcite spar except for identifiable grain replacements. For

simplified measurement of crystal size, very finely crystalline and aphanocrystalline crystals (<16 μm) were counted as micrite.

Cement spars account for about 27% in total volume. They are mostly equant, and have various types with the radiaxial fibrous, dripstone, granular, and blocky types as the most common. Content, size, and shape of the cement spars can vary greatly based on the severity of diagenesis the rock experienced. For instance, samples from middle to toe slope contain up to 45% of cement spars; and many grains are coated by sparry calcite rims. In comparison, cement spars only account for about 5% and there are few to no rims on the grain surface in sand-rich rocks from the foundation. In addition, cement spars are commonly coarse to very coarse in the middle to tow slope, and occur as isopachous sparry calcite rims and are fibrous to bladed shaped. In contrast, cement spars are commonly circumgranular and medium to fine sand-sized in the middle to upper slope, thinner than the isopachous rims, and are equant to bladed in shape. The preferential occurrence of cement spars of different size and shape along a clinof orm indicate varying degrees of diagenesis, such as aggrading neomorphism.

3.4. DIAGENESIS

The clinof orm deposits have been greatly altered by complex, multi-episode diagenetic processes, as indicated by abundant sparry calcite and common diagenetic structures, such as stylolites or seams suggest that. Early diagenesis is suggested by lithified algal mats in samples rich in microbial structures, which formed micritic micropeloidal structures associated with microsparite and sparite cements. The main process is probably microbial precipitation (e.g., Dupraz et al., 2004).

Neomorphic recrystallization and replacement are the most common processes. Folk (1965) defined neomorphism as a process that original crystals are consumed, and their place is simultaneously occupied by new crystals of the same mineral or by a polymorph. Metastable carbonate mud experiences coalescive transformation, aggrading to micrite and later to larger micro- to pseudospars. Hence, the content and size of cement spars reflect the degree of diagenesis if neomorphism is an aggrading type. Point counting data (Table 3.3) of samples from a single clinof orm (samples S7-26A-H) indicate that the rocks in toe to mid-lower slope seems to experience more diagenesis

than those in the mid-upper clinoform, as reflected in a trend of reduced spar content and an overall increase in micrite content from upper part to the toe. The uppermost part of the slope shows a reduction in cement content, which may be caused by a separate episode of diagenesis. However, an opposite trend developed in another single clinoform package (samples S7-24U and L). Samples in the lower clinoform have a similar amount of cement spars as in the previous clinoform. However, samples from the upper clinoform contain much more cement spars, slightly more than 60%. This indicates that diagenetic process varied laterally from clinoform to clinoform.

Secondary compaction structures indicate that the studied rocks had experienced burial processes, although it is suggested that deep burial diagenesis is not intense in carbonates deposited in continental basins (Tucker and Wright, 1990). Seams and stylolites, although not abundant, occur in many samples. Some samples contain fractures and dissolution pipes filled by late sparry calcite or micrite. At the toe part of the clinoforms, thin layers of calcareous shale were brecciated and disturbed by cone-in-cone structures (Figure 3.3A), which displacive cementation, shoving aside the surrounding materials (Folk 1965). Such displacive cements might contribute to some of the fibrous sparry rims as well. Many rims in the clinoform rocks show clear directional growth patterns. The patterns differ from dripstones in vadose zone to show a pendant structure, but are common growth vertically in two opposite directions and, thus, were probably formed during burial diagenesis. In addition, abundant coarse to very coarse calcite spars themselves show deformation and breakage, and even slightly undulatory extinction, which likely formed by physical and/or chemical processes of compaction, mechanical deformation, and crystallization during burial.

Silicification of carbonate minerals also occurred during burial. Silicifying fluids permeated almost the entire area close to the toe slope and uppermost foundation of the clinoforms (S7-23; Figure 3.3B, C), resulting in pervasive chertification. Bustillo et al. (2002) suggest that such process will selectively silicify stromatolites, oncolites, and other microbial carbonates, leaving behind ghost minerals and/or structures of primary carbonates. Common sources for the silica are redistributed biogenic silica, such as diatoms (e.g., Denys et al. 1998), but diatoms were not present in Permian. The silica, hence, might be originated from less common sources, such as detrital siliceous and

silicate minerals and lithics (e.g., Peterson and Von der Borch, 1965), which are common in the samples. Much silification of continental carbonates is associated with the upper regressive sequences, which were deposited in shallow lake to palustrine settings, and where water-level fluctuations caused emergence of the carbonate sediments (Bustillo et al., 2002).

Meteoric fabrics like circumgranular rims and epitaxial spars are present, but mostly have mixed with or masked by neomorphic pseudospars, making them hard to be differentiated. Many of the completely replaced grains could have formed by meteoric dissolution-precipitation; and some of the clean spars may have a meteoric origin as well. The sample beneath the clinoform foundation (S7-3; Figure 3.3D) has vesicular structures that could formed by meteoric dissolution. They are filled by clean secondary calcite spars that indicate burial dissolution and reprecipitation (e.g., Arp, 1995).

Diagenetic fabrics in the clinoforms could not be formed only neomorphic recrystallization, but multi-episode diagenesis, such as neomorphism, meteoric dissolution-precipitation, and some other unknown processes. The fabrics vary in structure, origin, and location in clinoforms. Detailed geochemical studies are needed to better understand the processes.

3.5. PETROFACIES

Petrofacies study is accomplished using point counting statistics and observations. Only non-biogenic samples are used in petrofacies analysis here; and other samples will be discussed in the next part.

Rocks in the clinoform packages are mainly mixed siliciclastic-carbonated types, especially in the body and some non-biogenic foundation parts. Though carbonate constituents are dominant in most of these mixed rocks, it is still suggested that carbonate rocks containing between 10 and 50% of terrigenous admixtures be distinguished in nomenclature from pure carbonate (Flügel, 2010). Mount (1985) suggests that sediments containing more than 10 volume% of the antithetic component should be considered as mixed. Previous classification has been discussed and proposed by Pettijohn (1975), Folk (1969), Zuffa (1980), and Mount (1985). Zuffa synthesized works from Pettijohn and Folk to give a three-dimensional classification of mixed-composition rocks for

quantitative analysis, based on the content of intra- and extra-basinal noncarbonated and carbonate grains. However, the author's observations of the studied samples and Mount's (1985) discussion suggest that Zuffa's classification aims mainly for arenites and ignores the implication of the matrix and cement and, thus is not adequate for classification of the studied samples. In addition, differentiation between intra- and extra-basinal grains, especially carbonate grains, is difficult. Therefore, Zuffa's classification scheme is not used in the study of petrofacies here.

On the other hand, Mount's (1985) first-order descriptive classification uses two components: (1) Siliciclastic component including siliciclastic sand (S) and non-carbonate mud (Mu), and (2) carbonate components including allochems (A) and micrite (Mi). It is mainly intended for descriptive purposes and the general classification of mixed sediments. He specifically mentioned that this classification does not include any genetic interpretation because of differences in nature of the siliciclastic and carbonate sediments, which makes it unequal in determination of their compositional and textural maturity. Mount's classification is useful to this study. Prefixes and adjectives may be added to the rock names to include more information of the rocks, if needed.

One obstacle to the application of Mount's classification is the pervasive diagenetic alteration and products in the Lucaogou samples, which obscure the identification of both siliciclastic and carbonate component. Carbonate components, owing to their metastable chemical composition, should be affected more than the siliciclastic grains, mainly through aggrading neomorphism of micrite to pseudo-spars and dissolution of carbonate grains. To compensate the effect of neomorphism, it is assumed that all cement spars are derived from recrystallized micrite, that is, all cement spars are pseudo spars. This assumption will definitely cause bias because cement spars can also form by passive precipitation in pore spaces, dissolution-precipitation by meteoric processes, alteration of carbonate or siliciclastic grains, or even transportation from another sources as a carbonate grain. But the author's observations indicate the assumption is reasonable in most cases in this study and, thus, for samples that had not experienced extreme diagenesis, the assumption may not cause great deviation from the reality. However, some samples had experienced extreme diagenesis, such as samples S7-26U and S7-38, that more than 50% of the volume has been altered to sparry calcite. In

these cases, the assumption may cause a major bias. Hence, extremely-altered samples will not be used in petrofacies classification.

Three petrofacies are identified from 12 samples based on their S, A, Mi compositions (Figure 3.5). Petrofacies A of a mean composition of $S_{29}A_{11}Mi_{60}$ is the main type of the clinofom rocks and some foundation rocks. Petrofacies B ($S_{60}A_{15}Mi_{21}$) occurs in the sand-rich clinofoms. Petrofacies C ($S_8A_3Mi_{89}$) occurs only in the foundation rocks in the lowermost part, bordering the lower non-clinofom deposit. These petrofacies differ mainly in grain composition and texture. Petrofacies A contains more carbonate components and rich in micritic content, whereas Petrofacies B contains more siliciclastic grains. Petrofacies B is a micritic sandstone, which is dominated by siliciclastic grains and have similar amount of micrite and allochems. Petrofacies C is strongly micrite dominated with few sand-sized grains, mostly siliciclastic.

3.5.1. Petrofacies A. Petrofacies A is characterized by a high content of micrite and siliciclastic sand. The micrite is dominant; and siliciclastic grains are more than carbonate grains with an average S:A ratio of 5:2. For detrital grains, lithics, especially the volcanic lithics, dominate at 55%. Feldspars only accounts for 11% and are mainly plagioclase. Quartz grains are rare at 0.6%. The carbonate grains include mainly intraclasts, aggregate grains, and peloids, which account for 79% of the volume of carbonate clasts on average.

3.5.2. Petrofacies B. Petrofacies B is dominated by detrital grains. It has a much higher grain content (78.3%) than the other two petrofacies. The ratio between siliciclastic and carbonate components is about 5:3; and the S/A ratio is 9:2. For detrital grains, similar to Petrofacies A, the volcanic lithics are dominant, accounting for 56% of the siliciclastic component. For carbonate component, carbonate grains have a similar volume to micrite (A:Mi = 5:7); and peloid is the main grain type, accounting for ~56% of the carbonate grains. This petrofacies had experienced less diagenetic alteration than Petrofacies A that only 4.8% of the volume is occupied by cement spars.

3.5.3. Petrofacies C. Petrofacies C is characterized by the highest micrite content, accounting for 89% of the total SAMi composition. Grain content is only 11.7%, 85.8% of which are siliciclastic grains, 6.3% carbonate grains, and the rest completely replaced grains. Lithics dominate in siliciclastic grains at 74%, with sedimentary mud clasts more

than volcanic lithics with a Ls:Lv ratio of 3:2. Carbonate grains are bioclasts and peloids. No high-energy intraclasts and aggregate grains are present.

3.6. LITHOFACIES AND THEIR DEPOSITIONAL ENVIRONMENTS

Lithofacies were identified based on grain composition, texture, fossil content, sedimentary structures, and stratigraphic evidence including stratigraphic thickness and geometry, grain size trend, and stacking pattern. Overall four major lithofacies were identified, and each of which is subdivided into subfacies on the basis of facies component listed above.

Nonmarine carbonates are characterized by their own kinds of particles and fabrics (Arp, 1995). Lacustrine limestone, owing to common biogenic effects and terrestrial influence, may not be well classified using Folk's (1959, 1962) scheme, which emphasizes on hydrodynamic conditions. In contrast, Dunham's (1962) classification, expanded by Embry and Klovan (1972), is established by assuming that the fabrics are determined by hydromechanical or biogenic conditions (Dunham, 1962; Tucker & Wright, 1990; Arp, 1995). Wright (1992) revised this classification by adding diagenetic alterations of depositional fabrics, which is more suited for some of the highly diagenetically-influenced rocks in the clinofom packages. In this study, Wright's modified Dunham classification is heavily used.

As discussed previously, Mount's classification ignores the cement and grain contacts. For a better delineation of diagenetic and grain relationship, the author prefers Wright's revised version to classify lithofacies, aided by Mount's classification on petrofacies. The comprehensive lithofacies descriptions and depositional environment interpretation are shown in Table 3.4.

3.6.1. Mixed Siliciclastic-Carbonate Lithofacies. Mixed siliciclastic-carbonate lithofacies is characterized by a mixed composition of siliciclastic and carbonate grains and matrix. It is non-biogenic. Sediments containing more than 10 volume% of the authigenic component is defined as mixed (Mount 1985). The mixed siliciclastic-carbonate lithofacies can be subdivided into carbonate component dominated and siliciclastic component dominated. Grains are mostly both texturally and compositionally immature, medium to coarse sand sized, moderately sorted. All units have a sharp top,

and well current laminated, without obvious biogenic and bioturbation structures. They are interpreted as being deposited in a high energy littoral to lake plain environment on the basis of their composition, grain texture, and sedimentary structure.

3.6.1.1. Diagenetic lithic packstone and wackestone subfacies. Diagenetic lithic packstone and wackestone is a major facies of the clinoform package, composed of both siliciclastic and carbonate components. It correlates to Petrofacies A as sandy micrite from Mount's classification. Grain content averages 43% of the total volume; and the average ratio between siliciclastic and carbonate grains is 5:2. Siliciclastic grains are compositionally and texturally immature, and dominated by lithics, especially basic to intermediate volcanic lithics, coarse sand-sized in the clinoform body and medium sand-sized in the foundation, moderately sorted, and subangular to subrounded. Carbonate grains are dominantly blackened peloids, intraclasts, and aggregate grains, with minor ooids and few bioclasts, fine to coarse sand sized and mostly coarse sand sized, moderately well to moderately poor sorted, commonly more poorly sorted than siliciclastic grains in the same sample, and mainly subrounded to subangular. Matrix is dominantly micrite, admixed with little clay and organic matter. This subfacies is commonly strongly altered, containing 2.3-47.8% of sparry calcite. It is commonly single to double layered and current laminated. It commonly overlies a peloidal sandstone clinoform to form a couplet with a sharp top, termed as clinoform high-order cycles (Yang et al., 2008). The abundance of coarse blackened peloids, rip-up intraclasts and aggregate grains, and detrital lithics, and common current laminations suggest that the subfacies were deposited in a high energy environment, such as littoral and beach.

3.6.1.2. Micritic lithic sandstone subfacies. This lithofacies is characterized by the abundance of detrital grains and minor carbonate components (Figure 3.3E). It correlates with to Petrofacies B, as micritic sandstone, as indicated by observations of only one thin section. Field and microscopic observations indicate that the subfacies is grain supported, subarenaceous, and angular to subrounded, moderately sorted. The grains are mainly medium to fine detrital lithic sand where close to the toe, and medium to coarse or even fine lithic pebbles in the main clinoform body. Carbonate grains are mainly blacken peloids, some ooids and bioclasts, and few intraclasts and aggregate grains. They are fine sand-sized and moderately sorted. The reduced amount of intraclasts

and aggregate grains cause the overall grain size of carbonate grains to be finer than those in the packstone and wackestone subfacies. Current laminations are abundant; some parts lenticular; and the lower part has symmetrical ripples. This subfacies constitutes the sandy clinoform of the clinoform high-order cycles. The abundance of lithics and current lamination indicates a high energy littoral to beach environment, similar to that of packstone and wackestone subfacies. But the limited amount of carbonate components indicates different controlling factors from those of packstone and wackestone facies.

3.6.2. Microbial Carbonate Lithofacies. Microbial carbonate lithofacies is common and contains microbially-induced sedimentary structures (cf. Noffke et al., 2001). They are dark gray, organic rich, and contain bound grains of various types and sizes. They are subdivided into two subfacies on the basis of microbial structures.

3.6.2.1. Boundstone subfacies. This lithofacies is characterized by abundant planar or domal non-skeletal microbially-induced sedimentary structures, such as stromatolite (Figure 3.3F) and bound grains. It is dominated by dark organic-rich micrite, with early microbial precipitated sparry calcite and bound grains. The amount of bound grains varies from 13-36% and lower to 13%. The trapped grains are detrital or carbonate, mostly medium to fine sand sized, and up to very coarse sand sized if grains are oncoids. In some samples granule to pebble-sized volcanic lithics are present. These lithics are vertical oriented and break some of the algal layers, interpreted as dropstone (Figure 3.4A, B). Trapped detrital grains are dominantly volcanic lithics; and carbonate grains dominantly oncoids or peloids. Intraclasts and aggregate grains are rare. Grains are moderately to moderately poor sorted, angular to subrounded. This subfacies is knobby on the outcrop, showing growth structures and occur in both clinoform and foundation rocks. The subfacies is interpreted as being deposited in the shallow littoral zone. Oncoids near the toe indicate a water depth deeper than the normal wavebase, where agitation is minimal.

3.6.2.2. Thrombolitic microbialite subfacies. Thrombolitic microbialite is identified by its biogenic composition and texture, which is mainly composed of organic rich, small spherical micritic thrombolitic mats gluing together. These mats are peloidal, very fine to fine sand sized. Less than 5% detrital grains are trapped. They are mostly chert or highly altered detrital grains, fine to very fine sand sized, moderately to poorly

sorted. This subfacies occurs in the beds underneath the clinoform foundation, ~5m beneath the clinoform package. Burrows contain soft sediment fills. Pedogenic pisoids and meteoric dissolution networks with later sparry calcite filling develop within the subfacies, indicating subaerial exposure. The depositional environment is interpreted as supralittoral lake plain.

3.6.3. Mudrock Lithofacies. Mudrock lithofacies can be subdivided into three subfacies as interlaminated siltstone and mudstone, organic-rich mudstone, and calcareous shale. They are differentiated by composition, texture, sedimentary structure, and may have been deposited in different environments.

3.6.3.1. Interlaminated mudstone-very fine sandstone subfacies. This subfacies is characterized by the interlaminated very fine sandstone and micritic mudstone. The micritic mudstone laminae are usually neomorphized to form microspars, with some late dolomitization, resulting in a light color in the sample. It correlates to Petrofacies C as sparse micrite from Mount's classification. Very fine sandstone laminae are either grain or matrix supported. Grains are mainly detrital, rich in volcanic lithics and plagioclase with minor quartz, very fine to fine sand sized, equant, angular to subrounded, and moderately sorted, and crudely normal graded. Carbonate grains are mainly peloids and some bioclasts, such as shell fragments and pieces of lithified algal mat, very fine sand sized, and moderately sorted. Micrite in mudstone laminae are mixed with clay and other siliciclastic silts. The latter seem to be aphano- to micro-crystalline, homogeneous, and in some cases, parallel laminated. The occurrence of siliciclastic silts is hard to explain, but possibly formed by silicification. Very fine sandstone laminae are common with clay cement, which form continuous or discontinuous partings and are parallel to bedding (Figure 3.4C). No obvious bioturbation was observed; and some parts contain symmetrical ripple marks. This subfacies occur at the lowermost part of the clinoform foundation and were interpreted as being deposited in a sublittoral to littoral environment with weak wave agitation. The normal-graded sandstones may be tempestites.

3.6.3.2. Organic-rich mudstone subfacies. Organic-rich mudstone is composed of organic-rich micrite. It is massive without obvious sedimentary structures, but rich in bioturbation, such as burrows. Some of the micrite contain spherical, very fine sand sized

micritic nodules, indicating a probably microbial origin. Rare detrital grains are very fine sand sized and poorly sorted. The organic-rich mudstone occurs in the foundation and are thick bedded and laterally persistent. It is interpreted as lake-margin mud flat deposit.

3.6.3.3. Calcareous shale subfacies. Calcareous shale is commonly organic-rich, dark grey to grey, dense, and contains coarse silt sized detrital or carbonate grains. It is calcitic or dolomitic, and mixed with clayey and silty grains. In some cases, it is interlaminated with organic-poor shale forming light and dark interlaminations. This subfacies occurs underneath the toe or above the top of the clinoforms. Close to the toe slope, it is commonly split into pieces by displacive cements. The shale at the top contains abundant medium to coarse sand sized grains, which are dominantly volcanic lithics, subrounded to angular, and moderately sorted. These grains float in the dense dark micritic mud with random orientations, similar to a floatstone but grains are detrital (Figure 3.4D). They may be of an eolian origin (Yang et al., 2008). This subfacies is interpreted as a sublittoral to profundal deposit.

3.6.4. Highly Diagenetically-Altered Limestone Lithofacies. This lithofacies is characterized by a highly diagenetically-altered texture. At least 50% of total volume is cement spars. They are divided into non-oblitative and oblitative subfacies based on Wright's (1992) classification, termed lithic cementstone and sparstone. Their depositional environments cannot be interpreted because the original fabrics were extensively altered, but can be inferred from their stratigraphic position and adjacent rocks.

3.6.4.1. Lithic cementstone subfacies. This lithofacies contains dominantly cement spars interspersed with floating grains (Figure 3.4E). Cement content is more than 50%. Detrital grains dominate over carbonate grains. The rarity of carbonate grains may be caused by their dissolution and/or recrystallization during diagenesis. Detrital grains are dominantly lithics, angular to subrounded, medium sand sized, moderately sorted and, thus, compositionally and texturally immature. Carbonate grains are dominantly peloids. Cement spars are commonly coarse to very coarse sand sized. This subfacies occurs in clinoforms, indicating uneven diagenesis within the clinoform package. Originally it may be similar to the diagenetic lithic wackestone or packstone subfacies because they are observed in same clinoform beds.

3.6.4.2. Sparstone subfacies. Sparstone subfacies is identified by the oblitative diagenesis texture. It is mainly composed of coarse to very coarse sparry calcite crystals forming a blocky mosaic (Figure 3.4F). Stylolites and seams are present at the boundary between mosaics. Almost no relict texture is present, except some patches of organic rich siltstone. It is speculated that the original lithology is similar to the organic-rich calcareous shale subfacies.

3.7. LATERAL AND VERTICAL FACIES CHANGES IN CLINOFORMS

Facies changes occur laterally and vertically. Lateral facies change along a single clinoform is termed well-zoned if sedimentary structures, sediment fabrics and biota all form well-defined facies belts. A gradual zone, on the other hand, is defined if no precise contact can be located; and a nil to weak zone if no obvious facies juxtaposition occurs (Quiquerez and Dromart. 2006). Vertical facies change between stratigraphically adjacent beds or group of beds is termed significant if the structure, sediment fabric, or biota change sharply or termed weak to none if the change is insignificant (Quiquerez and Dromart. 2006).

The field and petrographic study of a carbonate-dominated clinoform (samples S7-26A-H) suggest that a relatively segmented facies zonation and facies in each segment change gradually. From the toe to the upper slope, the grain content increases from 33.2 to 50.6%. The proportion of detrital grains in total grains is 69% at the toe slope, decreases to 54.1% at a slightly higher location, increases to 65.7% at the middle slope, decreases to 49.7% at middle-upper slope, and dramatically increases to 80.8% at the uppermost slope. The proportion of carbonate grains increases from 15.5% at the toe to 33.1% at the toe-middle slope, decreases to 23.7% at the middle slope, increases to 31.2% at the middle-top slope, and finally drastically decreases to 19.2% at the uppermost slope. The grain size is persistent at about 0.75Φ closed to the toe slope, increases to 0.54Φ at the middle slope, decreases from 0.86Φ at middle-upper slope to 0.95Φ in the uppermost slope (Figure 3.6). Overall the grain size is persistently coarse. Grain size trend of detrital grains is similar to the abundance trend, whereas the size trend of carbonate grains is variable and differs from that of abundance trend.

Trend in the degree of sorting is weak (Figure 3.7). Sorting of detrital grains varies without a clear trend, largely moderately the standard deviation from 0.7 to 0.89. Sorting of carbonate grain is relatively poor in the middle slope and better in the uppermost slope, changing from moderately sorted to poorly sorted then back to moderately sorted. Overall sparry calcite content decreases upslope with the smallest amount at the middle-upper slope. In general, the textural and compositional trends in this carbonate-dominated clinoform is relatively stable. The changes are gradual in the middle to toe slope, and somewhat erratic from the middle to top slope.

The textural and compositional trend of a single sand-rich clinoform is not documented in this study. Field observations alone are not detailed enough to delineate the trends.

Finally, the sand- and carbonate-dominated clinoforms in a couplet show significant vertical changes in facies. The carbonate-dominated clinoforms consists carbonate component more than siliciclastic component (Petrofacies A) to form diagenetic lithic packstone and wackestone. The sand-dominated clinoform take more siliciclastic component than the carbonate (Petrofacies B) to form micritic sandstone. This change is mainly compositional.

Table 3.1. Raw point-counting data

Samp le #	G	M	C	P	S	Q m	Q p	Lv	Lvt	Lv m	Lvl	L vv	Lvf	Lund	P	K	A M	Ls	Ls m	Lss	Ls c	A	In t	A g	O o	O n	Pi s	Pe l	Bi o	CR C
S7-2	61	26	24	0	7	0	0	1	0	1	0	0	0	3	0	0	0	3	3	0	0	51	0	0	0	0	0	9	42	3
		5																												
S7-3	22	92	33	0	8	1	0	0	0	0	0	0	0	3	0	0	0	4	0	0	4	20	3	2	17	1	57	85	9	12
		5																				5	4							
S7-5	50	13	16	0	3	1	0	0	0	0	0	0	0	0	0	0	0	2	1	0	1	20	3	0	0	0	0	11	6	27
		3	7																											
S7-17	89	23	26	1	74	8	0	11	2	9	0	0	0	13	16	0	0	26	12	0	14	3	0	0	0	0	0	1	2	12
		4																												
S7-18	11	10	12	0	57	5	1	16	3	12	1	0	9	14	6	0	1	14	10	0	4	29	2	2	1	1	0	20	3	33
		9	8	3																										
S7-19	94	12	12	0	72	2	1	29	0	26	3	0	0	19	3	0	4	14	9	1	4	6	0	0	1	0	0	4	0	17
		8	8																											
S7-20	27	57	17	2	20	3	0	112	21	66	24	0	1	49	3	0	9	24	2	22	0	46	3	4	8	1	0	26	3	28
		4			0																									
S7-21	17	14	31	1	10	1	0	65	8	44	9	4	0	8	0	2	1	28	6	20	2	41	4	7	8	0	0	22	0	27
		3	5		5																									
S7-22	13	50	16	3	83	2	0	47	7	28	12	0	0	6	3	0	0	25	11	14	0	26	2	8	4	4	0	8	0	21
		0	7																											
S7-23	12	18	37	0	25	0	1	15	0	15	0	0	0	1	0	0	0	7	0	7	0	10	0	6	1	89	0	4	1	0
		6	7																			1								
S7-24L	12	93	13	0	83	0	0	30	7	13	10	0	0	21	6	1	0	25	11	13	1	44	0	29	11	0	2	2	0	0
		7	0																											
S7-24U	52	87	21	0	34	0	0	17	2	14	1	0	0	8	3	0	0	6	5	0	1	13	0	4	1	0	0	7	1	5
			1																											
S7-26A	69	12	15	0	66	6	0	29	6	16	4	1	2	7	7	0	1	15	15	0	0	2	1	0	0	0	0	1	0	1
		4	7																											
S7-26B	11	82	15	0	79	0	0	35	4	28	2	0	1	24	2	0	0	19	14	2	3	18	7	8	2	1	0	0	0	18
		6	2																											

Table 3.1. Raw point-counting data (Cont.)

S7-26C	13	85	13	1	72	0	0	48	4	35	8	0	1	17	7	0	0	0	0	0	0	32	1	0	1	2	0	10	4	29
	3		1																			5								
S7-26D	13	10	11	0	78	1	0	43	2	36	5	0	0	19	12	0	0	3	3	0	0	43	1	2	4	0	0	19	1	9
	0	8	2																			7								
S7-26E	11	11	12	2	90	1	0	21	1	18	2	0	0	18	0	0	0	50	48	0	2	14	1	1	3	5	0	3	1	7
	1	7	0																											
S7-26F	16	83	98	0	11	0	0	79	9	58	12	0	0	13	14	0	0	5	1	0	4	40	1	3	5	1	0	13	4	18
	9				1																	4								
S7-26G	18	15	8	2	94	0	0	54	9	36	6	0	3	25	3	0	2	10	6	0	4	59	1	2	7	3	1	24	7	36
	9	1																				5								
S7-26H	17	97	76	0	14	0	0	70	18	35	17	0	0	36	25	1	0	11	5	1	0	34	3	0	0	0	0	4	0	0
	7				3																									
S7-27	15	18	13	0	11	1	0	54	18	32	4	0	0	20	28	1	1	7	6	0	1	34	1	5	5	0	0	8	0	8
	4	3			2																	6								
S7-35	41	27	36	0	27	2	0	8	0	8	0	0	0	5	0	0	0	12	8	0	4	10	0	0	0	0	0	6	4	4
		3																												
S7-38	12	36	18	0	10	3	0	60	9	41	9	1	0	12	16	0	1	18	16	0	2	8	2	0	1	2	0	3	1	9
	7		7		9																									

Table 3.2. Derivative data calculated from raw point-counting data

Sample #	G (%)	M (%)	C (%)	Mi (%)	P (%)	Mz(G)	$\sigma_1(G)$	S/G(%)	Mz(S)	$\sigma_1(G)$	A/G(%)	Mz(A)	$\sigma_1(A)$
S7-2	17.4	75.7	6.9	82.3	0	2.21	1.19	11.5	2.08	1.52	83.6	2.30	1.05
S7-3	64.3	26.3	9.4	35.7	0	1.30	1.51	3.5	2.62	1.04	91.1	1.97	1.49
S7-5	13.3	38.0	47.7	81.1	0	1.75	1.19	6.0	1.63	0.59	40.0	1.84	1.16
S7-17	25.4	66.9%	7.4	34.9	0.3	2.98	0.88	83.1	2.94	0.90	3.4	3.52	0.92
S7-18	34.0	30.9	35.1	61.7	0	2.45	0.68	47.1	2.57	0.61	24.4	2.30	0.72
S7-19	26.8	36.6	36.6	67.4	0	2.11	1.01	76.6	2.15	1.04	5.3	3.10	0.89
S7-20	78.3	16.3	4.8	18.9	0.6	2.04	0.73	73	1.95	0.65	16.8	2.24	0.89
S7-21	49.4	41.4	8.9	49.4	0.3	2.02	0.76	60.7	1.94	0.70	23.7	2.11	0.83
S7-22	37.1	14.3	47.8	58.9	0	1.19	0.84	63.8	1.37	0.90	20.0	0.98	0.79
S7-23	36.0	53.4	10.6	52.0	0	-0.20	0.44	19.8	0.26	0.93	80.2	-0.36	0.27
S7-24L	36.3	26.6	37.1	63.7	0	0.91	0.82	65.4	0.97	0.84	34.6	0.80	0.77
S7-24U	14.9	24.9	60.2	85.1	0	1.65	0.74	65.4	0.72	0.76	25.0	1.10	0.90
S7-26A	19.7	35.4	44.9	74.3	0	1.63	1	95.7	1.63	0.96	2.9	2.00	1.82
S7-26B	33.2	23.4	43.4	66.8	0	0.77	0.89	69	0.83	0.89	15.5	0.23	0.72
S7-26C	38.0	24.3	37.4	64.4	0.3	0.75	0.82	54.1	0.62	0.75	24.1	0.62	0.78
S7-26D	37.1	30.9	32.0	62.9	0	0.75	0.85	60.0	0.70	0.76	33.1	0.81	1.02
S7-26E	31,7	33.4	34.3	66.9	0.6	0.97	0.98	81.1	0.98	0.98	12.6	0.89	0.97

Table 3.2. Derivative data calculated from raw point-counting data (Cont.)

S7-26F	48.3	23.7	28.0	51.7	0	0.54	0.82	65.7	0.56	0.73	23.7	0.55	0.92
S7-26G	54.0	43.1	2.3	44.9	0.6	0.86	0.70	49.7	0.80	0.63	31.2	0.93	0.76
S7-26H	50.6	27.7	21.7	49.4	0	0.95	0.77	80.8	0.94	0.74	19.2	0.96	0.56
S7-27	44.0	52.3	3.7	55.1	0	1.05	0.76	72.7	1.02	0.74	22.1	1.09	0.78
S7-35	11.7	78.0	10.3	81.7	0	2.37	1.29	65.9	2.30	1.39	24.4	2.30	1.26
S7-38	36.3	10.3	53.4	58.6	0	1.65	0.74	85.8	1.65	0.76	6.3	1.75	0.55

Table 3.3. Cement spar distribution in clinoform deposits

		S7-26A	S7-26B	S7-26C	S7-26D	S7-26E	S7-26F	S7-26G	S7-26H	S7-24L	S7-26U
C%		44.9	43.4	37.4	32.0	34.3	28.0	2.3	21.7	37.1	60.2
Crystal size (%)	Finely Crystalline	21.7	1.3	0.8	0	1.1	0	16.7	25.0	0	0.5
	Medium Crystalline	46.5	13.8	9.9	3.6	55.6	11.3	66.7	26.3	6.9	5.2
	Coarsely Crystalline	28.0	61.8	32.8	48.2	33.3	50.5	16.7	47.4	38.5	60.7
	Very coarsely crystalline	3.8	23.0	56.5	48.2	3.4	38.1	0	1.3	54.6	33.6
Crystal shape (%)	Equant	48.4	53.3	81.7	94.6	1.7	88.7	83.3	78.9	95.4	89.1
	Bladed	35.0	21.1	21.5	0	61.4	0	0	0	1.5	0.5
	Fibrous	16.6	25.7	16.8	5.4	34.2	11.3	16.7	21.1	3.1	10.4

Table 3.4. Characteristics, interpreted depositional environments, and occurrence of lithofacies in studied samples

Lithofacies	Grain composition	Sedimentary texture	Depositional environment	Occurrence
1 Mixed siliciclastic-carbonate rock				
a. Diagenetic lithic packstone and wackestone	Volcanic lithics, minor sedimentary lithics, intraclasts, aggregate grains, and peloids, micrite and sparry calcite abundant	Coarse to medium sand, angular to subrounded, moderately sorted	High-energy littoral	Carbonate-rich clinof orm and foundation, S7-26A-H, S7-21,22,24L
b. Micritic lithic sandstone	Volcanic lithics, minor sedimentary lithics and peloids, less micrite and sparry calcite	Fine to coarse sand, upper part coarser, angular to subrounded, moderately sorted	High-energy littoral	Siliciclastic-rich clinof orm and foundation, S7-20
2 Microbial carbonate rock				
a. Boundstone	Volcanic lithics, minor sedimentary lithics and peloids, oncoids depending on location	Medium to fine sand for uncoated grain, oncoids size random, moderately to moderately poor sorted, angular to subrounded	Near-shore zones, slight wave or current agitation	Clinof orm foundation and underlain beds, S7-5,6,8,10,18,19,23

Table 3.4. Characteristics, interpreted depositional environments, and occurrence of lithofacies in studied samples (Cont.)

b.	Thrombolitic microbialite	Pisoids and peloids, algal mats, minor in-situ intraclasts, ooids, and bioclasts	Various pisoid size, other grain fine to very fine sand, moderately poorly sorted	Lake plain, supralittoral	Overlain by clinof orm deposits, S7-3
3	Mudrock				
a.	Interlaminated mudstone-very fine sandstone	Volcanic lithics, plagioclase, mudrock lithics and chert, microsparry micrite	Detrital grains very fine to fine, moderately sorted, angular to subrounded, crude normal grading, carbonate mud laminae	Sublittoral to littoral	Base of clinof orm foundation, underlain beds, S7-7, 17, 35,37
b.	Organic rich mudstone	Micrite, algal mats, minor bioclasts	Very fine algal mats and other grains, micritic mud	Mud-flat	Lowermost deposit, S7-2
c.	Calcareous shale	Calcareous mud, clay and organic matter mixed, eolian sand	Organic-rich and poor laminae, eolian sand medium to coarse, subrounded to subangular, floating, moderately sorted	Sublittoral to profundal	Clinof orm toe and overlapping, parts of S7-26A,E, S7-27,40

Table 3.4. Characteristics, interpreted depositional environments, and occurrence of lithofacies in studied samples (Cont.)

4	Highly diagenetic influenced limestone				
	a. Lithic cement stone	Volcanic lithics, minor sedimentary and carbonate clast, sparry calcite rich	Medium sand, angular to subrounded, moderately sorted	Suspected high-energy littoral	Clinoform foundation and body, S7-24U, 38
	b. sparstone	Sparry calcite crystals, minor silt	Organic rich silt patches	Suspected low-energy sublittoral	Suspected clinoform body or foundation, S7-36

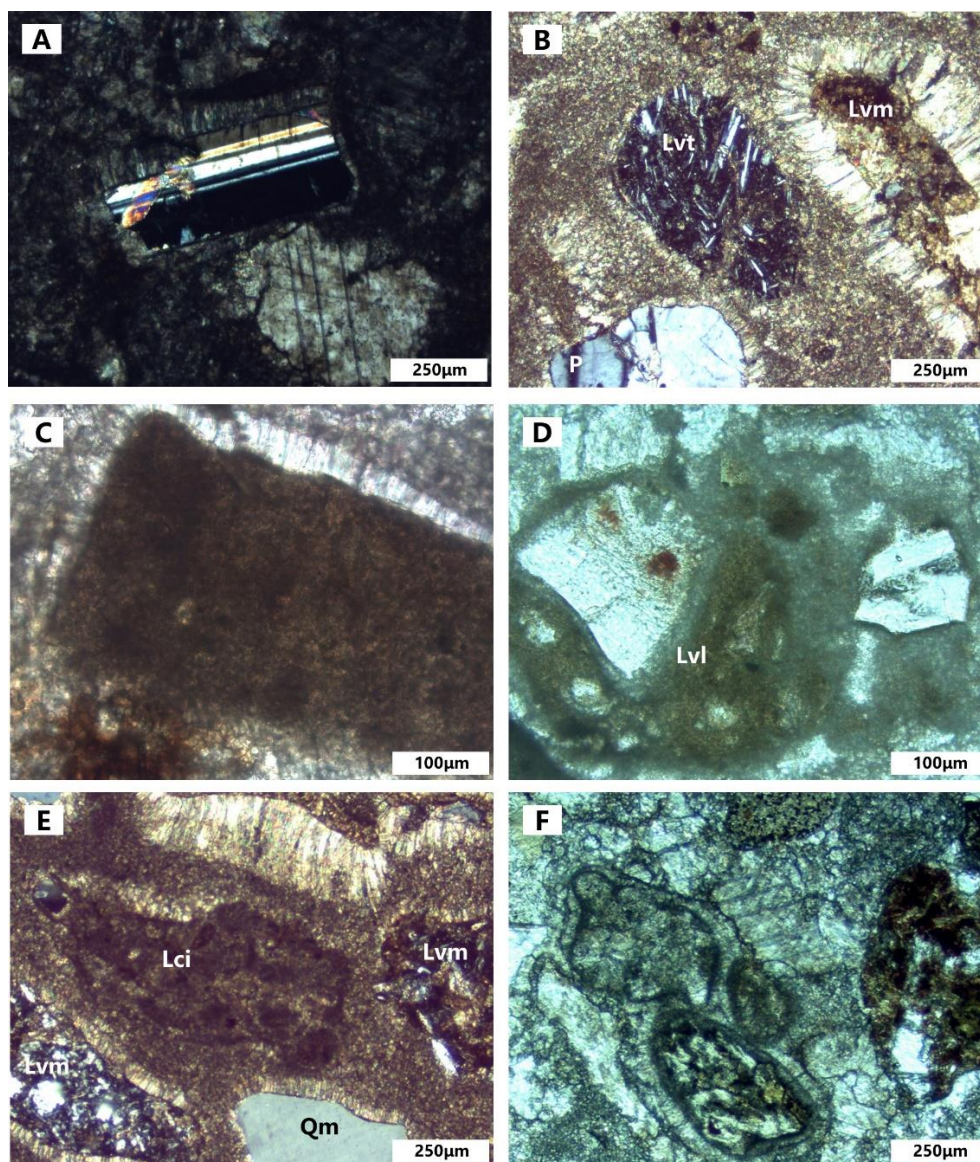


Figure 3.1. Photomicrographs showing various grains. (A). S7-26D (XL), a plagioclase with a bladed sparry calcite rim and in a point contact with a grain that is completely replaced by sparry calcite. (B). S7-26H (XL), several detrital clasts in micritic matrix. Central part is a volcanic lithic with trachytic texture (Lvt), interpreted as an intermediate type. Right part is a highly altered volcanic lithic with microlitic texture (Lvm) with a rim of bladed to fibrous calcite. Lower left part is a plagioclase grain. (C). S7-26D (PL), a mud clast with anequant to bladed rim. (D). S7-26F (PL), an intraclast with multiple grains internally. The biggest part is a highly altered lathwork basaltic volcanic lithic (Lvl), surrounded by some plagioclase grains. (E). S7-26H (CL), an intraclast (Lci) in the central part, with multiple very fine internal grains, more organic and clay content than the surrounding matrix. Lower part is a monocrystalline quartz (Qm). (F). S7-26F (PL), an aggregate grain with three grains glued together. Note the glued grains are smaller than the nearby unglued volcanic lithic. The zigzag outline of the aggregate grain may be a torn mark, indicating a rip-up origin.

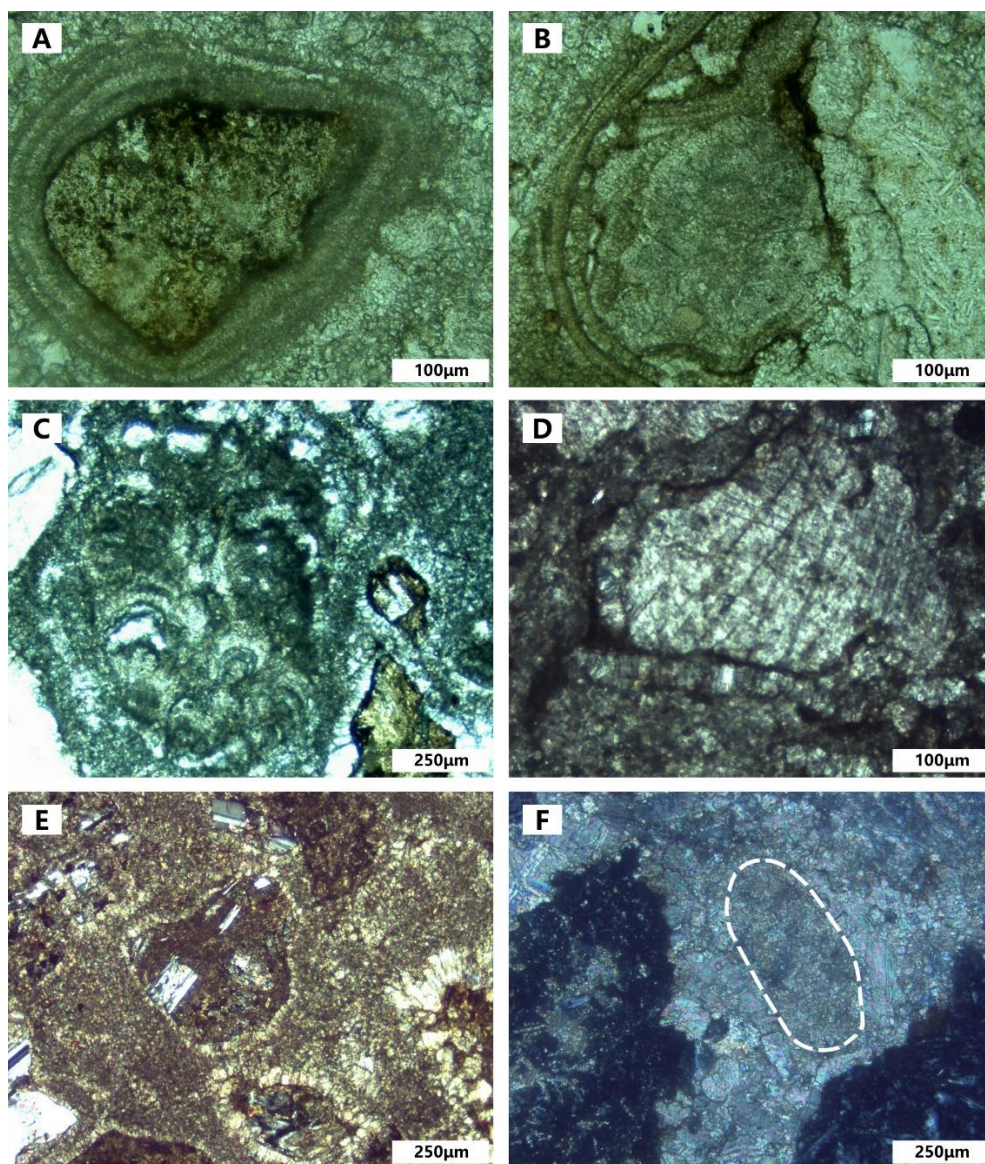


Figure 3.2. Photomicrographs showing various grains and matrix. (A). S7-26F (PL), an ooid with a volcanic lithic as nucleus. (B). S7-26F (PL), a superficial, partially broken ooid, indicating reworking and abrasion during transport. (C). S7-26F (XL), Bioclast with microbial growing structures and some trapped very fine sand-sized grains. (D). S7-26C (XL), a completely replaced grain with little relics at the edge, which is not enough for identification. (E). S7-26H (XL), Grains in micritic matrix. The micrite is the main type of matrix type in clinoform package. Color intensity varies with amount of mixed clay and organic matter. (F). S7-26F (XL), neomorphosed matrix to form micro- and pseudo-spars. The dashed line outlines a relic of micrite or a micritized grain.

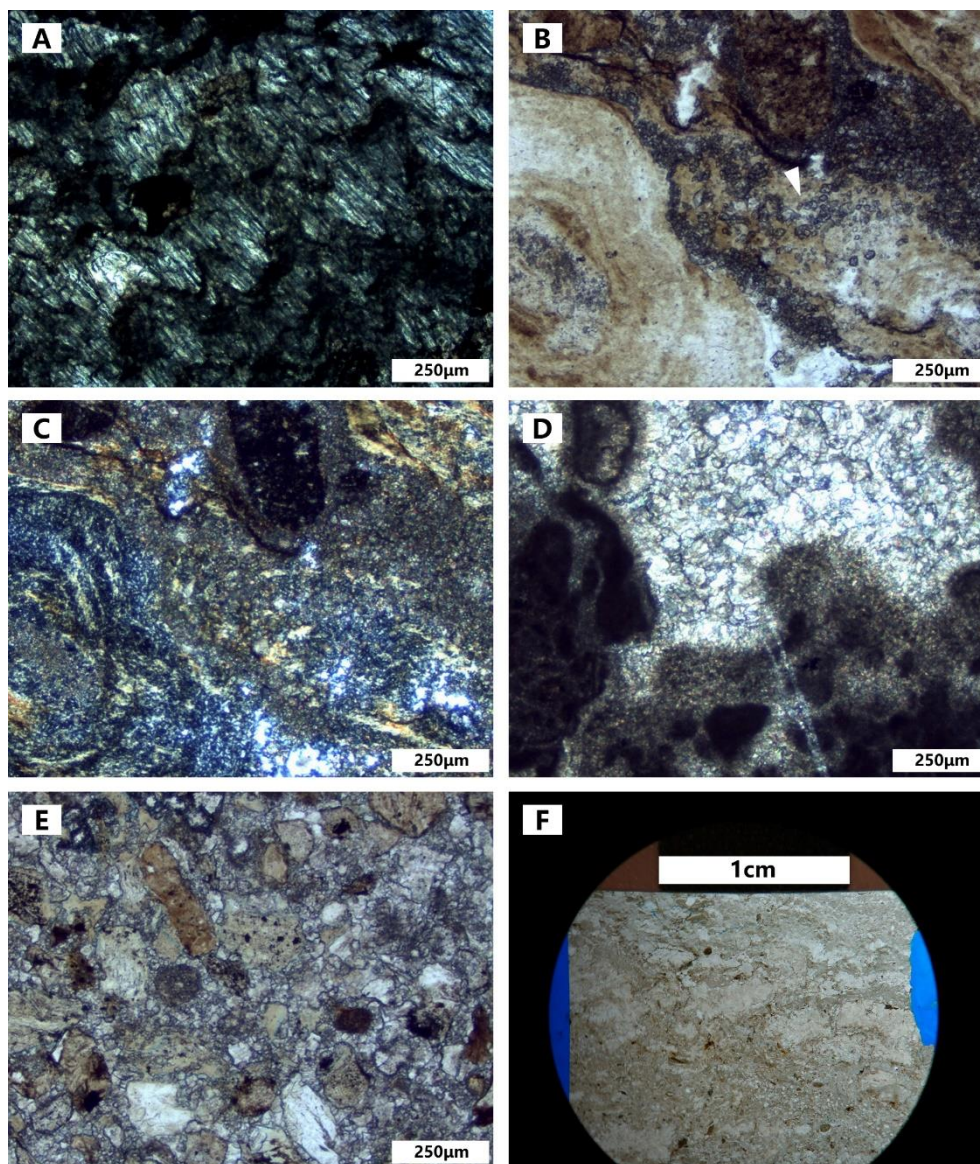


Figure 3.3. Photomicrographs showing various interesting features. (A). S7-27A (XL), a cone-in-cone structure. Displacive fibrous to bladed sparry calcite crystals fracture original shale layer into pieces during burial. (B). S7-23 (PL), a boundstone with oncoids and algal lamination with possible tiny dolomite rhombs (white arrow). (C). S7-23 (XL), the same photo in cross-polar, showing intense silicification and some siliceous cements in lower part. (D). S7-3 (XL), a vesicular structure filled by sparry calcite, indicating meteoric dissolution and reprecipitation during subaerial exposure. (E). S7-20 (PL), a micritic sandstone rich in detrital grains with microcrystalline micrite. (F). S7-19, a stromatolitic structure with microbial lamination and fenestrae filled by sparry calcite.

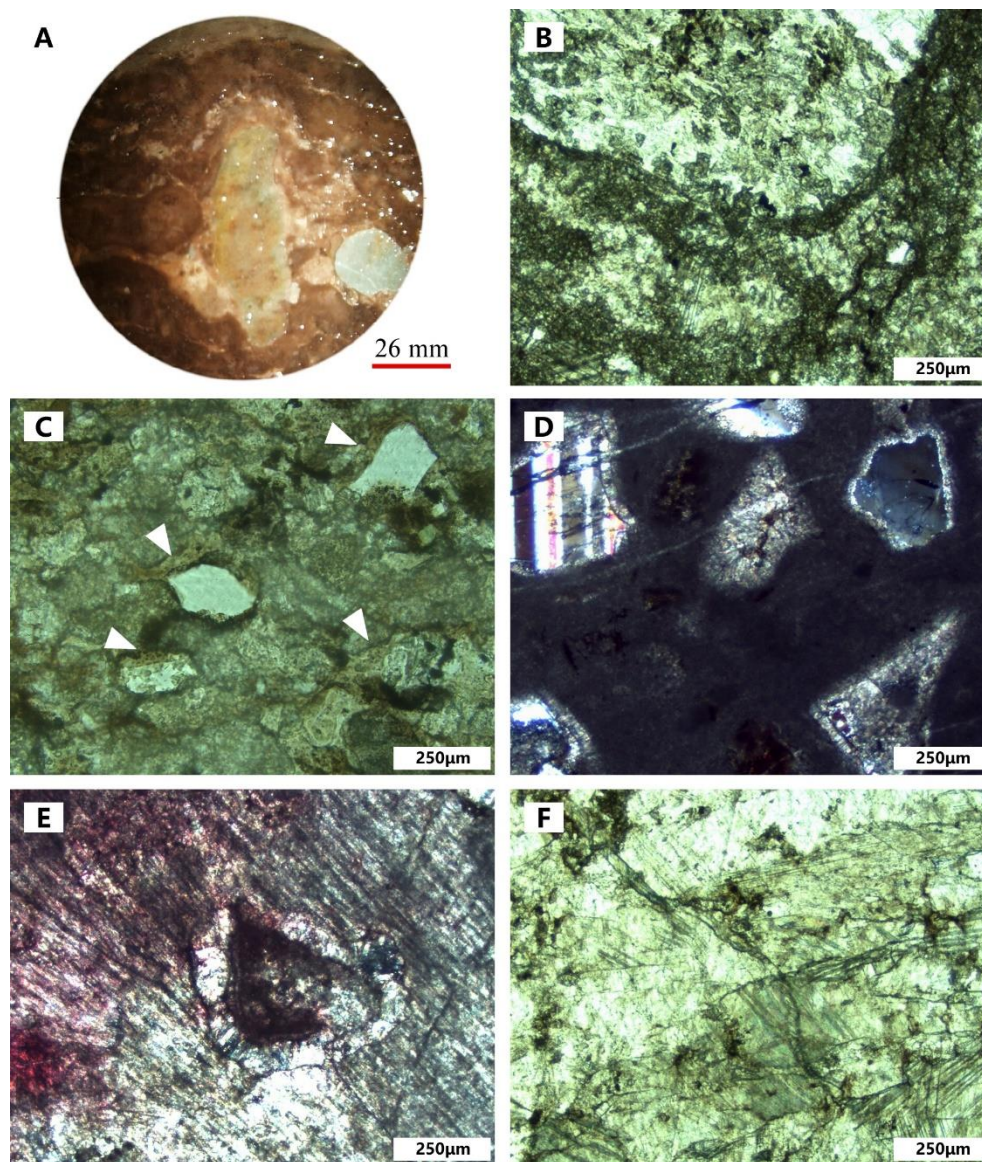


Figure 3.4. Photomicrographs of interesting features. (A). S7-6, hand sample containing multiple granule-pebble sized dropstone grains in microbial carbonate, vertically oriented, suggesting a seasonally frozen lake. From Yang et al. (2008). (B). Thin section of the sample in (A), showing pebble sized volcanic lithic with trachytic texture of the dropstone (PL). (C). S7-17 (PL), very fine quartz, lithics, and plagioclase grains in micritic matrix. White arrows point to clay cement surrounding grains that are generally parallel to bedding. (D). S7-28 (XL), calcareous shale with floating angular to subangular eolian sands. Matrix is dark gray, organic rich, and micritic. (E). S7-26C (PL), severely diagenetically-altered rock with grains floating in the cement. Red color is partially stained calcite. (F). S7-36 (PL), extremely diagenetically-altered fabric composed of only coarse calcite spars. Seam and fracture in the middle indicate burial processes.

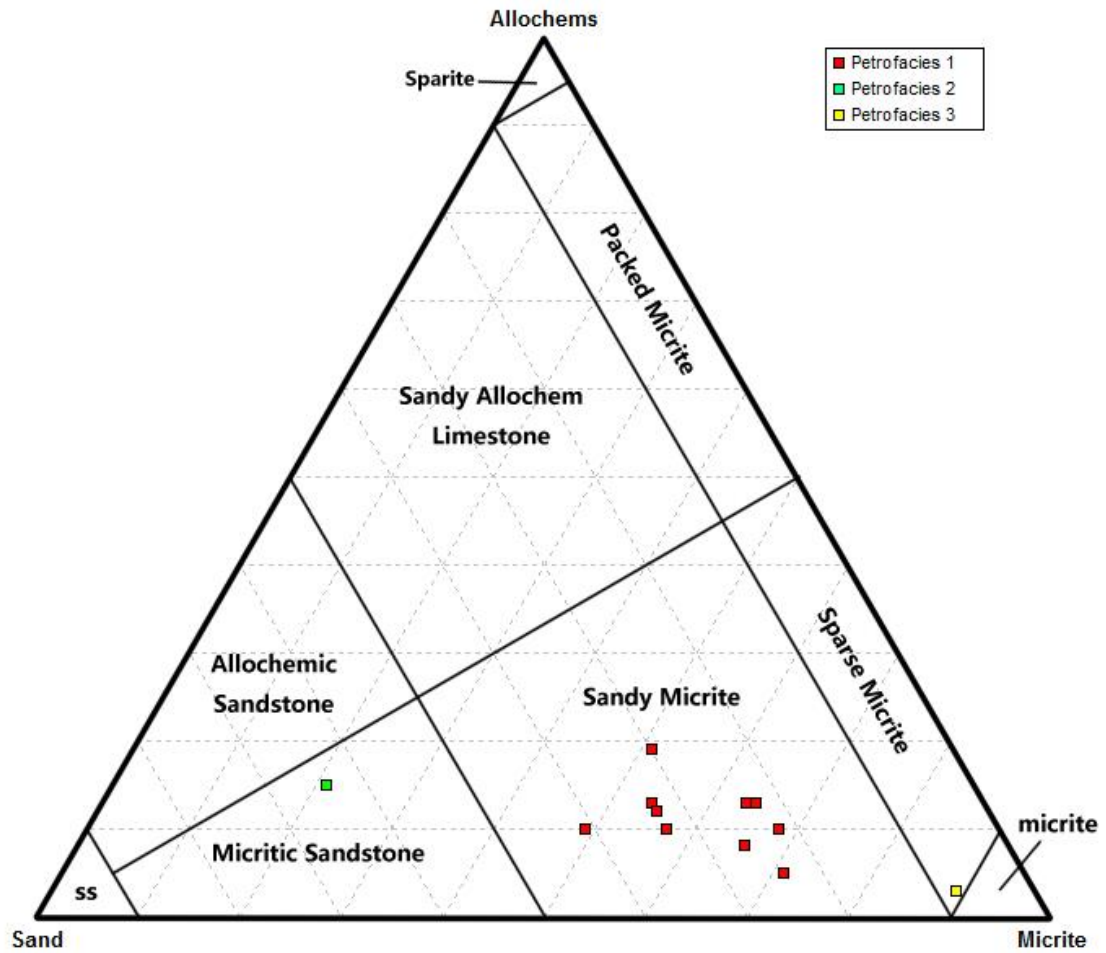


Figure 3.5. ASMi ternary diagram showing non-microbially-induced, relatively weakly diagenetically-altered samples in clinoform package. Modified from Mount (1985).

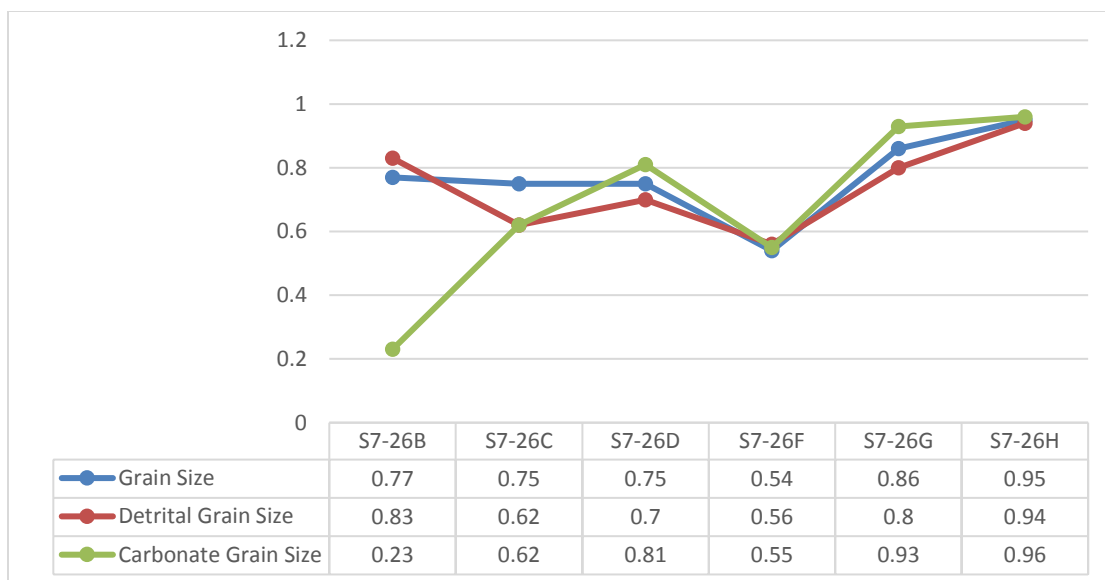


Figure 3.6. Lateral change of grain size from toe to upper slope of a carbonate-rich clinoform. The left side is the toe and right side is the top.

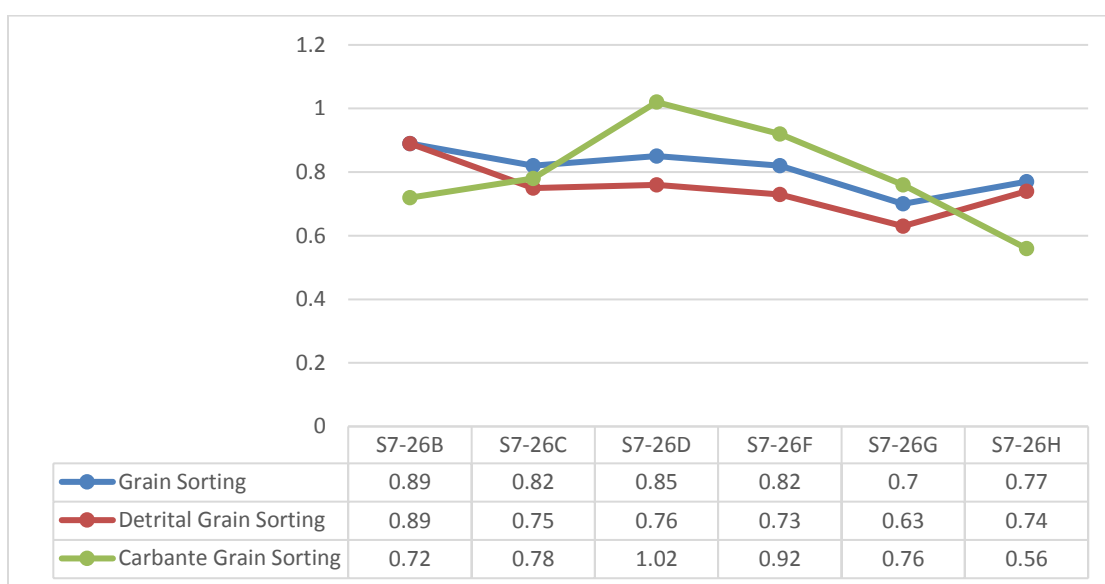


Figure 3.7. Lateral change of grain sorting from toe to upper slope of a carbonate-rich clinoform

4. DISCUSSION AND INTERPRETATION

4.1. FORMATION OF CARBONATE-RICH CLINOFORMS

Field observations indicate that the carbonate-rich clinoforms prograde from a shallow subaqueous carbonate platform and flat, where carbonate production was active (Yang et al., 2008). The clinoform foundation is dominated by microbial rich boundstone. The lakeward accretion foresets are composed mainly coarse-grained deposits and have a symmetrical-asymmetrical sigmoidal shape that are similar to Gilbert-type delta foresets in dip section. However, the sedimentary fabrics that lack of mud-sized fractions on toe slope and any fluvial evidence on the upper slope preclude a deltaic interpretation. In addition, the repetition of carbonate and- siliciclastic-dominated clinoform couplets is hard for an origin of stable river inflow.

Sedimentary texture and structures in the carbonate-dominated clinoforms indicate a high energy environment with strong wave and current activities. Carbonate clasts are dominated by intraclasts, aggregate grains, and peloids. Aggregate grains commonly have incomplete cement rims and loss of glued grains, with broken and torn edges, indicating they were not in-situ but transported and redeposited. Some intraclasts are composed of small micritic segments, patchy, and glued by sparry calcite. This indicates non-biogenic cementation as in aggregate grains. The cements are late calcite precipitation, indicating a rip-up process that tore these intraclasts during strong wave activities. Besides, both siliciclastic and carbonate grains are generally coarse to very coarse. These textures, associated with the abundant current laminations, suggest a wave and current-induced sediment transport.

A recent study indicates that accretion of low-relief (< ~25m) carbonate clinoforms is primarily influenced by wave-induced sediment transport (Quiquerez & Dromart, 2006). Waves can erode and deposit sediments along the lake shore. Strong wind triggers wave to form currents, transporting the eroded materials as a shore drift and forming embankment prograding to the deep water when the shoreline or current diverges. When the coastline turns abruptly landward, like a bay, the embankment can take the form of a spit or a bar close to the inflexion, and when the current diverges from the coast line, the diverged flow can form wave-built terraces, dipping lakeward. Wave-

built constructive terraces form preferentially at the head of a triangular bay, into which the waves from a large body of water are rolled without obstruction (Gilbert, 1890). Such progradational littoral depositions induced by strong wave-derived currents have been exemplified by accretionary foresets in Lake Bonneville (Gilbert, 1885, 1890) and the Glens Ferry Formation, Snake River plain (Swirydczuk, Wilkinson & Smith, 1979, 1980). The coarse to very coarse grains, micrite, or even some of the calcite spars in the clinofoms can be transported from the nearby carbonate rich environment (i.e. carbonate factory) by strong currents to be deposited as clinofoms.

Carbonate wave-constructed terrace in the Glens Ferry Formation was composed of abundant high-energy ooids due to the strong wave agitation facing the shore. The ooids are thin coated by low-Mg cortices and crenulated by algae, and coarse sand-sized. In contrast, ooid is not common in the lower Lucaogou carbonate-dominated clinofoms; and nuclei are mainly of a medium to medium-coarse sand size. Many of them are coated by organic rich micrite, interlaminated with radial microcrystalline calcite or aragonite, more likely to have a microbial origin (Davaud & Girardclos, 2001). Besides, many ooids are broken. Dominant carbonate clasts, such as aggregate grains and intraclasts, contain generally dark organic-rich micrite with none or few fine to very fine detrital grains and microbial relics. They are interpreted as being derived from a nearby low-energy carbonate platform or mud flat. The detrital clasts in the clinofoms are generally coarse to very coarse sand sized, indicating that nucleating detrital grains and those in the clinofoms were not from the same origin. These indicate that coated and aggregated grains are not in situ, and most of the detrital grains did not form ooids in such a carbonate rich environment. The wave progradation probably did not face the lake margin; and the clinofoms are probably a spit or bar. Whether the clinofoms formed a spit, bar, or wave-built terrace, a landward embayment of the coastline is required. This probably indicates that the lake shore morphology was not continuous when the clinofom was developed (Figure 4.1).

4.2. FACIES CHANGES IN CLINOFORM PACKAGE

As discussed previously, the facies in a single carbonate-dominated clinofom is laterally divided into two zones, each of which shows gradual facies changes,

respectively. Detrital grains show a coarsening-upward then fining-upward trend. Carbonate grains show two fining-upward trends updip. Grain type distribution shows a segmented lateral zonation as well, but not as obvious and linear as the grain size trend, which may be caused by later severe diagenesis. The transition point is close to the middle slope, near the maximum declivity along the clinoform. It has been observed that the most granular, grain-supported fabrics often coincides with the position of maximum declivity along the high-relief carbonate clinoform (Kenter, 1990; Adams & Schlager, 2001), but for a low-relief carbonate clinoform, facies differentiation is often not directly related to clinoform shape, height, or declivity, instead, may result from hydrodynamic zonation with increasing water depth (Quiquerez & Dromart, 2006). Zonation in the carbonate-rich clinoform thus probably is induced by two different flow regimes of a different energy level. However, field observation does not show evidence of oscillatory flows, such as hummocky cross-beds on the middle to toe slope. Thus, the mechanism of how upper and lower flow regimes influence the lateral facies change at the middle slope is unsure. Alternatively, sediment gravity flows, such as grain flow or sand avalanching, may result in lateral facies transition, but probably more likely in high-relief clinoforms (Mullins et al., 1983; Kenter, 1990). For instance, zonation of grain size grading in Glens Ferry Formation, which was interpreted as sand avalanching, is opposite to that in the studied sample (Swirydczuk, Wilkinson & Smith, 1980). Above all, a mature interpretation of the causes of lateral facies change in the carbonate-dominated clinoform is still pending.

The vertical facies change in a carbonate-siliciclastic clinoform high-order cycle, is significant. It can be explained by intermittent strong current activities in Vauchigmon, Turkey (Quiquerez & Dromart, 2006). Wave activities were probably stronger during the development of siliciclastic-rich clinoforms, because transporting abundant coarse sand and, in some cases, even granule-sized basaltic to intermediate lithic grains from an embayed flat to form a well-washed siliciclastic-dominated clinoform requires high physical energy. When currents were not strong enough to transport abundant siliciclastic lithics, lighter carbonate grains were transported to form carbonate-rich clinoforms with more matrix.

Alternatively, the significant vertical facies change can be caused by variations in climatic conditions. The carbonate factory may have been more productive under a semiarid condition, and less productive under a subhumid condition. High resolution stratigraphic interpretation has indicated high-frequency changes between humid and semiarid-arid conditions at the high-order cycle scale in the NE Tarlong section (Yang et al., 2010). Field observations suggest that the siliciclastic-rich clinofolds have an upward-coarsening trend from medium to fine to medium sand at the lower slope coarse to even granule and fine-pebble in the upper slope. The trend suggests that water inflows carrying sediments downslope deposited the sediments to form the clinofolds. This interpretation is tentative because only one thin section of the siliciclastic-rich clinofolds was studied. Overall the depositional environment had a relatively high energy because both carbonate and siliciclastic-rich clinofolds have abundant current laminations. As a result, climatic changes resulting variations in carbonate productivity in the factory may be a more reasonable explanation. The carbonate-siliciclastic clinofold couplets can either reflect a cycle of seasonally-recurrent wave activities, or high frequency, repetitive seasonal variations in precipitation and evaporation, or a combination of both.

4.3. PROBLEMATIC ASPECTS

The existence of water inflow is unsure. Northern Tarlong has been interpreted as both the depositional and subsidence centers by Yang et al. (2009, 2010). The northward prograding of the clinofolds is probably more suited for a water inflow origin from the south and prograding lakeward than a coastline morphology-induced wave-built deposit. However, the ability of wave to transport heavy lithics is unknown. Both of the two clinofold types are rich in coarse lithics. How strong the wave should be to transport the heavy lithics and how long the transport distance is are unknown for the existing data. Nevertheless, a mechanism of transport and deposition by water inflows may give an easier explanation of lithic transport, origin, and hydrodynamic equilibrium. This explanation, although supported by some field observations, cannot be confirmed by petrographic data. Hence, a wave-built deposit is probably a more appropriate explanation for the clinofold sets based on petrographic data. If the clinofold package

was a primarily wave-induced product, the shoreline morphology should have played a more significant role than lake level change.

The other problem is the high content of micritic matrix. If the clinoform was formed in a high energy environment, the matrix content, theoretically, should be low. But the assumed micrite content (Mi) is relatively high and reaches to 66.8% in some toe parts. One possibility for the high matrix content is the result of severe diagenesis. To simplify the complex multi-episode diagenesis, cements were all assumed as aggraded neomorphic micrite for a simpler diagenetic and petrofacies study. This may cause bias, especially in highly diagenetically-altered samples at the toe slope. Some original grains may be counted as micrite, resulting in an increase in matrix content. In addition, micritization, which is common at a variable degree throughout the samples, may be the reason for a high matrix content. Some bioclasts are highly micritized so that they are hard to identify. Finally, the content of assumed micrite content generally increases down slope, which may be caused by water inflow. The role of water inflow process remains uncertain.

4.4. LAKE CONTRACTION AND EXPANSION

The clinoform foundation overlies a microbial boundstone with a sharp boundary. Upward change from littoral to sublittoral lithofacies indicates that the lake level rose during the deposition of clinoform foundation. Overall the clinoform package shows a general upward shallowing trend with stacks of interlaminated mudstone-very fine sandstone to microbial boundstone to mixed carbonate-siliciclastic packstone/wackestones from the lowermost foundation to the clinoform body, with upward coarsening and thickening. But the interval of thin mudstone/shale, microbial boundstone, mixed siliciclastic-carbonate rock occurs in both clinoform foundation and clinoform body, separated by a flat boundary. The relationship suggests that the clinoform package is a separated sequence. The carbonate-dominated clinoform package was truncated sharply and overlain by calcareous shale, which is interpreted as profundal deposit (Yang et al., 2008). No transgression lag was observed, indicating a sudden deepening of the lake. The profundal calcareous shale was highly bioturbated and

contains scattered eolian sands, indicating strong wind activities during the lake level rise.

4.5. PROVENANCE OF SILICICLASTIC SEDIMENTS

Carbonate grains are interpreted as from a nearby carbonate platform or mudflat; and siliciclastic grains rich in volcanic lithics probably from sand-rich lakeshore or/and littoral environment, or being transported by river inflow. It is necessary to understand the provenance of the siliciclastic grains in the mixed siliciclastic-carbonate rocks since it is an important component of the clinoforms. The result of QpLvLs (Figure 4.2) distribution shows that all samples fall in the field of magmatic arc, while results of QmFLt (Figure 4.3) distribution indicates that most samples are associated with a subduction-complex: a recycled-orogen source where the subduction complexes composed of oceanic sediments and lavas were uplift, and an undissected arc source, where the arc was young with a continuous volcanic cover, supplying abundant volcanic clasts shedding from volcanogenic highlands. The diversity of the samples from the same clinoform package on the ternary diagrams may be caused by: (1) bias caused by severe diagenesis that affects one or multiple parameters; (2) bias caused by insufficient sample size of mixed siliciclastic-carbonate rocks; and (3) lateral facies change of grain distribution along a clinoform. The clinoform deposits had experienced severe and complex diagenetic processes. They will alter the low-resistance components, such as carbonate and volcanic grains to increase the relative quantity of high-resistance grains like plagioclase and quartz. In lithic packstone/wackestones, carbonate components are dominant. Thus, the amount of detrital grains may not be sufficient to provide a reliable statistical result. Finally, lateral facies change can cause an uneven grain type distribution. That is, samples from different locations within the same clinoform may have variable proportions of different grain types, and affect the ternary plot results.

The magmatic arc origin of detrital grains of the carbonate-dominated clinoforms package conforms with the regional tectonic setting. Previous studies suggested that northern Tianshan was a major source area (Shao et al., 2001; Greene et al., 2001), where Devonian to Carboniferous arc-related intermediate volcanic rocks with

sparse Upper Devonian sedimentary rocks were present. This interpretation was questioned by a later petrographic study in the Tarlong-Taodonggou area (Guan, 2011). The northern Tianshan area is lack in source of basaltic lithic, but the clinofoms deposit contains averaged 19% of total volcanic lithics. The low survivability of basaltic lithics does not support the lithics being transported to the Tarlong-Taodonggou half graben from northern Tianshan over a long distance. Textural statistics show that all the plotted samples have more than 50% of volcanic grains in a subangular to angular shape, rarity of rounded grains, and a large (10-20%) volume of angular grains. Sedimentary lithics also are mainly subangular and angular. These observations suggest that a significant amount of detrital grains probably were derived from a close local source. The Upper Carboniferous oceanic arc basalt has been noted (Carroll et al., 1990; Graham et al., 1993), and may be exposed at rift shoulders to serve as the local source (Yang et al., 2010; Yang et al., 2013; Obrist-Farner, 2015).

4.6. CLIMATE AND LAKE TYPE

Paleoclimatic conditions were interpreted in terms of precipitation/evaporation (P/E) ratio, or net precipitation, which can be inferred from sedimentary evidence. The overall carbonate abundance indicates that the climate was generally relatively arid during the development of carbonate-dominated clinofom package (Yang et al., 2008). The cycles of carbonate-rich to siliciclastic-rich clinofoms suggest that climate conditions oscillated in a relatively high frequent. Clay-rich laminae occur in the lowermost part of the clinofom foundation indicates a dry and seasonally icy climate (Yang et al., 2010). The wave activities indicate strong but intermittent wind activities. Dropstones found in the microbial boundstones indicate that the lake was seasonally frozen (Yang et al., 2010).

Lake classification is based on a sequence-stratigraphic depositional model of Bohacs et al. (2000, 2003), on the basis of the climate, basin subsidence pattern, stratal stacking patterns, lithology, shoreline stability, surface water inflow, hydrological condition, organic matter origin, and hydrocarbon type. They classified ancient lakes into three types, overfilled, balanced-filled, and underfilled. Lack of evaporative facies precludes the underfilled lake type. The carbonate-dominated clinofoms, microbial

dominant organic matter, and unstable to stable shoreline indicate a balanced-filled lake during the formation of the clinofoms package.

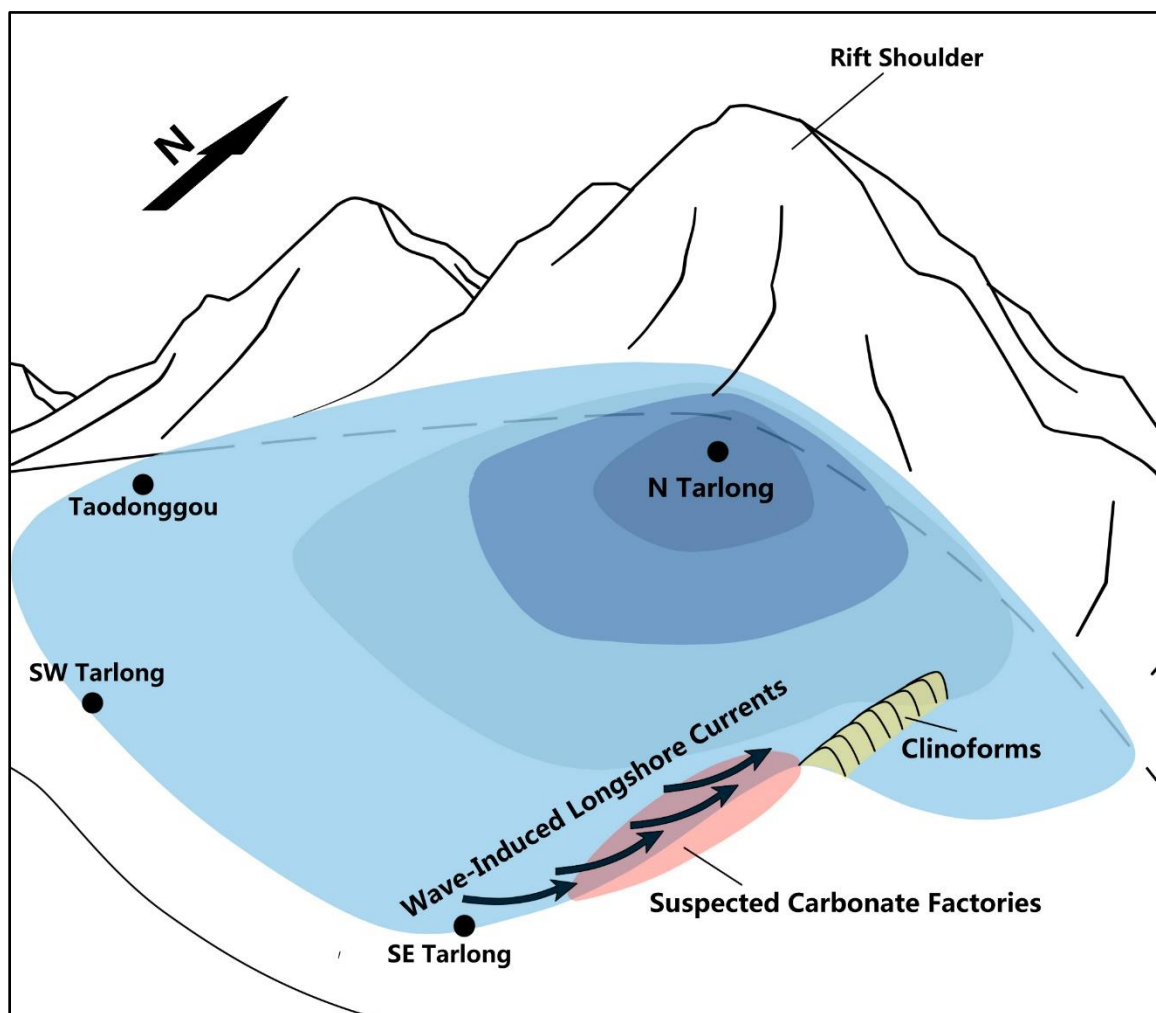


Figure 4.1. Schematic diagram showing the paleogeography during the formation of the carbonate-dominated clinofom package in the study area. Wave-induced longshore currents transported both siliciclastic and carbonate sediments to the depositional site, forming clinofoms where lake shoreline curved. The carbonate sediments were originally produced from a nearby carbonate factory, while siliciclastics from lake plain sand and mud flats.

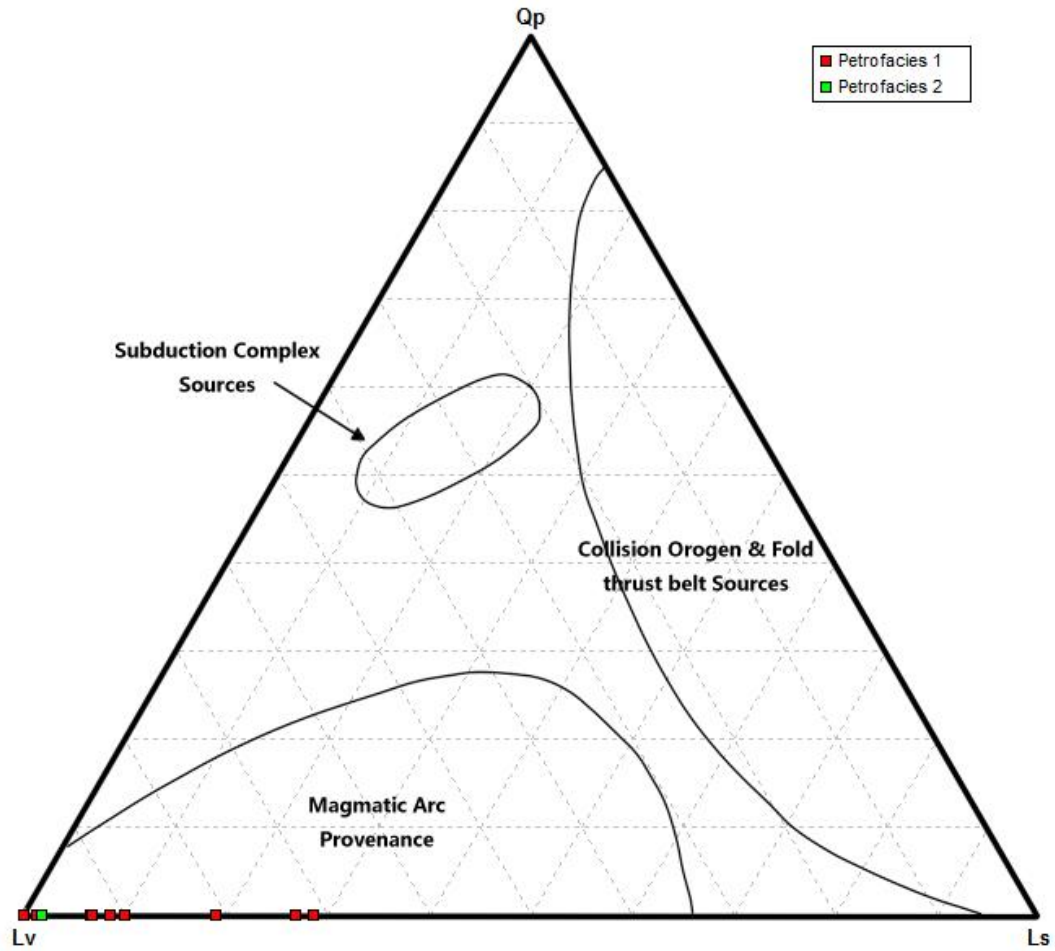


Figure 4.2. QpLvLs ternary diagram of detrital grains in samples. It shows all samples have a magmatic arc provenance. Modified from Dickinson (1985)

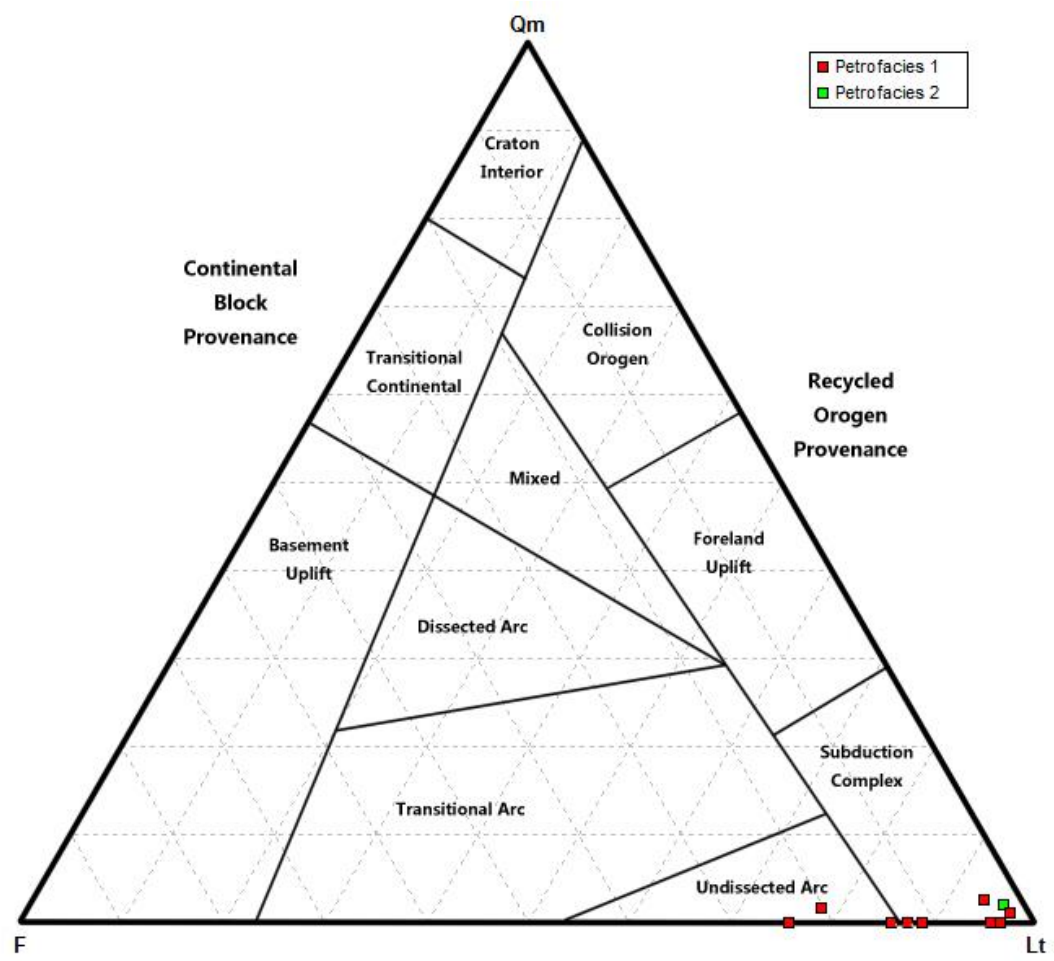


Figure 4.3. QmFL ternary diagram of detrital grains in samples. It shows that detrital grains were derived from rocks in a subduction complex and undissected arc, which suggest a mixed source. Modified from Dickinson (1985).

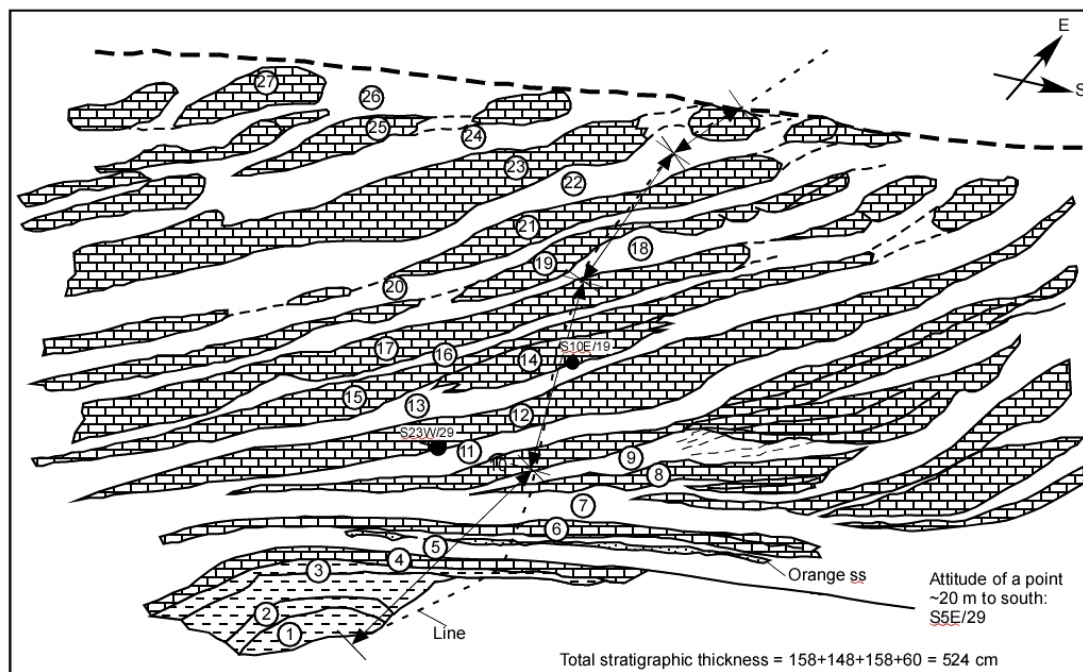
5. CONCLUSION

The carbonate-dominated clinoform package in lower Lucaogou LC serves as an example of how shoreline morphology and climate oscillation affect sediment deposit in a half-graben lake. The carbonated-dominated clinoform is interpreted to be a wave-induced spit or bar in a high-energy littoral environment. Sediments were eroded and transported from nearby lake margin by strong wave and current activities, and deposited when the coastline forms an embayment. The upper carbonated-rich clinoform and lower siliciclastic-rich clinoform in one clinoform couplet indicate high-frequency climate oscillation. The lake level was generally shallowing upward with small oscillations during the clinoform formation. Detrital grains are have multiple sources on the basis of composition and texture. Grains with a relatively high textural maturity were probably derived from the distant north Tianshan region, whereas basaltic lithics with a relatively low textural maturity from a local rift shoulder source. The Lucaogou lake was balanced-filled, in a seasonal, generally semiarid climate.

Questions remain for the forming mechanisms of the clinoforms, because of severe diagenetic alterations and insufficient data. Whether river inflow played a role in the clinoform development and lateral facies change is unsure. The original quantity of carbonate grains and matrix is questionable due to the highly-altered diagenetic fabrics. Finally, dynamic changes of shoreline morphology during the development of clinoforms are uncertain. All of these questions are waiting for solution, and need more work in the future.

APPENDIX A
SKETCH AND DESCRIPTIONS OF CLINIFORM PACKAGE IN DIP
DIRECTION

(by Dr. Wan Yang in 2008)

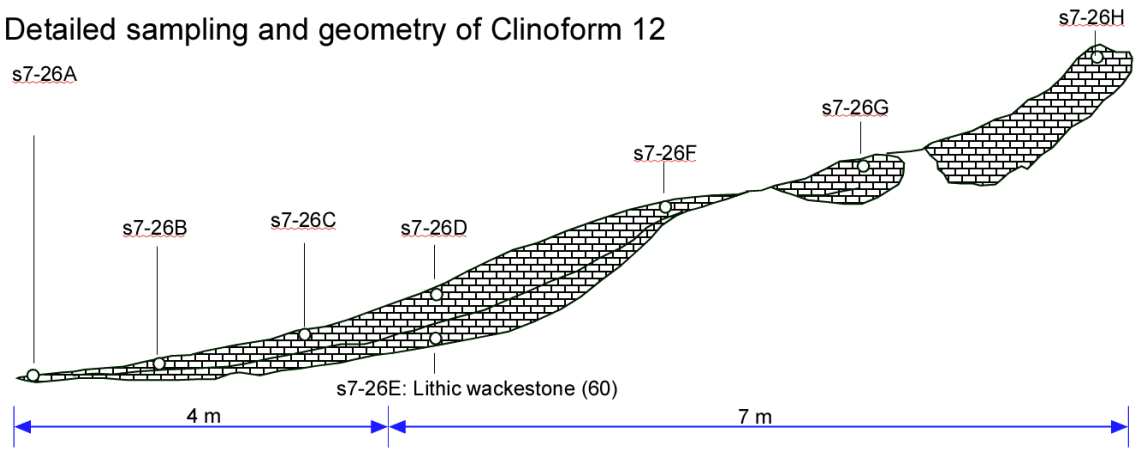


1. Lower part, shale, thick laminated, moderately calcareous, some silt and vf sandstone. Upper part, upward increasing lithic and shell debris, interlaminated, very calcareous. Sharp nonerosional top. S7-17 (upper part).
 - a) Orientation of dip cut: N85W; orientation of strike cut: N (uncorrected magnetic declination).
2. Basal 2-5 cm, current laminated, LSA, some shell debris, lenticular. Upward decreasing lithics, finer (m sand), wackestone, gray, lateral persistent. Sharp top. S7-18 (upper part).
3. Wackestone/packstone, gray, well medium laminated, abundant lithics and shell debris. Could be siltstone or very calcareous vf-f sandstone. Persistent. 5 cm thick. Sharp top.
4. Wackestone (70%), gray, dense, 1-3 layers, laterally persistent, well bedded, floor of clinofolds, many algal-coated grains, common lithics, some algal filaments, gray, dense, sparse lenses of blackened granules. Knobby, algal laminated top with ~5-cm relief. S7-19.
5. Shale or argillaceous, lithic wackestone, gray, well thick laminated. Uppermost part a layer of very calcareous sandstone or lithic wackestone, discontinuous basinward. Thickens to south from 1 to 5-10 cm, yellowish orange, c-vc, moderately to poorly sort. Distal part ripple (symmetrical) topped. Laterally persistent. Sharp top. S7-20.

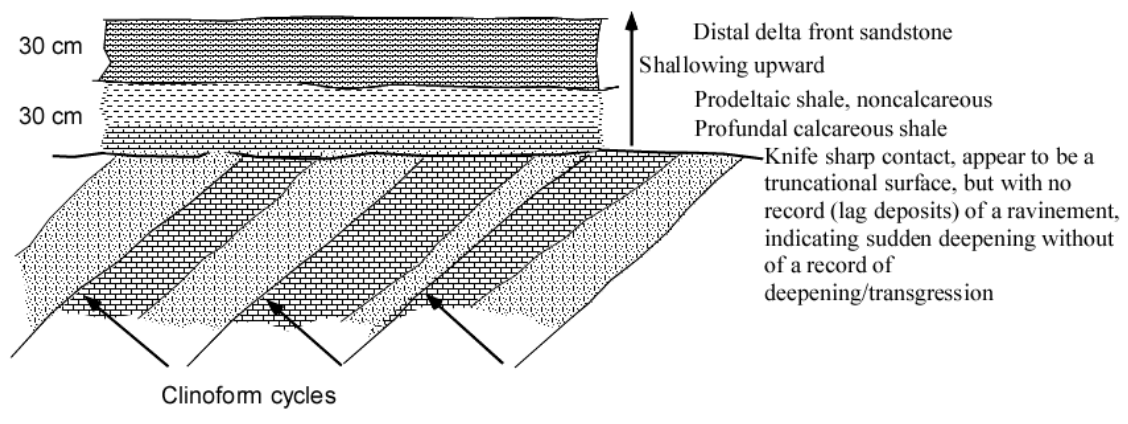
6. Sandstone, whitish gray, LSA, very calcareous, abundant shell fragments (?), moderately to poorly cemented, can be grouped with underlying orange sandstone. Thickness varies, but overall thickens to north from 5 to 10 cm. Laterally persistent. Sharp top. S7-21.
7. An interval of amalgamation of clinoform toes, as a condensed interval. Persistent thickness of 10-15 cm. Well thick laminated, sandy (m-vc) shale or siltstone, or sandstone (LSA/LW), moderately calcareous. Lenses of sandstone and blackened clasts, thin beds, mm laminated. Sharp to gradational top.
8. Packstone/wackestone at toe, gray, 20% lithics, m-c, sand-size peloids and shale fragments. Terminates to south in 4 m. A clinoform. Changes to south to very calcareous LW with peloids, c-vc, current laminated in lower part. Sharp top. S7-22 (toe of clinoform).
9. Sandstone, dark gray, weathered grayish green, LW/LSA, moderately to poorly cemented, very calcareous, common to abundant peloids (coated grains, limestone clasts/composite grains, shell fragments), in places, lithic wackestone, locally current laminated. Peloids crease to south. Some thin (< 1 cm), discontinuous micrite laminae. Sharp top. S7-23.
10. Wackestone, lithics rich, or peloidal LW/LSA, crude current laminations, light gray, upward decreasing lithics. Amalgamates with 3-4 clinoforms to the south to form a thick (~50 cm) interval of limestone. Sharp top.
11. Sandstone, weathered yellowish green, dark gray, m-vc, conglomeratic, LW/LSA, very calcareous. Current laminated, interlamination of wedge/lenses/layers of peloidal LW/LSA, 1-5 cm thick. Abundant granule to some fine pebbles (up to 5 cm in diameter), limestone clasts dominant. Clasts oriented. Many blackened clasts. Thickens to south up clinoform. A 25-cm long, 5 cm thick limestone lens (may be allochthonous), Sharp top.
12. 2 layers/intervals. Lower part, light gray, peloidal LW/LSA, c-vc, or lithic rich wackestone/packstone, extra-clasts rich, current laminated, 5-10 cm thick, sharp/gradational contact with the upper part. Upper part: lithic (20%) peloidal packstone/wackestone (70%), dense, gray. 10-20 cm thick. This 2-layer pattern is also present in other limestones. Sharp top. To be sampled in detail.

13. Sandstone, yellowish green, well sorted and rounded, LSA, c-vc, lenses of concentrated blackened clasts. Apparently current laminated. Clasts in sandstone and limestone are mostly oriented parallel to bedding plane in all cases or slightly imbricated. Moderately to poorly cemented. Sharp top.
14. Part of bed 13, better cemented. Sharp top.
15. Wackestone/packstone in south, lithics rich wackestone or peloidal sandstone (c-vc) in northern end. 2-layered pattern in northern lithics rich part. Sharp top. S7-24.
16. Sandstone, peloidal, abundant layers/laminae with abundant granular blackened clasts, LSA, c-vc, very calcareous, thin. Sharp top.
17. Wackestone/packstone, lithics increasing to south. Middle part a persistent 3-cm thick layer with blackened clasts, sharp top and base, some clasts with blackened coats. Sharp top.
18. Wackestone, shaley, mainly blackened, elongate clasts, thin, poorly cemented, apparently laminated. Sharp top.
19. Packstone, peloidal, <5% lithics in north. Quartzose m-c LSA in south with 10% peloids. Sharp top.
20. Similar to bed 18. Sharp top.
21. Packstone, peloidal in north, lower part ~10% lithics, upper part <5%, many blackened clasts with one in complete cvet(?). Lithics rich, peloidal wackestone in south. Lower part apparent faint current laminations. Sharp top.
22. Similar to Bed 18. Sharp top.
23. 2-layered pattern. Upper part (~30 cm), peloidal wackestone (70), dense, yellowish gray. Lower part (10 cm thick) has a persistent 3-cm thick layer with concentrated blackened clasts, encased in sandstone or sandy limestone. Sharp top.

Detailed sampling and geometry of Clinoform 12






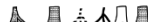




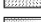





















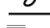

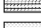







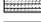


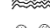









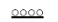





















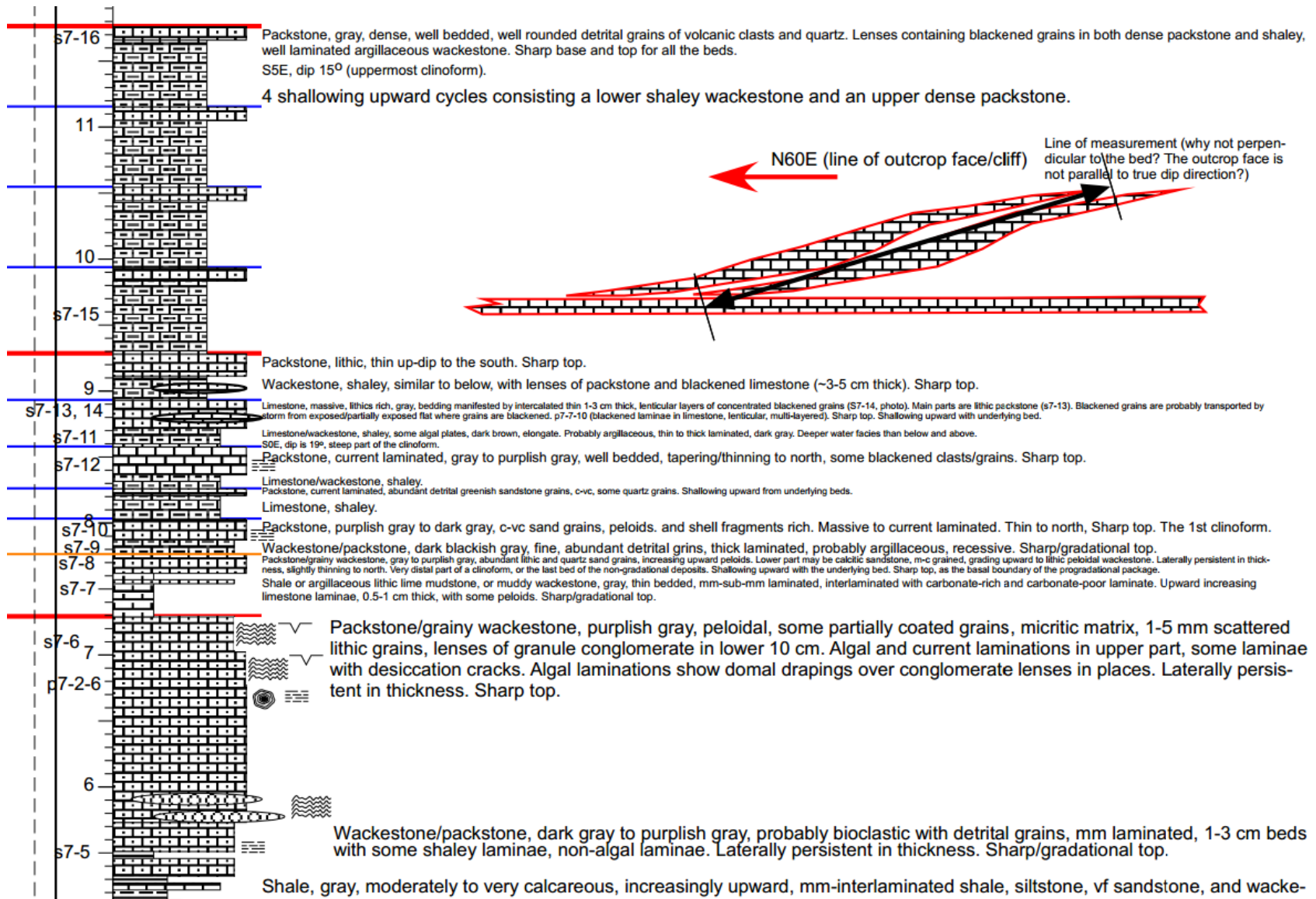
Termination of Progradation

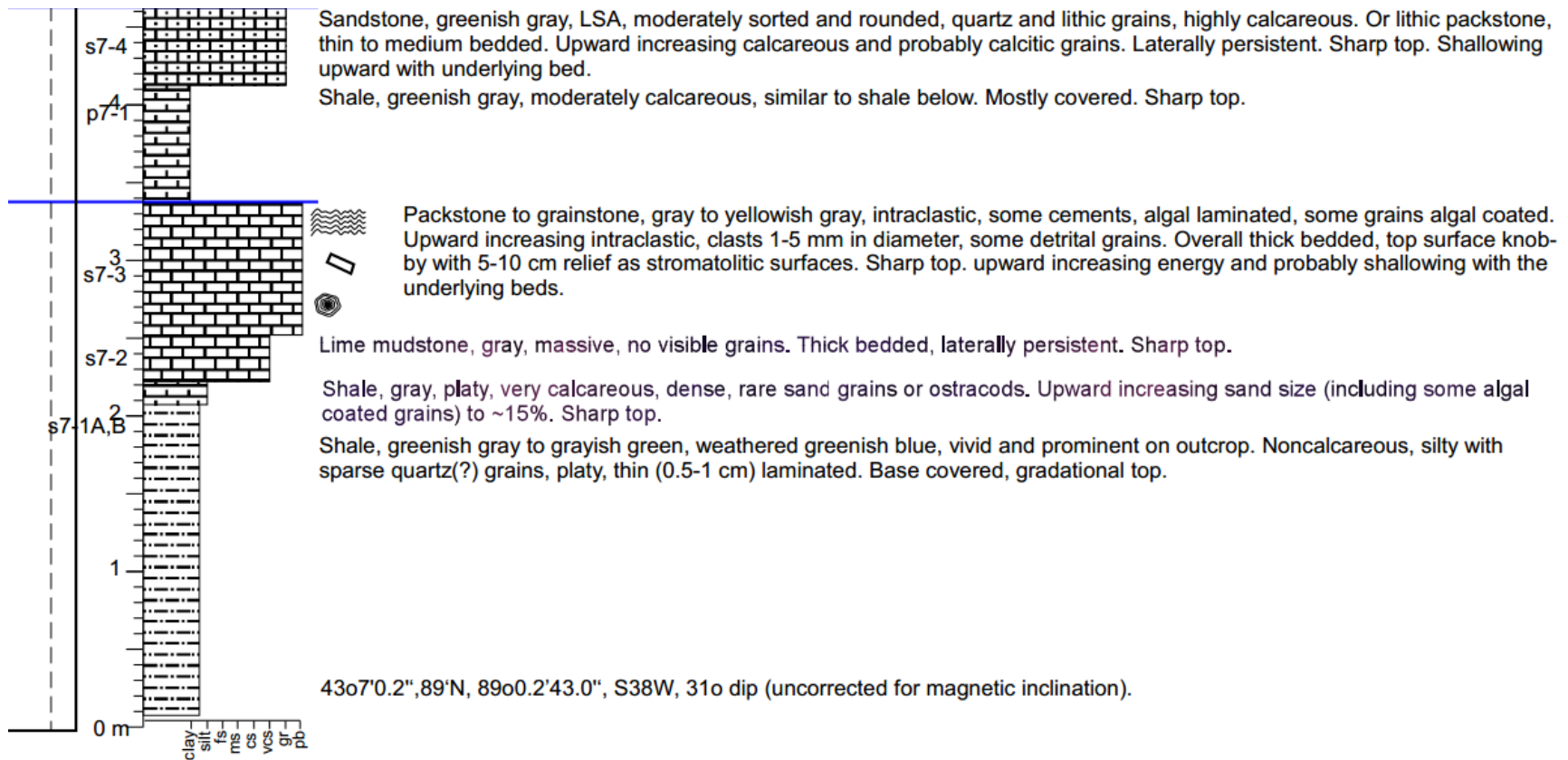


APPENDIX B
MEASURED SECTION 2 IN STRIKE DIRECTION

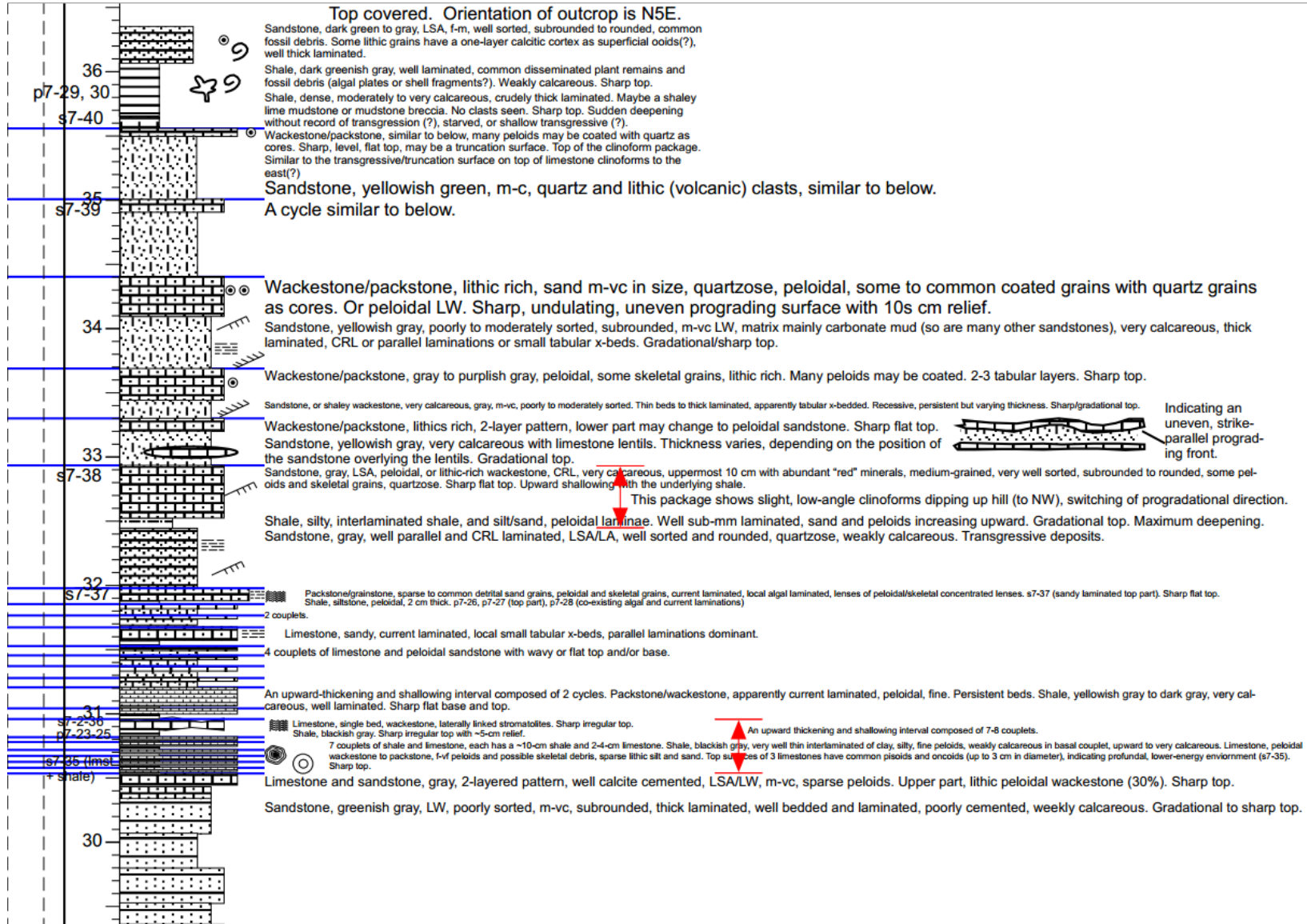
Legend

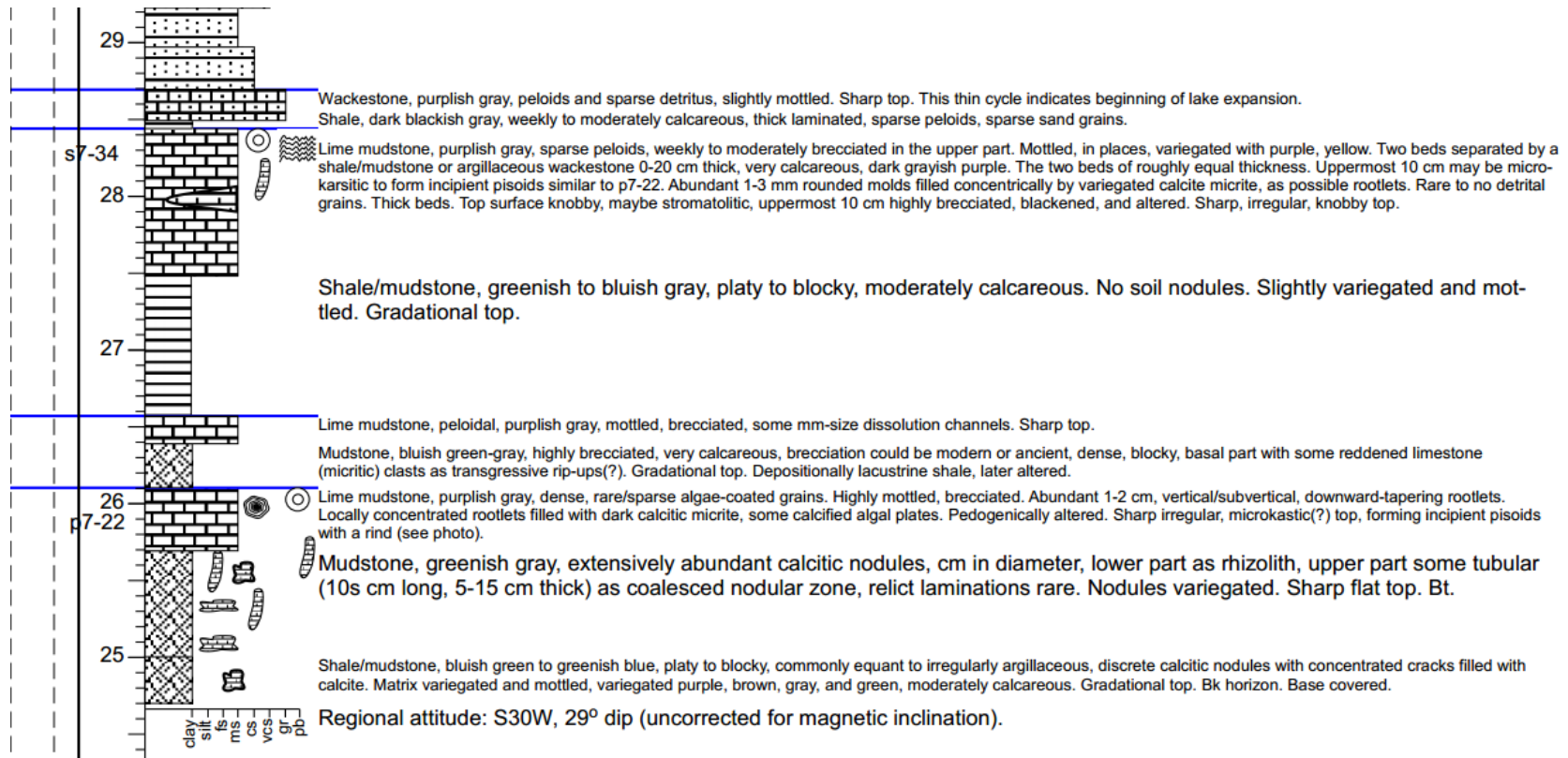
LITHOLOGY	SEDIMENTARY TEXTURE AND STRUCTURE
 Normal graded conglomerate or sandstone	 Soil slickensides
 Reverse graded conglomerate or sandstone	 Illuviated muddy sediments
 Clast-supported conglomerate	 Root mold, silicified/calcified stumps or branches
 Matrix-supported conglomerate	 Calcareous claystone and sandstone nodules, commonly root mottled
 Sandstone	 Rhizoconcretion or calcitic nodules
 Well-bedded sandstone	 Limonitic clayey soil pisoid
 Well-laminated sandstone	 Mud cracks
 Cross-bedded sandstone	<hr/>
 Conglomeratic sandstone	 Mud chips, rip-up clasts
 Calcareous sandstone	 Pisoids
 Muddy sandstone	 Ooids and superficial ooids
 Interbedded sandstone and shale/siltstone	 Invertebrate bone fossils
 Shale	 Trace fossils
 Silty shale	 Plants and plant debris
 Calcareous shale or mudstone	 Plant remains and fragments, carbonaceous laminae
 Dolostone	 Fish or fish scale fossils
 Shale, dolomitic.	 Shell fragments
 Mudstone	 Burrows, mottling structure
 Conglomeratic mudstone	<hr/>
 Calcrete or altered palustrine limestone	 Planar, tabular, and/or trough x-bedding
 Paleosol	 Erosional surface
 Limestone with shale partings	 Internal erosional surface
 Limestone	 Ripple and climbing ripple laminations
 Arenaceous limestone	 Hummocky cross stratification (HCS)
 Argillaceous limestone	 Contorted bedding
 Oolitic packstone/grainstone	 Cryptalgal lamination
 Pyroclastic breccia	 Symmetrical ripple marks
 Extrusive igneous rocks	 Vesicles filled with calcite or other minerals
 Modern salt accumulation	 Normal graded bedding
 Intrusive igneous rocks	 Reverse graded bedding
 Pillow basalt	 Algal coated pisoid and oncoid
 Mafic porphyry	 Microfaults
 Felsic porphyry	 Dissolution cavities/vugs
 Breccia	 Extensive brecciation structure
 Tuffaceous sandstone	<p>LA - Lithic arenite LSA - Lithic subarenite LW - Lithic wacke CRL - Climbing ripple laminations</p>
 Tuffaceous shale	 High-order cycle boundary
 Oolitic sandstone	 Low-order cycle boundary
 Gypsiferous sandstone	<p>Lst xx Cycle number</p>
 Bedded halite	<p>tr xx s7-xx Sample TDxx sz14-xx</p>
 Bedded gypsum	
 Gypsum and shale interlaminate	



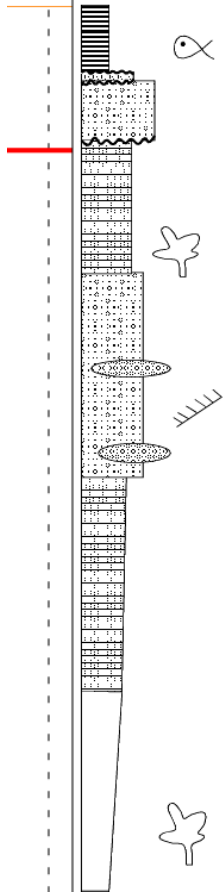


APPENDIX C.
MEASURED SECTION 3 IN STRIKE DIRECTION





APPENDIX D.
MEASURED SECTION 4 IN STRIKE DIRECTION



Shale, black, sub-mm laminated, wkly calc. Few thin (~2 cm) of wkst. Some fish scales. Profundal.

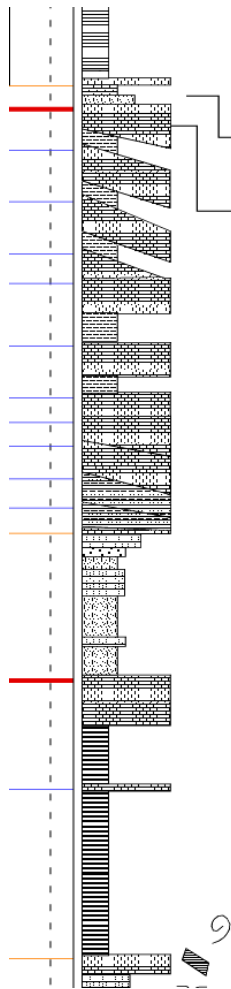
Ss, gray, f-m, v calc., lenticular (0-10 cm thick), erosional top & base. Some fossil debris.

Ss, blackish gray, c-vc, laminated to massive. Fossil fragments. Erosional top & base. Transgressive deposits.

Ss, gray, f-m, rare fine pebbles, well thin bedded. Plant debris throughout. Small tabular x-beds.

Ss, conglomeratic, and lenses of conglomerate. Ss, m-c, well sorted, lithic arenite, plane beds, normal graded beds, and low-angle tabular x-beds, some internal erosional surfaces. Local convoluted beds. Non-calcareous. Clasts well rounded, pebbles parallel to bedding. Upper contact sharp. Channel mouth bar deposits.

Slst & ss, well laminated, wkly calc., rare pebble and plant debris. Coarsening upward from siltstone to f-vf sandstone. Some mud chips. Distal delta front deposits. Base gradational, top sharp.



Conglomerate, laterally changes into calc. slst, to fine ss. Clasts fine pebble, clast-supported. Capping underlying progradational package. Thickness varies from 3-10 cm. Transgressive lag.

2 beds of ss & lmst intercalated with calc. sh. Lower ss, m, v calc., w-laminated, fossiliferous, ~10 cm thick. Upper peloidal wkst. Relatively concentrated clasts (4 cm max.) on top surfaces and throughout. High-energy shallow littoral.

4 beds of pkst/wkst with shale interbeds (each 20-30 cm thick), forming northward prograding clinofolds. L. lmst lithic-rich, u. ones pure, gray. Sh & silty sh contain f-ss laminae. On the top surfaces, lmst nodules algal-laminated to form stromatolites.

3 beds of arenaceous packstone to grainstone, gray, each ~30 cm thick, common shell fragments, sparse granule to pebble-size clasts. Beds are graded, plane bedded, or low-angle x-bedded.

Shale and silty shale interbeds, dark gray to light brown, 20-40 cm thick, very calcareous, well laminated, abundant shell and fossil fragments. High-energy shallow littoral with periodic deepening.

4 beds of northward prograding clinofolds. Basal bed, ~20 cm, v calc. ss, m, l. part with fossil molds, interbedded with gray-black, fissile, fossiliferous sh. 2nd bed more fossiliferous, less sandy. 3rd and 4th beds arenaceous pkst/wkst, gray, beds 20-30 cm thick, wedge shaped. Sparse sed. clasts throughout. Algal-parallel laminated, some tab x-beds.

Wkst, brown-gray, argil., some clasts, clayey/silty matrix-supported fossil debris.

Ss, conglomeratic, m-c, clasts are fossil debris, increasing upward. Reworked lag deposit.

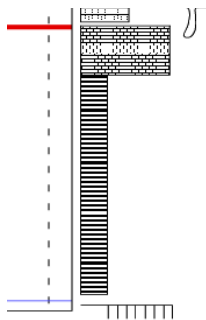
Slst, with f ss, gray, v. calc., w-laminated. Top ss x-laminated. Mid ss & slst with many limonite nodules, ~1 mm in size, mottled with relict laminations. L. ss, m, climbing ripple laminated, symmetrical ripple marks and shell fragments throughout. Base sharp, top gradational.

Pkst/grnst with shale partings, blackish gray, sub-mm algal laminated. Each bed is 5-10 cm.

Shale, black to greenish gray, fissile laminated, calc. A pkst in middle, black, fossiliferous, organic rich.

Micrite or peloidal wackestone, gray, abundant 1 cm or less mud chips. Lake shore deposit.

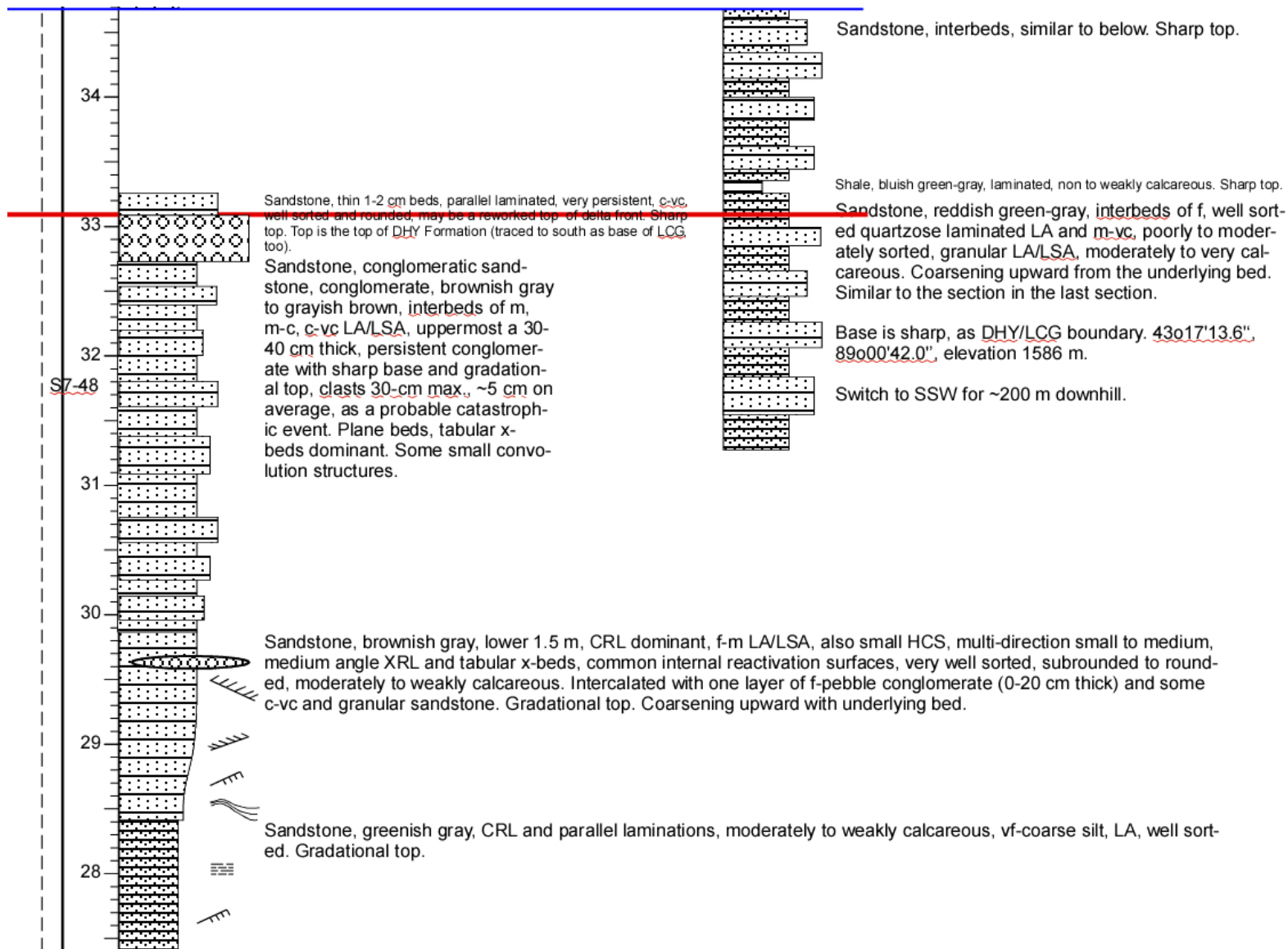
Ss, green, f-m, abundant shell fragments and clasts, crudely thin bedded, mottled.

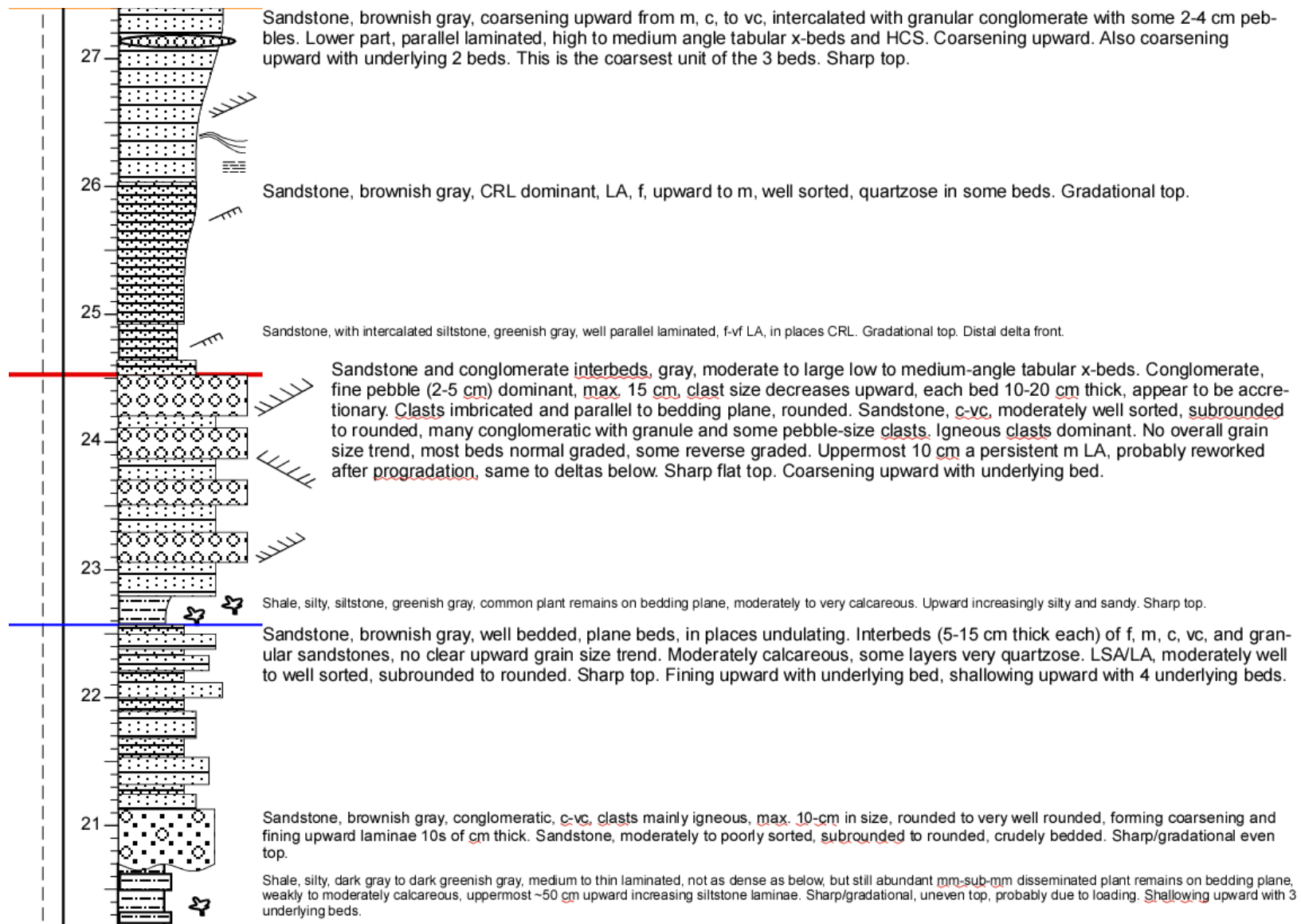


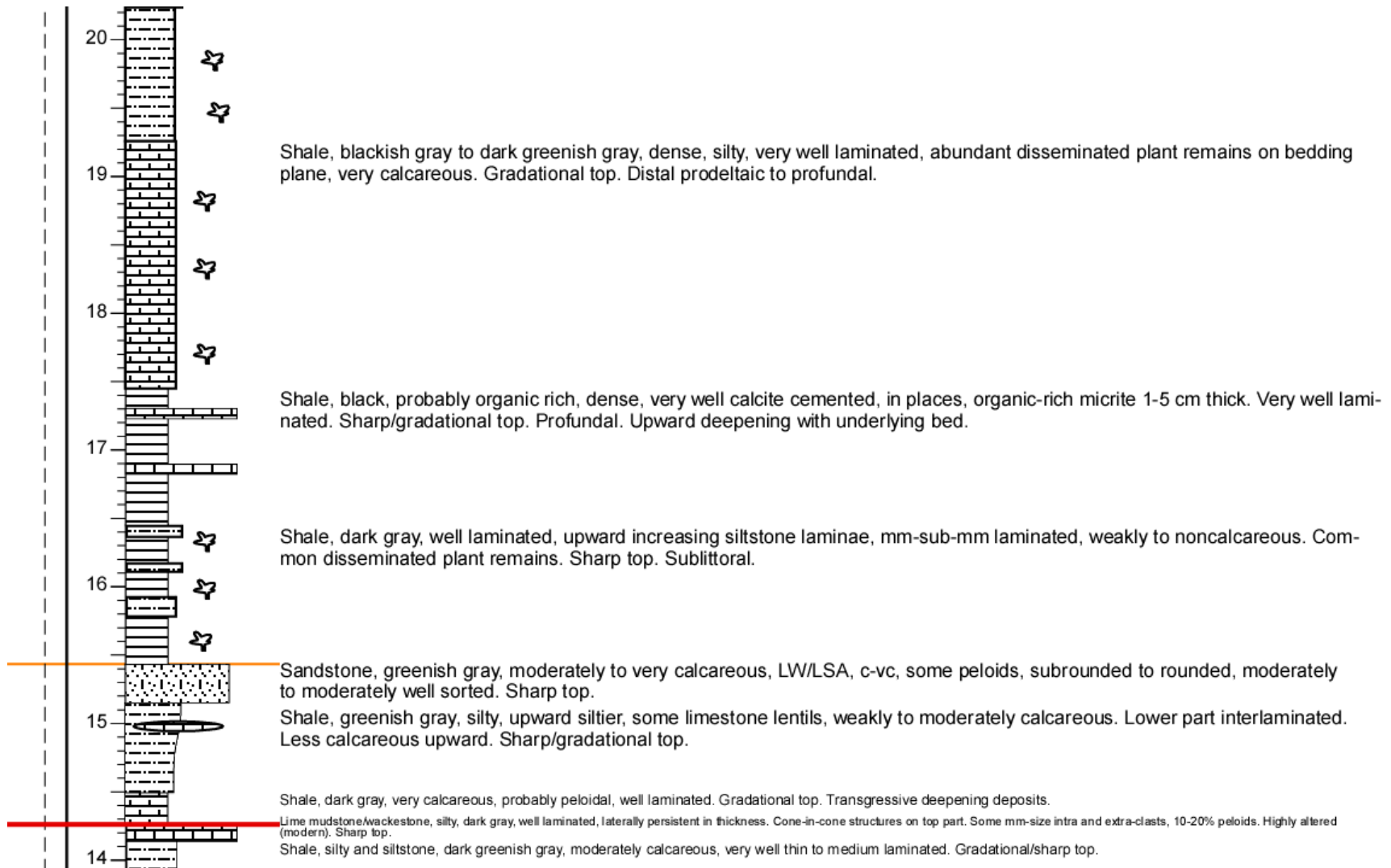
Micrite, peloidal, sparse shell fragments. Top intraclastic pkst/grnst, irregular and knobby, with ~15 cm relief, interlaminated with black fissile shale between knobs, an algal/stromatolite origin.

Shale, greenish gray, slightly calcareous, platy, no fossils seen.

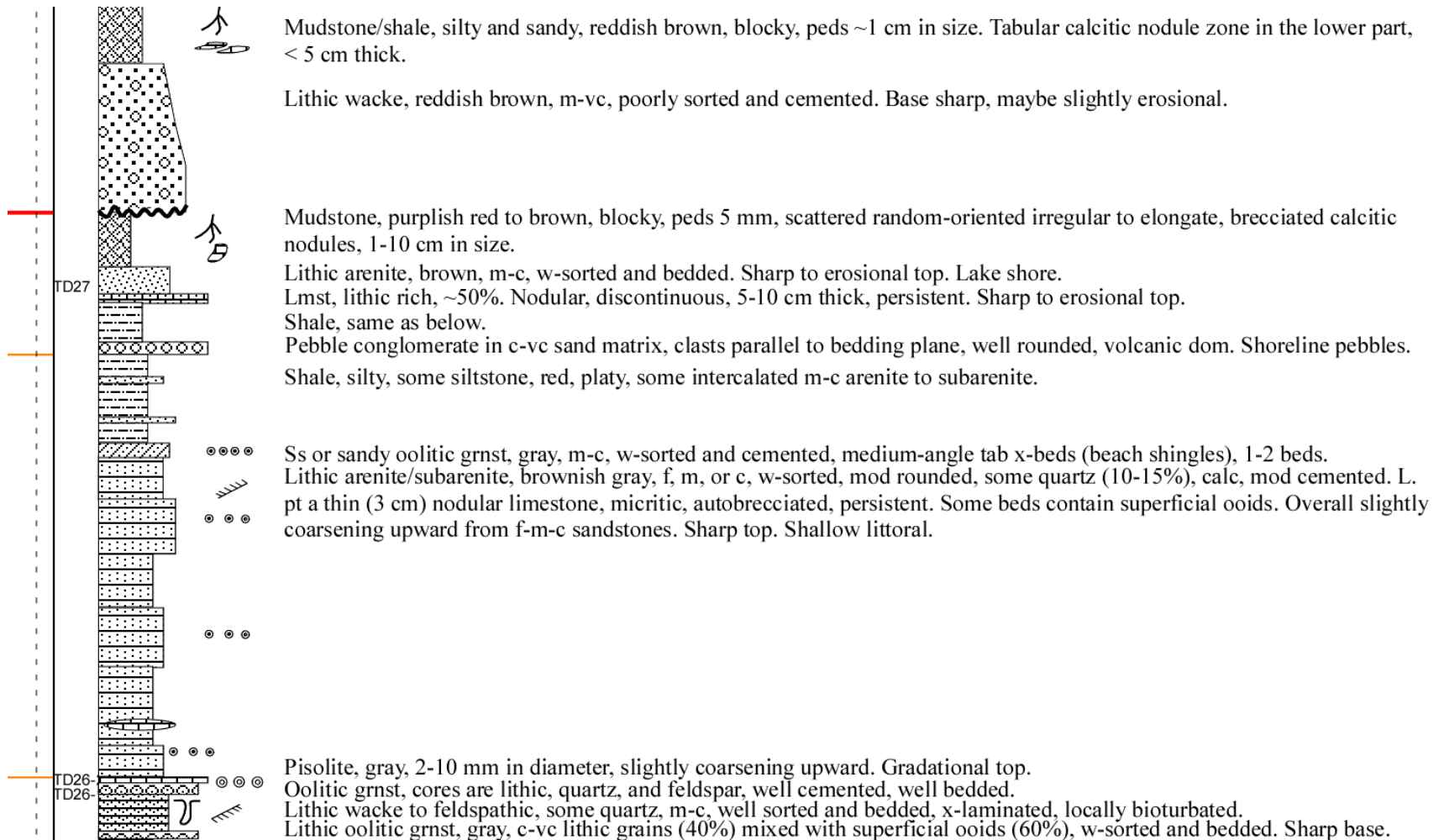
APPENDIX E.
MEASURED SECTION 5 IN STRIKE DIRECTION

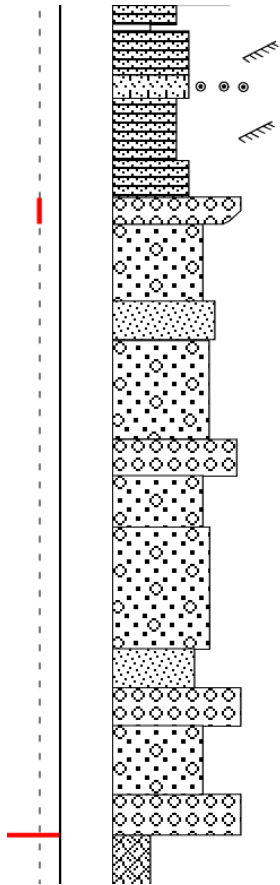






APPENDIX F.
MEASURED SECTION 6 IN STRIKE DIRECTION



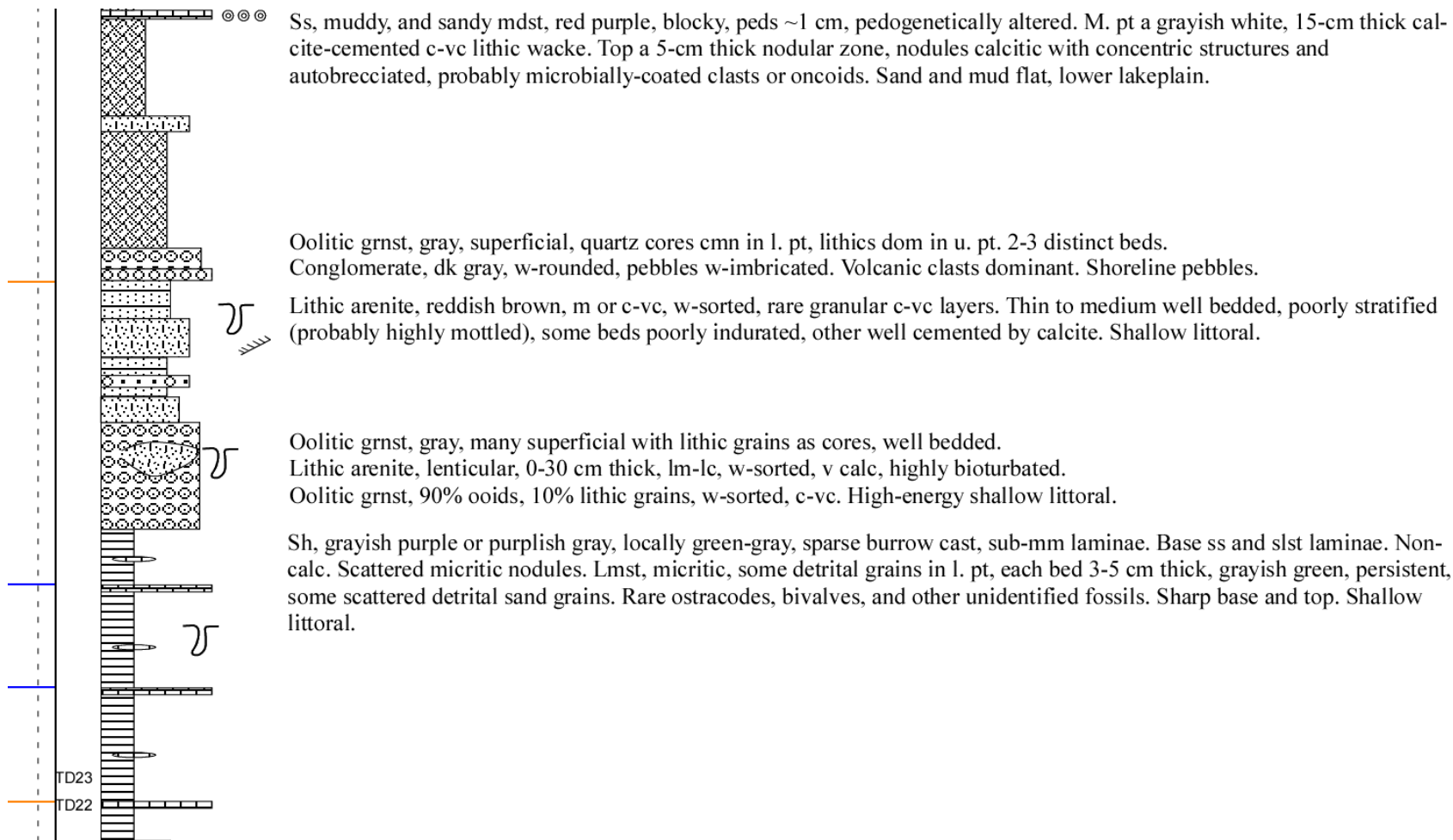


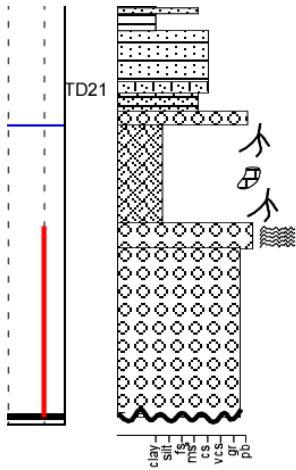
Arenite, brown, w-sorted, f or m, w-bedded and laminated, some ripple x-laminated, thin beds 10s cm. One bed v calc, gray, with some superficial ooids. One thin (<5 cm) red shale in the uppermost part. Shallow littoral.

Conglomerate, gray, coarsening upward from fine pebble to cobble (10-15 cm), imbricated, parallel to bedding, volcanic clasts. Shoreline pebbles.

Conglomeratic sandstone and sandy conglomerate, light pale pink, light gray, very poorly cemented, granule to fine pebble clasts. Weathered into loose sediments. Interbeds with sandy conglomerate with granule to fine pebble clasts, poorly sorted. 2 beds (~25 cm thick each) well sorted c-vc arenite. The rest is poorly sorted. Partially covered. Sharp base. Braidplain/lakeplain deposits.

Mudstone, dark purplish red. Lakeplain mud flat.



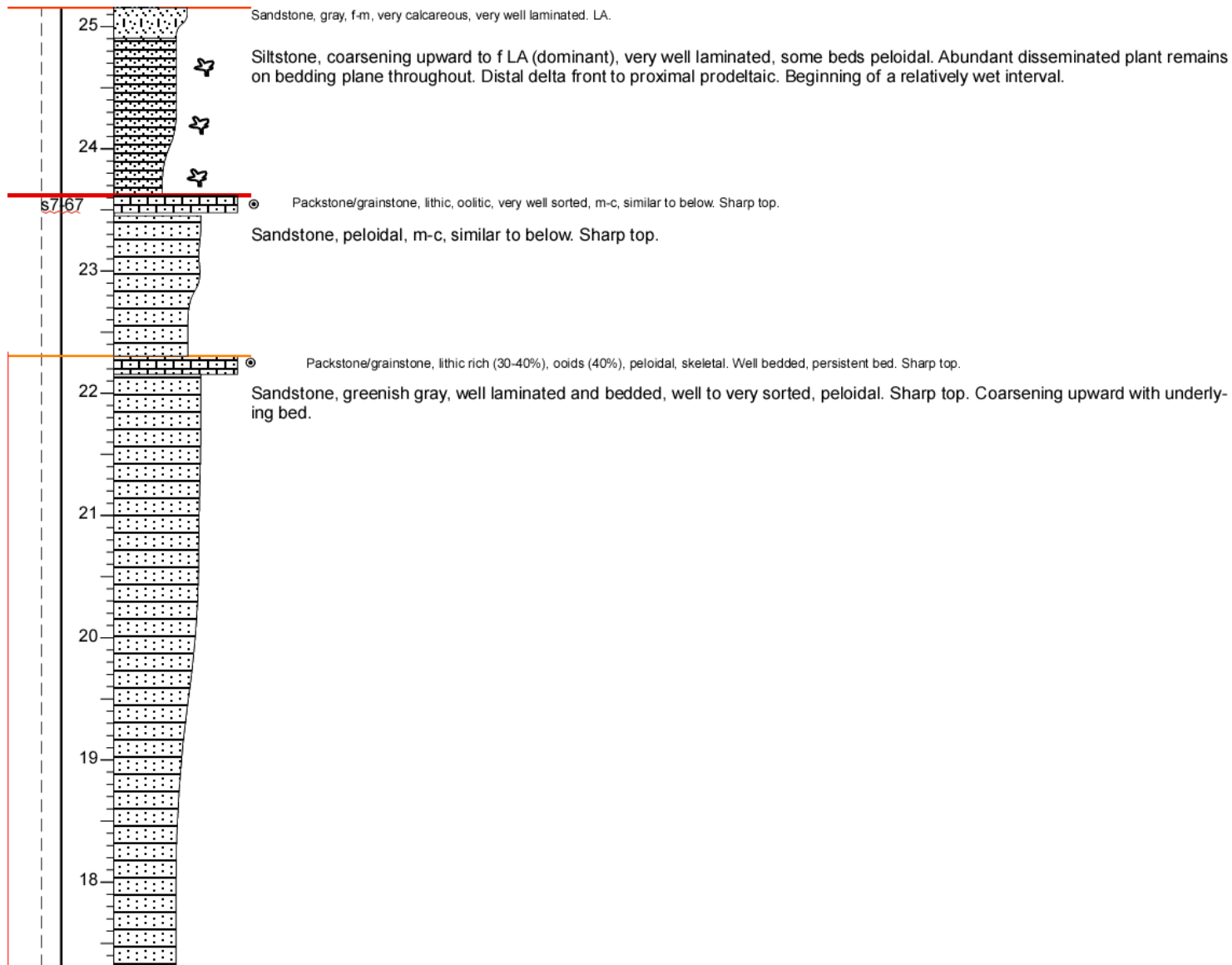


Sandstone, brown, c, w-sorted, mod-rounded, multi-directional x-bedded, trough and tabular. Lakeshore-shallow littoral.
 Lithic arenite, gray, f-c, mod-sorted, v calc, persistent. Sharp base and top.
 Lithic arenite, reddish brown, m, w-sorted, mod-rounded, laminated.

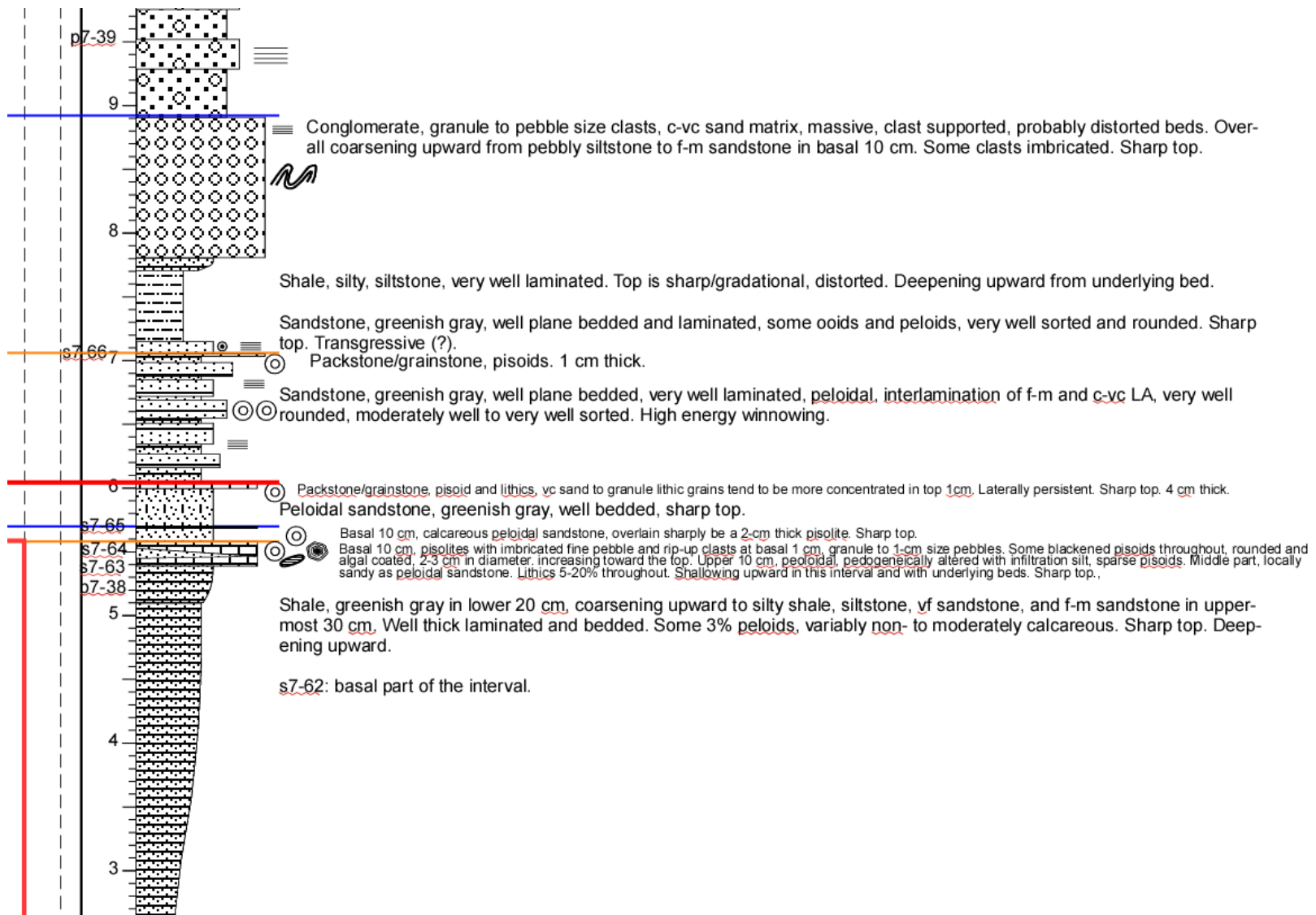
Conglomerate, blackened, vw-rounded, 5-20 cm, w-imbricated, persistent. Sharp base and top. Shoreline pebbles.
 Mdst, reddish purple, slightly silty, peds 2-3 mm, scattered irregular to elongate calcitic nodules. Calcitic paleosol, lakeplain mud flat.

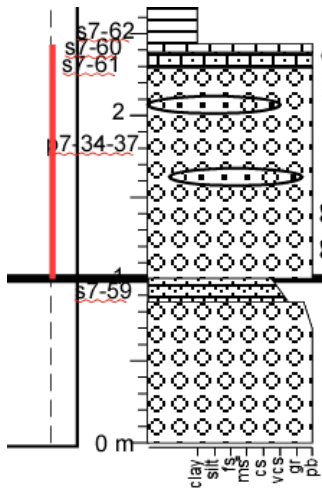
Conglomerate, grayish red, granule to fine pebble size, w-imbricated. Two parts, although with same composition and are a single sedimentation unit. U. pt much better calcite cemented; many clasts superficially coated by algae or microbes.
 Braidplain, upper lakeplain deposits.

APPENDIX G.
MEASURED SECTION 7 IN STRIKE DIRECTION







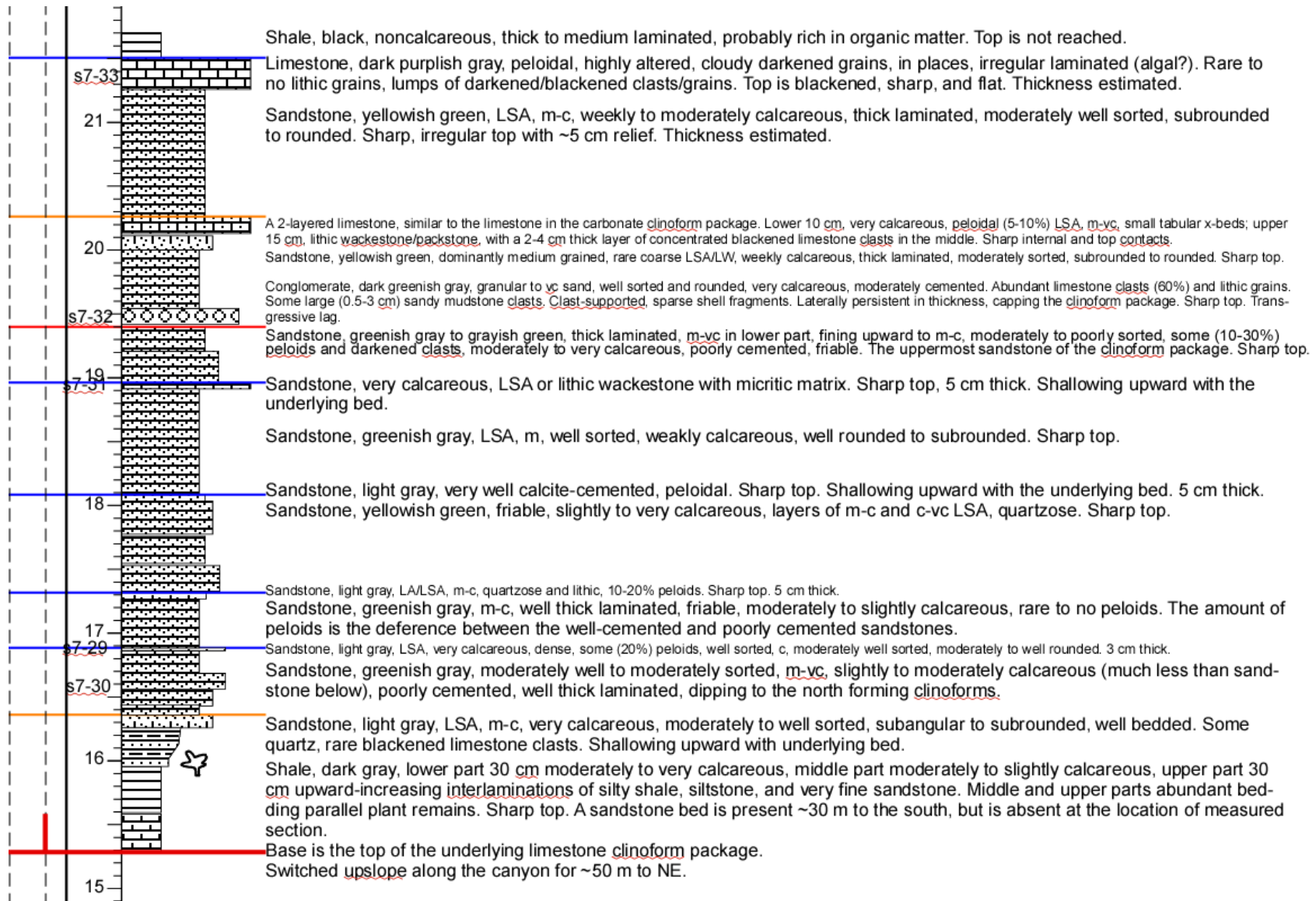


◎ ◎ Conglomerate, dark gray, clast supported, plane beds, 1-5 cm thick, some bases are gently concave. Clasts granule to fine pebble, very well imbricated and/or parallel to bedding plane. Laminae of conglomeratic c-vc LA, moderately well to moderately sorted, well rounded. Upper part 4 cm, pisoids, 2-3 mm in diameter, probably algal coated, reverse or normal graded, 2-3 beds, each ~2 cm thick, core of pisoids is very well rounded, probably a high-energy origin; cortex may be of algal origin, indicating starvation, thus, the top/interval suggests maximum lake expansion and most evaporative condition. Below the top ~10 cm, some skeletal and peloidal grains. Scattered rounded to equant 1-3 cm calcitic nodules in lower part. Transgressive shoreline pebbles. Sharp, flat, persistent top, as maximum transgressive surface.

Conglomeratic sandstone, gray to greenish gray, in the upper 10 cm, c-vc, moderately well sorted, LA/LSA, downward change to f-pebble to pebble (max. ~10 cm in size) conglomerate, clast supported. Tabular lentils of calcite deposits, 5-20 cm thick, parallel to bedding plane in upper part (groundwater calcite?). This is the uppermost braided stream cycle in DHY. Gradational base. Sharp top, slightly concave (~5 cm), as the first transgressive surface of LCG Formation.

43o14'45.0"N, 89o03'11.9"E, elevation 1523 m. Attitude, N17E dip direction(uncorrected), 44o dip angle.

APPENDIX H.
MEASURED SECTION 1 IN STRIKE DIRECTION



BIBLIOGRAPHY

- Adams, E. W., Morsilli, M., Schlager, W., Keim, L. & Van Hoek, T. 2002. Quantifying the geometry and sediment fabric of linear slopes: examples from the Tertiary of Italy (Southern Alps and Gargano Promontory). *Sedimentary Geology* 154, 11–30.
- Allen, M.B. and Natal'in, B.A., 1995. Junggar, Turfan and Alakol basins as Late Permian to? Early Triassic extensional structures in a sinistral shear zone in the Altaid orogenic collage, Central Asia. *Journal of the Geological Society*, 152(2), pp.327-338.
- Allen, M.B., Windley, B.F., Chi, Z., ZHONG-YAN, Z.H.A.O. and GUANG-REI, W.A.N.G., 1991. Basin evolution within and adjacent to the Tien Shan Range, NW China. *Journal of the Geological Society*, 148(2), pp.369-378.
- Arp, G. 1995. Lacustrine bioherms, spring mounds, and marginal carbonates of the Ries-Impact-Crater (Miocene, southern Germany). *Facies*, 33, 35–90.
- Blott, S.J. and Pye, K. (2001) GRADISTAT: a grain size distribution and statistics package for the analysis of unconsolidated sediments. *Earth Surface Processes and Landforms* 26, 1237-1248.
- Bosellini, A., 1984, Progradation geometries of carbonate platforms: Examples from the Triassic of the Dolomites, northern Italy: *Sedimentology*, v. 31, p. 1-24.
- Bustillo, M.A., Arribas, M.E., Bustillo, M., 2002. Dolomitization and silicification in low-energy lacustrine carbonates (Paleogene, Madrid Basin, Spain). *Sed. Geology* 151, 107-126.
- Carroll, A.R., Brassell, S.C. and Graham, S.A., 1992. Upper Permian Lacustrine Oil Shales, Southern Junggar Basin, Northwest China (1). *AAPG Bulletin*, 76(12), pp.1874-1902.
- Carroll, A.R., Graham, S.A., Hendrix, M.S., Ying, D. and Zhou, D., 1995. Late Paleozoic tectonic amalgamation of northwestern China: sedimentary record of the northern Tarim, northwestern Turpan, and southern Junggar basins. *Geological Society of America Bulletin*, 107(5), pp.571-594.
- Carroll, A.R., Liang, Y., Graham, S.A., Xiao, X., Hendrix, M.S., Chu, J., and McKnight, C.L., 1990, Junggar basin, northwest China: Trapped late Paleozoic ocean: *Tectonophysics*, c. 191, p. 1-14.
- Carroll, A.R., Yunhai, L., Graham, S.A., Xuchang, X., Hendrix, M.S., Jinchi, C. and McKnight, C.L., 1990. Junggar basin, northwest China: trapped Late Paleozoic ocean. *Tectonophysics*, 181(1-4), pp.1-14.
- Cheng, Z.-W., Lucas, S.G., 1993. A possible nonmarine GSSP for the Permian–Triassic boundary. *Albertiana* 12, 39–44.

- Davaud, E., Girardclos, S., 2001. Recent freshwater ooids and oncoids from western Lake Geneva (Switzerland): indications of a common organically mediated origin. *Journal of Sedimentary Research* 71, 423-429.
- Denys, L., Kiden, P., Verbruggen, C., 1998. Opaline concretions in Weichselian Late-Glacial lake marl from Flanders, northern Belgium. *Journal of Paleoclimatology* 20, 91-98.
- Dickinson, W.R., 1970. Interpreting detrital modes of graywacke and arkose. *Journal of Sedimentary Research*, 40(2).
- Dickinson, W.R., 1985. Interpreting provenance relations from detrital modes of sandstones. In *Provenance of arenites* (pp. 333-361). Springer Netherlands.
- Dunham, R.J., 1962. Classification of carbonate rocks according to epositional texture. – In: Ham, W.W. (ed.): *Classification of carbonate rocks. A symposium.* – Amer. Ass. Petrol. Geol. Mem., 1. 108-17
- Dupraz, C., Visscher, P.T., Baumgartner, L.K., and Reid, R.P., 2004, Microbe-mineral interactions: early carbonate precipitation in a hypersaline lake (Eleuthera Island, Bahamas): *Sedimentology*, v. 51, p. 745–765.
- Embry, A.F., Klovan, J.E., 1971. A late Devonian reef tract on northeastern Banks Island. N.W.T. – *Bull. Canadian Petrol. Geol.*, 19. 730-891.
- Flügel, E. 2010. *Microfacies of CarBONATE Rocks: Analysis, Interpretation and Application*. Second edition. Berlin, Heidelberg, Springer-Verlag. 984p.
- Folk, R.L., 1959. Practical petrographic classification of limestones. *AAPG Bulletin*, 43(1), pp.1-38.
- Folk, R.L. 1962. Petrography and origin of the Silurian Rochester and McKenzie Shales, Morgan County, West Virginia: *Jour. Sed. Petrol.*, v. 32, p.539-578.
- Folk, R.L., 1962, Spectral subdivision of limestone types, in Ham, W.E., ed., *Classification of carbonate Rocks-A Symposium: American Association of Petroleum Geologists Memoir* 1, p. 62-84.
- Folk, R.L., 1965. Some aspects of recrystallization in ancient limestones. In: Pray L C, Murray R C (eds.) *Dolomitization and Limestone Diagenesis*. (SEPM Special Publication, vol 13. pp 14–48.
- Folk, R.L., 1974. The natural history of crystalline calcium carbonate: effect of magnesium content and salinity. *Journal of Sedimentary Research*, 44(1).
- Folk, R.L., 1980, *Petrology of sedimentary rocks*: Hemphill Publishing Company, Austin, Texas, 184 pp.
- Gierlowski-Kordesch, E. H. 2010. Lacustrine carbonates. In: Alonso-Zarza, A. M. & Tanner, L. H. (eds.) *Carbonates in Continental Settings. Developments in Sedimentology*. 61, 1-101.

- Graham, S.A., Hendrix, M.S., Wang, L.B. and Carroll, A.R., 1993. Collisional successor basins of western China: Impact of tectonic inheritance on sand composition. *Geological Society of America Bulletin*, 105(3), pp.323-344.
- Greene, T.J., Carroll, A.R., Hendrix, M.S., Graham, S.A., Wartes, M.A. and Abbink, O.A., 2001. Sedimentary record of Mesozoic deformation and inception of the Turpan-Hami basin, northwest China. *Paleozoic and Mesozoic tectonic evolution of central and eastern Asia*, 194, p.317.
- Greene, T.J., Carroll, A.R., Wartes, M., Graham, S.A. and Wooden, J.L., 2005. Integrated provenance analysis of a complex orogenic terrane: Mesozoic uplift of the Bogda Shan and inception of the Turpan-Hami Basin, NW China. *Journal of Sedimentary Research*, 75(2), pp.251-267.
- Guan, W., 2011, Provenance Analysis of Upper Permian-Basal Triassic Fluvial-Lacustrine Sedimentary Rocks in the Greater Turpan-Junggar Basin, Southern Bogda Mountains, NW China. Master thesis, Wichita State University.
- Hendrix, M.S., Graham, S.A., Carroll, A.R., Sobel, E.R., McKnight, C.L., Schulein, B.J., Wang, Z., 1992. Sedimentary record and climatic implications of recurrent deformation in the Tian Shan: evidence from Mesozoic strata of the north Tarim, south Junggar, and Turpan basins, northwest China. *Geol. Soc. Am. Bull.* 104, 53–79.
- Jacquin, T., Arnaud-Vanneau, A., Arnaud, H., Ravenne, C. & Vail, P. 1991. Systems tracts and depositional sequences in a carbonate setting, a study of continuous outcrops from platform to basin at the scale of seismic lines. *Marine Petroleum Geology* 8, 122-39.
- Kelts K. and Talbot M.R. 1990. Lacustrine carbonates as geochemical archives of environmental change and biotic-abiotic interactions. In: Tilzer M.M. and Serruya C. (eds), *Ecological Structure and Function in Large Lakes*. Springer-Verlag, Berlin, pp. 290-317.
- Kenter, J. A. M. 1990. Carbonate platform flanks: slope angle and sediment fabric. *Sedimentology* 37, 777–94.
- Kenter, J. A. M. & Campbell, A. 1991. Sedimentation on a Lower Jurassic carbonate platform flank: geometry, sediment fabric and related depositional structures (Djebel Bou Dahar, High Atlas, Morocco). *Sedimentary Geology* 72, 1–34.
- Liao, Z., Lu, L., Jiang, N., Xia, F., Song, F., Zhou, Y., Li, S., Zhang, Z., 1987. Carboniferous and Permian in the western part of the east Tianshan Mountains. *Eleventh Congress of Carboniferous Stratigraphy and Geology, Guidebook Excursion 4*. Beijing, China, 50 pp.
- Liu, Zhaosheng, 2000. The Permo–Triassic boundary at the northern margin of Tu–Ha Basin. *J. Stratigr.* 24, 310–314 (in Chinese with English abstract).
- Mount, J. F., 1985. Mixed siliciclastic and carbonate sediments: a proposed first-order textural and compositional classification: *Sedimentology*, v. 32, p. 435-442.

- Mullins, H., Heath, K. C., Van Buren, H. M. & Newton, C. R. 1983. Anatomy of a modern open-ocean carbonate slope: northern Little Bahamas Bank. *Sedimentology* 31, 141–68.
- Obrist-Farner, J., 2015. Origin and stratigraphic architecture of the Middle Permian lower and upper Quanzijie low-order cycles, Bogda Mountains, NW China.
- Obrist-Farner, J., Yang, W. and Hu, X.F., 2015. Nonmarine time-stratigraphy in a rift setting: An example from the Mid-Permian lower Quanzijie low-order cycle Bogda Mountains, NW China. *Journal of Palaeogeography*, 4(1), pp.27-51.
- Peterson, M.N.A., Von der Borch, C.C., 1965 Chert: modern inorganic deposition in a carbonate-precipitating locality. *Science* 14. 1501-1503.
- Pettijohn, F.J., 1975. *Sedimentary rocks* (3rd ed.): New York, Harper and Row, 628 p.
- Pettijohn, F.J., Potter, P.E. and Siever, R., 1972. *Sand and sandstone*.
- Pomar, L. 1991. Reef geometries, erosion surfaces and high-frequency sea level changes, Upper Miocene reef complex, Mallorca, Spain. *Sedimentology*, v. 38, p. 243-269.
- Quiquerez, A. & Dromar, T.G. (2006) - Environmental control on granular clinoforms of ancient carbonate shelves. *Geological Magazine*, 143, 343-365.
- Richter, D. K. (1983). Calcareous ooids: a synopsis". In: *Coated grains*. Springer, pp. 71-99.
- Shao, L., Stattegger, K. and Garbe-Schoenberg, C.D., 2001. Sandstone petrology and geochemistry of the Turpan basin (NW China): implications for the tectonic evolution of a continental basin. *Journal of Sedimentary Research*, 71(1), pp.37-49.
- Shao, L., Stattegger, K., Li, W., Haupt, B.J., 1999. Depositional style and subsidence history of the Turpan Basin (NW China). *Sed. Geol.* 128, 155–169.
- Swirydczuk, K., Wilkinson, B. H., and Smith, G. R., 1979, The Pliocene Glens Ferry Oolite: lake margin carbonatedeposition in the southwestern Snake River Plain: *Jour. Sed. Petrology*, v. 49, p. 995-1004.
- Swirydczuk, K., Wilkinson, B.H. and Smith, G.R., 1980. The Pliocene Glens Ferry oolite- II: Sedimentology of oolitic lacustrine terrace deposits: *Journal of Sedimentary Petrology*, v. 50, p. 1237-1247.
- Talbot, M. R., and Allen, P. A., 1996, *Lakes*, in Reading, H. G., ed., *Sedimentary environments, processes, facies and stratigraphy*, third edition, Blackwell Science, Oxford, p. 83-124.
- Talbot, M.R., Kelts, K., 1990. Paleolimnological signatures from carbon and oxygen isotopic ratios in carbonates from organic carbon-rich lacustrine sediments. In: Katz, B.J. (Ed.), *Lacustrine Basin Exploration: Case Studies and Modern Analogs*, AAPG Memoir 50, pp. 88-112.

- Tucker, M.E., Wright, V.P., 1990. Carbonate Sedimentology. Blackwell Science Publications, Oxford.
- Wright, V.P., 1992. A revised classification of limestones, *Sedimentary Geology*, 76, 177-185.
- Yang, W., 2008. Depositional Systems Analysis within a Seismic Sequence Stratigraphic Framework, Turpan-Hami Basin, NW China. Tu-Ha Oil Company Internal Report, PetroChina.
- Yang, W., Feng, Q., Liu, Y., Tabor, N., Miggins, D., Crowley, J.L., Lin, J. and Thomas, S., 2010. Depositional environments and cyclo-and chronostratigraphy of uppermost Carboniferous–Lower Triassic fluvial–lacustrine deposits, southern Bogda Mountains, NW China—A terrestrial paleoclimatic record of mid-latitude NE Pangea. *Global and Planetary Change*, 73(1), pp.15-113.
- Yang, W., Guan, W., Wang, Y., Feng, Q., Liu, Y., Tabor, N., 2008. Limestone-Sandstone Clinoforms in Middle-Permian Lacustrine Deposits, Implications for Progradational Infilling of Intermontane Lake Basins. AAPG Poster.
- Yang, W., Liu, Y., Feng, Q., Lin, J., Zhou, D. and Wang, D., 2007. Sedimentary evidence of Early–Late Permian mid-latitude continental climate variability, southern Bogda Mountains, NW China. *Palaeogeography, Palaeoclimatology, Palaeoecology*, 252(1), pp.239-258.
- Yin, H.F., Zhang, K., Tong, J., Yang, Z., Wu, S., 2001. The global stratotype section and point (GSSP) of the Permian–Triassic Boundary. *Episodes* 24 (2), 102–114.
- Zhou, T., Li, X., Yang, J., Hou, J., Liu, S., Cheng, Z., Wu, S., Li, Y., 1997. Research on Chinese nonmarine Permo–Triassic GSSP sections. *Xinjiang Geology* 15, 211–225 (in Chinese with English abstract).
- Zuffa G.G., 1980, Hybrid arenites: their composition and classification: *Jour. Sed. Petrology*, v. 50, p. 21-29.

VITA

Yiran Lu was born in Beijing, China. In May 2012, He recieved his Bachelor of Science in Geology, China University of Petroleum-Huadong, and Bachelor of Science in Geology, Missouri University of Science and Technology. He received his Master of Science in Geology and geophysics, Missouri University of Science and Technology, in December 2016

Yiran Lu has a publication of GSA annual meeting abstract in 2016.